

## Durham E-Theses

---

### *Debris flow dynamics: A flume study of velocity and superelevation*

PROCTER, CHRISTOPHER, MATTHEW

#### How to cite:

---

PROCTER, CHRISTOPHER, MATTHEW (2012) *Debris flow dynamics: A flume study of velocity and superelevation*, Durham theses, Durham University. Available at Durham E-Theses Online:  
<http://etheses.dur.ac.uk/3587/>

#### Use policy

---

The full-text may be used and/or reproduced, and given to third parties in any format or medium, without prior permission or charge, for personal research or study, educational, or not-for-profit purposes provided that:

- a full bibliographic reference is made to the original source
- a [link](#) is made to the metadata record in Durham E-Theses
- the full-text is not changed in any way

The full-text must not be sold in any format or medium without the formal permission of the copyright holders.

Please consult the [full Durham E-Theses policy](#) for further details.

**DEBRIS FLOW DYNAMICS:  
A FLUME STUDY OF  
VELOCITY AND  
SUPERELEVATION**

*Christopher Procter*

*MSc. (By Research)*

*Department of Geography*

*Durham University*

*December 2011*

## **Declaration and Statement of Copyright**

I confirm that no part of the material presented in this thesis has previously been submitted by me or by any other person for a degree in this or any other University. In all cases, where it is relevant, material from the work of others has been acknowledged.

The copyright of this thesis rests with the author. No quotation from it should be published without prior written consent and information derived from it should be acknowledged.

*Christopher M. Procter*

*Department of Geography,*

*Durham University*

*December 2011*

## Abstract

Debris flows are powerful, geophysical flows with the potential to cause fatalities and damage infrastructure. The hazard posed by these events is often related to the velocity of the flow. However, due to their spontaneous nature and rapid onset, opportunities to observe debris flows are rare. The aim of this investigation was to improve the understanding of debris flow dynamics in curved channels using a hardware laboratory flume model.

The purpose-built, variable slope, 8 m long flume enables a variety of debris flow boundary conditions to be studied. Here, 60 experimental tests were carried out at four slope of  $-15^\circ$ ,  $17^\circ$ ,  $23^\circ$  and  $25^\circ$ ; for both straight (12 tests) and curved channels (48 tests). The modular construction of the flume enabled purpose-made channel curves to be inserted in the straight channel. Four channel bends with differing geometries were tested; three radii of curvature – 0.4, 0.55 and 0.7 m (for a bend angle of  $40^\circ$ ) and one radius of curvature of 0.7 m for a  $20^\circ$  bend angle. For all runs the grain-size of the debris flow mixture consisted of a poorly sorted gravel/sand/clay mix (bulk density  $1880 \text{ kg m}^{-3}$ , water content 17%). A combination of direct and video-based observations were used to record debris flow behaviour including variation in superelevation and the average and local velocity of the flow.

Channel gradient is shown to be an important factor in controlling debris flow velocity. The straight channel results demonstrate a strong linear relationship between debris flow velocity and channel gradient. Modelling debris flow hydraulics reveals a power-law relationship, suggesting Newtonian turbulent flow conditions. The magnitude of superelevation was strongly linked to debris flow velocity, radius of curvature and bend angle. Superelevation was shown to increase in a power law relationship with debris flow velocity, which was greatest for tighter bend geometries. A decrease in radius of curvature resulted in a non-linear increase in superelevation, while decreasing the bend angle promoted a decrease in superelevation. When compared to observed superelevation, predicted values from the superelevation equation can substantially overestimate by up to 210% in some circumstances, suggesting that predicted values and back-calculated velocity estimates should be regarded as maxima. Furthermore, calculation of ' $k$ ' from experimental data suggests that ' $k$ ' was not constant (varying by two-fold) and has a value less than '1', contrary to the proposed theory.

This novel investigation has studied the influence of debris flow velocity, radius of curvature and bend angle upon superelevation, broadening the very limited knowledge base surrounding debris flow superelevation and its controls. For future studies it is recommended to: increase the number of experimental runs for each channel configuration; use a wider range of radii of curvature and bend angles; and improve the accuracy of the superelevation equation by introducing a parameter to account for bend angle, and to better define the significance and value of ' $k$ '.

## Acknowledgements

There are many people to whom I owe a debt of gratitude for their help in this project.

I would like to express my thanks to my supervisors Jeff Warburton and Bob Hilton who have guided me through this research. This project would not have been possible without Jeff's guidance, while his infectious optimism and ability to solve practical issues have proven invaluable time and again. Additionally, my thanks extend to Tim Davies who stepped into the breach and set aside large chunks of his time to improve my substandard knowledge of mathematical issues and fluid mechanics, without whom this project would be significantly weaker. It was a privilege working with you all.

Second, the department's technical staff were all incredibly helpful and without the support they provided it would not have been possible to undertake this project. In particular, I would like to single out Mervyn Brown for his endless assistance with the flume, his entertaining chat and for being an all-round star!

I am incredibly grateful to my fellow postgraduate students in the cave, the lack of daylight tried to defeat us but has provided us with a strong camaraderie and I would not have been able to get through this year without you all, and I hope vice versa! To those who assisted me with my numerous days of practical work in one way or another; Simon, Lizzie, Dickie, Ben (x2), Alex and Sam, thank you. Additionally, I am super-duper thankful to Mr. Edwin Baynes who has contributed in many ways to this investigation while simultaneously completing his own project. The days he dedicated to helping me with my practical work are uncountable, while his advice and level-headedness have been a valuable asset; Edwin, thanks mate!

Last but not least, thanks to Mum and Dad for their continued patience and financial support.

# Contents

<b>Declaration and Statement of Copyright .....</b>	<b>i</b>
<b>Abstract.....</b>	<b>ii</b>
<b>Acknowledgements.....</b>	<b>iii</b>
<b>Contents .....</b>	<b>iv</b>
<b>Figures.....</b>	<b>vii</b>
<b>Tables .....</b>	<b>xi</b>
<b>Equations .....</b>	<b>xii</b>
<b>Chapter 1: Introduction .....</b>	<b>1</b>
1.1. Debris flow definition and characteristics .....	1
1.2. Debris flow hazard.....	4
1.3. Research aim and objectives.....	7
1.4. Background and rationale: debris flow dynamics in channels .....	7
1.5. Effect of channel form on debris flow dynamics.....	9
1.6. Thesis structure .....	10
<b>Chapter 2: Theoretical and Experimental Background.....</b>	<b>11</b>
2.1. Derivation of the superelevation equation .....	11
2.2. Derivation of $k$ .....	12
2.2.1. Superelevation equation review.....	16
2.3. Material properties.....	18
2.3.1. Grain size analysis .....	18
2.3.1.1. Clay .....	19
2.3.1.2. Sand.....	19
2.3.1.3. Gravel .....	20
2.3.2. Experimental mixture composition and bulk density .....	21

2.4. Influence of temperature.....	21
2.5. Rheology and rheological models.....	22
<b>Chapter 3: Research Methods.....</b>	<b>24</b>
3.1. Flume facility.....	24
3.1.1. Bend construction.....	28
3.2. Determining sediment mix properties.....	33
3.2.1. Grain size analysis.....	33
3.2.1.1. Clay sized fraction.....	33
3.2.1.2. Sand sized fraction.....	36
3.2.1.3. Gravel sized fraction.....	38
3.2.2. Experimental mixture composition and bulk density.....	40
3.3. Experimental configuration.....	41
3.3.1. Release of sediment mixture.....	42
3.3.2. Image analysis.....	42
3.4. Experimental precision and statistical analysis.....	44
3.5. Summary.....	45
<b>Chapter 4: Results.....</b>	<b>46</b>
4.1. Straight channel results.....	47
4.2. Channel gradient versus velocity.....	50
4.3. Curved channel results.....	51
4.3.1. Superelevation versus velocity.....	51
4.3.1.1. Bend geometry: $R_c = 0.7$ m, $\theta = 20^\circ$ .....	51
4.3.1.2. Bend geometry: $R_c = 0.7$ m, $\theta = 40^\circ$ .....	53
4.3.1.3. Bend geometry: $R_c = 0.55$ m, $\theta = 40^\circ$ .....	55
4.3.1.4. Bend geometry: $R_c = 0.4$ m, $\theta = 40^\circ$ .....	57

4.3.2.	Spatial pattern of superelevation around bends .....	59
4.3.3.	Superelevation versus radius of curvature .....	62
4.3.4.	Superelevation versus bend angle .....	64
4.4.	Summary of results .....	65
<b>Chapter 5: Discussion .....</b>		<b>66</b>
5.1.	Effect of channel gradient upon debris flow velocity .....	66
5.1.1.	Velocity results .....	66
5.1.2.	Comparison with previous investigations and theory .....	68
5.2.	Curved channel experiments.....	70
5.2.1.	Velocity and superelevation.....	70
5.2.2.	Role of radius of curvature .....	71
5.2.3.	Role of bend angle .....	72
5.3.	Testing the superelevation equation .....	73
5.3.1.	Observed vs. predicted superelevation .....	73
5.3.2.	Comparison with previous studies of superelevation .....	76
5.3.3.	Variability and impact of 'k' factor .....	77
5.4.	Future investigations.....	79
<b>Chapter 6: Conclusions.....</b>		<b>83</b>
6.1.	Summary.....	83
6.2.	Primary conclusions.....	84
6.3.	Suggestions for further research .....	84
<b>References .....</b>		<b>86</b>

## Figures

<b>1.1</b>	Stress-Strain rate curves for four kinds of fluids	2
<b>1.2</b>	A cross-section of a superelevated bend (source: Prochashka <i>et al.</i> , 2008a)	5
<b>2.1</b>	Velocity profile in: <b>A.</b> laminar flow, <b>B.</b> turbulent flow	13
<b>2.2</b>	Values assigned to $k$ in the literature	15
<b>2.3</b>	Sensitivity analysis for $k$ , ranging from 0.1-10	15
<b>2.4</b>	Predicted superelevation curve	17
<b>3.1</b>	Visualisation of the experimental flume set-up, with the overhead camera frame	25
<b>3.2</b>	Headgate configuration, showing the alignment of the walls with the gate and the lever-arm release mechanism	26
<b>3.3</b>	A cross-section of the channel, demonstrating the parabolic shape	26
<b>3.4</b>	Visualisation of the artificial flume mounted on the stilts	27
<b>3.5</b>	A schematic representation of the experimental set-up, including the variation in channel gradient and the headgate configuration	27
<b>3.6</b>	An illustration of radius of curvature ( $R_c$ ) and bend angle ( $\theta$ ) in the bend complex	28
<b>3.7</b>	Manufacturing a channel bend	30
<b>3.8</b>	Channel arrangement for the moulding process	31
<b>3.9</b>	A completed bend having been reinforced, painted and a sand coating applied. Bend is $R_c = 0.55$ m, $\theta = 40^\circ$	32
<b>3.10</b>	Channel bend inserted into the flume structure. The geometry of the channel bend is $R_c = 0.7$ m, $\theta = 40^\circ$	32

<b>3.11</b>	Particle size distribution of clay samples tested using the Beckman Coulter LS230	35
<b>3.12</b>	Mean particle size distribution of the clay samples (n = 30) using the Beckman Coulter LS230	35
<b>3.13</b>	Average particle size analysis of kiln dried sand samples	37
<b>3.14</b>	Grain size distribution of sharp sand	37
<b>3.15</b>	Grain size profile of 10 mm and 20 mm gravels	39
<b>3.16</b>	Grain size distribution of the mixed aggregate	39
<b>3.17</b>	Graph to compare grain size distribution from the previous (Mixture 1) (Fairfield, 2011) and current (Mixture 2) composition	41
<b>3.18</b>	Demonstration of the recording of superelevation at the inside and outside walls of the channel	44
<b>4.1</b>	Average velocity profile for straight channel experiments at: <b>A.</b> 15, <b>B.</b> 17°, <b>C.</b> 23° and <b>D.</b> 25°	49
<b>4.2</b>	Average terminal velocity (ATV) and average velocity (AV) at each channel gradient	50
<b>4.3</b>	Average superelevation at each channel gradient for $R_c = 0.7$ m, $\theta = 20^\circ$	52
<b>4.4</b>	BEV of each debris flow with the respective maximum superelevation for $R_c = 0.7$ m, $\theta = 20^\circ$	52
<b>4.5</b>	Average debris flow BEV for each channel gradient and the respective average maximum recorded superelevation for $R_c = 0.7$ m, $\theta = 20^\circ$	52
<b>4.6</b>	Average superelevation at each channel gradient for $R_c = 0.7$ m, $\theta = 40^\circ$	54
<b>4.7</b>	BEV of each debris flow with the respective maximum superelevation for $R_c = 0.7$ m, $\theta = 40^\circ$	54

<b>4.8</b>	Average debris flow BEV for each channel gradient and the respective average maximum recorded superelevation for $R_c = 0.7 \text{ m}$ , $\theta = 40^\circ$	54
<b>4.9</b>	Average superelevation at each channel gradient for $R_c = 0.55 \text{ m}$ , $\theta = 40^\circ$	56
<b>4.10</b>	BEV of each debris flow with the respective maximum superelevation for $R_c = 0.55 \text{ m}$ , $\theta = 40^\circ$	56
<b>4.11</b>	Average debris flow BEV for each channel gradient and the respective average maximum recorded superelevation for $R_c = 0.55 \text{ m}$ , $\theta = 40^\circ$	56
<b>4.12</b>	Average superelevation at each channel gradient for $R_c = 0.4 \text{ m}$ , $\theta = 40^\circ$	58
<b>4.13</b>	BEV of each debris flow with the respective maximum superelevation for $R_c = 0.4 \text{ m}$ , $\theta = 40^\circ$	58
<b>4.14</b>	Average debris flow BEV for each channel gradient and the respective average maximum recorded superelevation for $R_c = 0.4 \text{ m}$ , $\theta = 40^\circ$	58
<b>4.15</b>	A schematic representation demonstrating varying location in the bend complex where maximum superelevation was observed. <b>A.</b> $R_c = 0.7 \text{ m}$ , $\theta = 20^\circ$ , <b>B.</b> $R_c = 0.7 \text{ m}$ , $\theta = 40^\circ$ , <b>C.</b> $R_c = 0.55 \text{ m}$ , $\theta = 40^\circ$ , <b>D.</b> $R_c = 0.4 \text{ m}$ , $\theta = 40^\circ$	31
<b>4.16</b>	Location of maximum superelevation in curves: <b>A.</b> where $\theta = 40^\circ$ , and <b>B.</b> where $\theta = 20^\circ$	62
<b>4.17</b>	Superelevation across varying radii of curvature with differing BEVs ( $n = 36$ )	63
<b>4.18</b>	Average superelevation at each radius of curvature across 3 complete BEV bands	63
<b>4.19</b>	Superelevation at differing BEVs for $\theta = 20^\circ$ and $\theta = 40^\circ$ at $R_c = 0.7 \text{ m}$	64

<b>5.1</b>	Demonstration of debris flow front position in video analysis	67
<b>5.2</b>	Demonstration of debris flow hydraulics using experimental and literature-based data	69
<b>5.3</b>	Predicted superelevation using power law trendline gradients for a constant BEV of $3 \text{ m s}^{-1}$ . Shaded area represents the range in predicted superelevation for a range of $k$ values	71
<b>5.4</b>	Discrepancy between predicted and observed superelevation values, with varying $k$ . Dashed line indicates 1:1 relationship	74
<b>5.5</b>	Box and whisker plot summarising $k$ values for each bend geometry	78
<b>5.6</b>	Demonstrating how the variability of $k$ can influence predicted superelevation curves	79

## Tables

<b>3.1</b>	Experimental configuration combinations	42
<b>4.1</b>	Summary of terminology, measurements and experimental error associated with each component	46
<b>4.2</b>	Summary of straight channel results at each channel gradient.	48
<b>4.3</b>	Summary of statistical results for $R_c = 0.7$ m, $\theta = 20^\circ$	53
<b>4.4</b>	Summary of statistical results for $R_c = 0.7$ m, $\theta = 20^\circ$	53
<b>4.5</b>	Summary of statistical results for $R_c = 0.7$ m, $\theta = 40^\circ$	55
<b>4.6</b>	Summary of statistical results for $R_c = 0.7$ m, $\theta = 40^\circ$	55
<b>4.7</b>	Summary of statistical results for $R_c = 0.55$ m, $\theta = 40^\circ$	57
<b>4.8</b>	Summary of statistical results for $R_c = 0.55$ m, $\theta = 40^\circ$	57
<b>4.9</b>	Summary of statistical results for $R_c = 0.4$ m, $\theta = 40^\circ$	59
<b>4.10</b>	Summary of statistical results for $R_c = 0.4$ m, $\theta = 40^\circ$	59
<b>5.1</b>	Summary of $k$ values for each bend geometry.	75
<b>5.2</b>	Summary of predicted and average observed superelevation from experiments where $\theta = 20^\circ$ , with overestimation included.	76
<b>5.3</b>	Summary of predicted and average observed superelevation from experiments where $\theta = 40^\circ$ , with overestimation included.	78

## Equations

1	Superelevation equation. Subject - $v$	10 & 66
2	Newton's second law of motion in a curve	11
3	Forced vortex equation	12
4	Reynold's equation	12
5	Momentum correction coefficient	14
6	Superelevation equation. Subject - $\Delta h$	16
7	Mean velocity of debris flow surges	68
8	Superelevation equation. Subject - $k$	77

## Chapter 1: Introduction

Debris flows are dynamic geophysical processes within mountain landscapes with immense, destructive power owing to their high energy and unpredictable nature (Berti *et al.*, 1999; Costa, 1984; Coussot and Meunier, 1996; Deangeli, 2008; Innes, 1983; Lorenzini and Mazza, 2004; Takahashi, 2000). Due to the very short timescales over which they can form and then terminate, monitoring their flow characteristics, erosion patterns and flow over complex terrain can be very difficult (Denlinger and Iverson, 2001; Denlinger and Iverson, 2004; Iverson and Denlinger, 2001; Prochaska *et al.*, 2008b). In particular, the velocity and rheology of a flow, the interaction of a flow with local channel topography (channel bends) and channel bed erodibility, are poorly known and understood. Further, the capability of a debris flow to escape the confines of a channel, particularly at bends, is a serious threat that has been little explored. As a flow moves through a bend, it banks around the corner and may overtop the channel walls, proceeding to flow in an unconfined manner across a debris fan and increasing the threat to infrastructure in the vicinity (USGS, 2001; Wieczorek *et al.*, 2001). These characteristics are crucial to understanding debris flow dynamics within channels for the prediction of run out areas, improved modelling developments and knowledge of the hazard posed (Berzi and Jenkins, 2009; D'Agostino *et al.*, 2010; Hungr, 1995; Mangeney *et al.*, 2010; Prochaska *et al.*, 2008b). A greater recognition of debris flow dynamics, particularly the behaviour of a flow in curved channels and the potential for channel breakout, would enable improved hazard management techniques to be developed to help mitigate the threat posed by such events (D'Agostino *et al.*, 2010; Guadagno *et al.*, 2005; Innes, 1983; Prochaska *et al.*, 2008b).

### 1.1. Debris flow definition and characteristics

Debris flows are widespread phenomena and occur in many mountain environments around the world (Bulmer *et al.*, 2002; Mangeney *et al.*, 2010). They are a key erosion and sediment transport mechanism and pose a significant environmental hazard (Berger *et al.*, 2011b; Davies, 1990; Iverson and Denlinger, 2001; Lorente *et al.*, 2003; Stock and Dietrich, 2006). Several definitions of debris flows exist within literature. However, the general consensus defines these phenomena as a form of mass movement whereby a non-uniformly saturated mass of water, and sediment of mixed grain size flows downslope under the influence of gravity, exhibiting fluid-like macroscopic behaviour

(Berti *et al.*, 1999; Costa, 1984; Davies, 1986; Hungr, 1984; Iverson *et al.*, 1997; Lorenzini and Mazza, 2004; Pouliquen and Vallance, 1999; Rickenmann and Zimmermann, 1993; Takahashi, 1981). It is the interaction of solid and fluid forces which differentiate these flows from other related phenomena such as fluvial flooding and rock avalanches (Berti *et al.*, 1999; Iverson *et al.*, 1997).

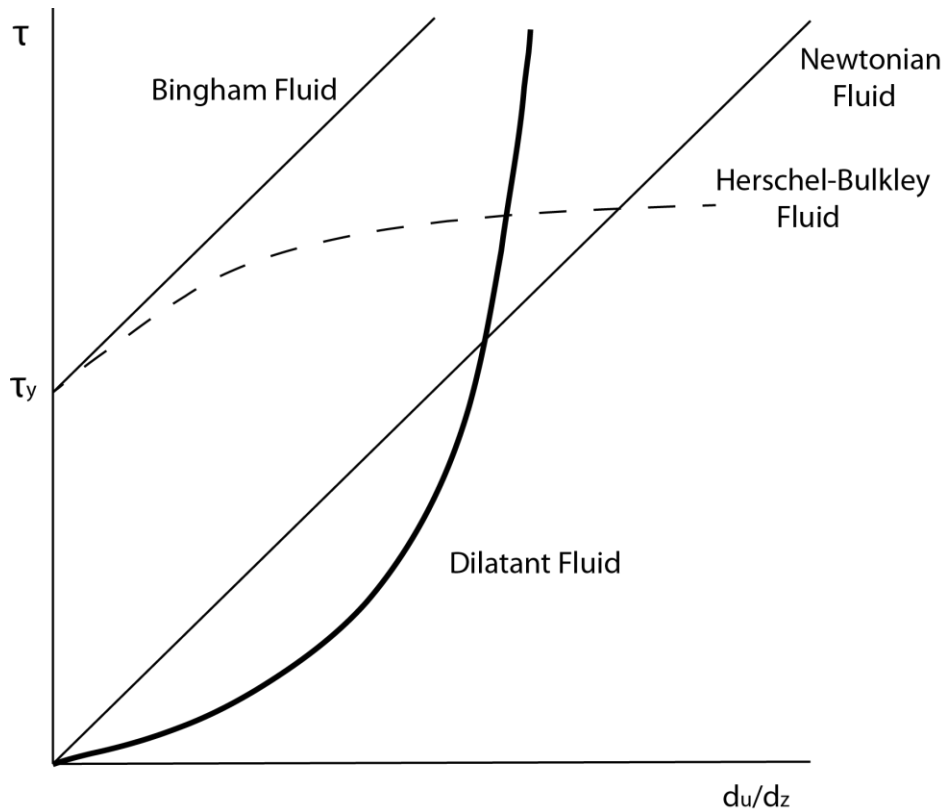


**Figure 1.1:** Stress-Strain rate curves for four kinds of fluids, where:

$\tau$  = stress,  $\tau_y$  = yield stress,  $du/dz$  = rate of strain. Bingham (cohesive), Herschel-Bulkley and Dilatant (non-cohesive) models have all been used to describe debris flow behaviour under non-Newtonian flow conditions.

*From Takahashi (2007) p. 39*

Debris flow motion is broadly classified as unsteady and non-uniform, typically exhibiting non-Newtonian laminar flow conditions (Figure 1.1) (Berzi and Jenkins, 2009; Davies, 1988; Davies, 1990; Iverson, 2003; Lorenzini and Mazza, 2004; Takahashi, 1981). Although debris flows consist of both solid and fluid fractions, it can initially be considered a one-phase flow due to the small difference in relative velocities of the two constituents (Coussot and Piau, 1994; Coussot and Meunier, 1996; Davies, 1990; Takahashi, 2000). The initiation of a debris flow is characterised by the

transformation of a granular mass to a flowing mixture of poorly sorted, cohesionless sediment with a relatively small water content; yet this water component is highly significant for mobilisation of a sediment mass (Berti *et al.*, 1999; Hampton, 1975; Innes, 1983; Iverson *et al.*, 1997; Iverson and Vallance, 2001). Grain size segregation is a characteristic of debris flows, where the head of the flow has a very high concentration of coarse granular material and is relatively dry, while the tail has a high proportion of fine sediment and is more fluid (Davies, 1988; Iverson, 1997; Iverson and Vallance, 2001; Lorenzini and Mazza, 2004). As an event proceeds, debris flow characteristics can evolve as material eroded from the river channel, predominantly via vertical rather than lateral scour, becomes entrained and transported, significantly enhancing an event's volume, runout distance and further erodibility (Berti *et al.*, 1999; Berger *et al.*, 2011a; Coussot and Meunier, 1996; Davies *et al.*, 1992; Evans *et al.*, 2001; Iverson, 2003; Mangeney *et al.*, 2010).

The sediment composition of debris flows can vary greatly between events, from very granular in nature, to those which are more fluid. The concentration of sediment in a debris flow is wide-ranging, from 25% by volume to 80-90% (Costa, 1984; Coussot and Meunier, 1996; Davies *et al.*, 1992; Takahashi, 1981). The water content of a typical event is relatively small, with reports ranging from 10-30% (Costa, 1984), although flow mobility is highly sensitive to and dependent upon this quantity (Van Steijn, 1989). For example, it has been stated that a change of 1% or 2% water by mass can alter the apparent viscosity of a slurry by a factor of two (Phillips and Davies, 1991). These fluid-solid mixtures are very dense, with recorded densities ranging from 1800-2500 kg m<sup>-3</sup> (Coussot and Meunier, 1996; Davies *et al.*, 1992; Innes, 1983; Iverson, 1997), and are capable of flowing at velocities of up to 20 m s<sup>-1</sup> (Davies, 1988; Deangeli, 2008; Evans *et al.*, 2001; Lorenzini and Mazza, 2004; Muñoz-Salinas *et al.*, 2007; Takahashi, 1981).

The hazard posed by debris flow events is heightened by their unpredictability, their transient nature and the large volumes of sediment that they are capable of transporting. Although typically debris flows are triggered by intense rainfall (Berti *et al.*, 1999; Davies, 1988; Rickenmann, 1999; Rickenmann and Zimmermann, 1993), it has been noted that they can also be initiated as a consequence of landsliding, the failing of temporary dams blocking river channels, snowmelt and high antecedent moisture conditions (Evans *et al.*, 2001; Lorenzini and Mazza, 2004; Pierson, 1985; Takahashi, 2000). In all cases, debris flow mobilisation is associated with the simultaneous and

synergistic presence of sediment, saturated with water and a sufficient slope gradient to initiate failure of the material (Davies, 1986; Innes, 1983; Iverson *et al.*, 1997; Iverson and Denlinger, 2001; Lorente *et al.*, 2003; Lorenzini and Mazza, 2004). Owing to the large range of potential initiation processes, predicting the onset of a debris flow is difficult. The unsteady, surge-like behaviour of a debris flow adds to the potential hazard (Takahashi, 2007). For example, Evans *et al.* (2001) reported 126 surges over a five hour period for a debris flow event in Jiangjia Ravine, China. Furthermore, the scale of such events can vary dramatically, from small-scale flows in temperate environments like Scotland where deposits rarely exceed 500 m<sup>3</sup> (Innes, 1983), to locations in China, most notably Jiangjia, where transported sediment volumes can regularly reach 5 x 10<sup>6</sup> m<sup>3</sup> (Coussot and Meunier, 1996), a range of over four orders of magnitude. The erosivity of debris flows and their ability to transport huge volumes of sediment is what makes them such an important geomorphic agent (Iverson, 1997; Lorente *et al.*, 2003; Wohl and Pearthree, 1991).

## 1.2. Debris flow hazard

The characteristics of debris flows make them a potentially powerful and destructive geophysical agent, with the ability to move large volumes of debris and destroy infrastructure (Lorente *et al.*, 2003; Iverson and Denlinger, 2001). The dangers of debris flows are at their greatest on alluvial fans, as this is where inhabited zones commonly occur in mountain landscapes (Berti *et al.*, 1999; Julien and Paris, 2010; Whipple, 1997; Wohl and Pearthree, 1991). For example, in Japan, debris flow events cause approximately 90 deaths every year (Takahashi, 1981), and many of these fatalities are associated with a lack of knowledge amongst the laypersons regarding the rapid onset and dangers posed by these events (Bowman and Davies, 2008; Coussot and Meunier, 1996). The United States Geological Survey (USGS) has categorised debris flows as amongst “the most serious landslide type hazards to human safety” (Innes, 1983; pg. 469). For these reasons, the development of appropriate hazard management strategies to counter the threat of debris flows is of paramount importance (Bowman and Davies, 2008; Innes, 1983; Guadagno *et al.*, 2005; Julien and Paris, 2010).

The risk posed by a debris flow increases considerably if an event manages to escape the confines of a channel on a fan and become unrestricted, which significantly increases the likelihood of damage to infrastructure, housing or fatalities. The breakout or avulsion of a flow event most commonly occurs at a channel bend, where a process

called ‘superelevation’ arises as a consequence of the centrifugal force experienced in the bend (Apmann, 1973; Muñoz-Salinas *et al.*, 2007). Superelevation is the inclination of the flow surface as a debris flow proceeds around a curve, causing a difference in elevation of the flow surface between the inside and outside walls of the bend at the same section (Figure 1.2) (Apmann, 1973). The magnitude of superelevation is related to the velocity of the flow (Apmann, 1973; Muñoz-Salinas *et al.*, 2007; Prochaska *et al.*, 2008a). This has been used to enable velocity to be back-calculated using the ‘superelevation equation’ (introduced in Section 1.5). If the magnitude of superelevation is greater than the height of the channel banks, debris flow breakout can occur, resulting in unrestricted flow and the potential for great damage.

The dangers posed by channel breakout were demonstrated in December 1999, when a sustained period of torrential rain caused landslides and debris flows in Venezuela (Sciblogs, 2010). In Caraballeda, northern Venezuela, a debris flow overwhelmed an engineered channel which was designed to contain debris flows through the city. At several locations, all associated with bends in the channel, the flowing debris escaped the channel (USGS, 2001; Wieczorek *et al.*, 2001). As a result of the bank overtopping, the debris flow inundated approximately one third of the city, destroying roads, demolishing many buildings and causing fatalities (USGS, 2001; Wieczorek *et al.*, 2001).

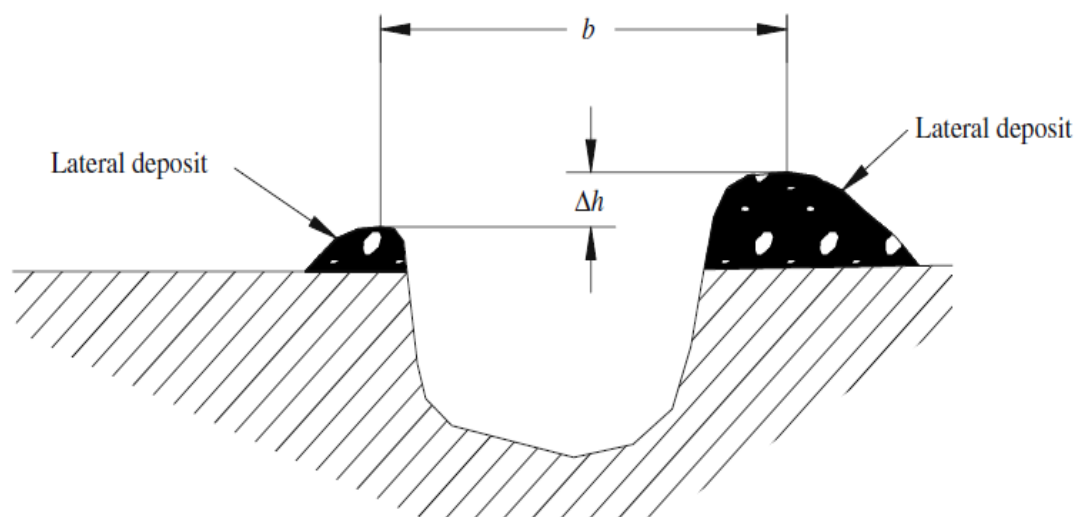


**Figure 1.2:** A cross section of a superelevated bend, demonstrating flow width ( $b$ ) and superelevation height ( $\Delta h$ ). From Prochaska *et al.*, (2008a), p. 2.

These observations demonstrate the urgent requirement for further research into the dynamics of confined, channelised debris flows in curved channels, and the factors governing channel breakout, which are very important elements for the creation of an effective hazard management framework. Owing to the unpredictability of naturally occurring debris flows, it is difficult to study these events in detail in the field (Davies, 1988; Davies, 1990).

In contrast, considerable progress has been made in understanding debris flow dynamics by replicating flow conditions in artificial flume facilities (Davies, 1988; Davies, 1990; Deangeli, 2008). Prior studies using an artificial flume facility have concentrated on studying debris flow dynamics in a straight channel, including observations of flow thickness, pore fluid pressure and basal normal stresses. Several experimental investigations have been performed using similar flume facilities, studying flow processes at a small scale in laboratory conditions (D'Agostino *et al.*, 2010; Davies, 1988; Deangeli, 2008; Mangeney *et al.*, 2010; Rickenmann *et al.*, 2003; Takahashi, 2007; Van Stieijn and Coutard, 1989). However, the construction of a 95 m, 31° rectangular, concrete flume in 1994 by the USGS has seen the greatest advances in the understanding of flow dynamics (Iverson, 1997; Iverson, 2003; Iverson *et al.*, 2010). This facility is capable of producing debris flows with a volume of approximately 10 m<sup>3</sup>, providing intermediate conditions between traditional, reduced-scale laboratory flumes and naturally occurring events, which may be much larger. Thus, the debris flows produced in the USGS flume can accurately mimic those under naturally occurring flow conditions (Iverson *et al.*, 2010).

As demonstrated above, experimental flume facilities provide an established and useful technique for studying debris flows, and therefore shall also be employed in this research. However, this approach has not been fully utilised for understanding flow in curved channels (Davies, 1990; Iverson, 1997; Iverson *et al.*, 2010). For example, only a couple of investigations have been performed which directly study debris flow behaviour in channel bends (Ashida *et al.*, 1981; Ikeya and Uehara, 1982).

Using a reduced-scale flume facility, the behaviour of debris flows can be readily studied in an accessible environment, where multiple combinations of flow event conditions can be replicated, permitting acquisition of well constrained results. Moreover, owing to the adaptable setup of the experimental flume used in this study, the channel can be configured in several ways, providing a wide range of boundary conditions that may be used to investigate such effects as the influence of gradient upon

an event and to study how a debris flow negotiates a bend in a channel. By maintaining a consistent grain size distribution and moisture content of the experimental mixture throughout this research, it is possible to isolate these influences upon flow dynamics.

### **1.3. Research aim and objectives**

The literature on debris flow dynamics is considerable, but there is much less information investigating the dynamics of channelised debris flows, and in particular how debris flows evolve whilst travelling around bends and through curved channels. The general goal of this research is to increase understanding of this topic, which has the potential for application in more effective hazard mitigation studies.

The aim of this research is:

- To explore debris flow dynamics in curved channels and assess the importance of controlling factors on debris flow superelevation.

Objectives:

- To determine the effect of channel gradient upon debris flow velocity.
- To explore the relationship between velocity and superelevation in curved channels
- To investigate how variations in radius of curvature can influence debris flow superelevation.
- To test the applicability of the ‘superelevation equation’ for estimating debris flow velocity in curved channels.

### **1.4. Background and rationale: debris flow dynamics in channels**

Channel gradient is an important controlling factor in debris flow propagation, influencing initiation, velocity, flow characteristics and deposition of an event. Coussot and Meunier (1996) discussed debris flow initiation, which typically occurs on steep slopes of  $\sim 30^\circ$  at the source area. However, this angle can often be much lower, in the region of  $\sim 18\text{-}20^\circ$  at approximately half the angle of repose (Berti *et al.*, 1999). This is because the sediment in the zone of failure is cohesionless and close to saturation, thus facilitating mobilisation. Mangeney *et al.* (2010) briefly studied the relationship between channel gradient and the velocity of an experimental debris flow in an artificial flume (not dissimilar from that to be used in the present research) and found an increase in velocity with steepening gradient. However, no quantitative relationship was given.

This is possibly because this was not the main aim of the investigation; rather, it was a requirement in order to study how the mixing of sediment in a flow was influenced by velocity. Somewhat surprisingly, Muñoz-Salinas *et al.* (2007) found no clear correlation between velocity and slope angle when using deposits from volcanic lahars to back-calculate velocity estimates.

Further literature exploring the link between channel gradient and debris flow velocity at the early and middle stages of a flow event is scarce, but there is more information which discusses the converse of this, notably the role of channel gradient upon deposition, which can be used as a proxy for velocity.

Debris flows deposit material in the form of either levees or lobes (Innes, 1983). Levees are formed when material at the head of the flow is pushed to the margins and deposited, whilst lobes are formed by the termination of flow as a whole (Costa, 1984; Coussot and Meunier, 1996; Davies, 1990; Innes, 1983; Takahashi, 1981). The primary zone of deposition for debris flows is on alluvial fans, where deposition arises because the gradient of the channel is no longer greater than the critical slope angle for flow, therefore terminating flow movement (Costa, 1984; Hampton, 1975; Innes, 1983). Davies (1990) explained that debris flow character evolves from an erosional to a depositional state where channel gradient is in the proximity of  $7^\circ$ . D'Agostino *et al.* (2010) noted that alluvial fans typically have a gradient between  $4-8^\circ$ , which is often approximately the mean gradient of the river channel upstream from the apex of the fan, and the channel downstream from the toe of the fan. These findings are broadly agreed within the literature and can be demonstrated in natural debris fans (Berti *et al.*, 1999; Bowman and Davies, 2008; Takahashi, 1981). This suggests that the relatively shallow gradients of alluvial fans are generally less than the critical slope angle for flow, and are therefore insufficient to dominate over the internal friction and shear strength of the flow, inducing a rapid decrease in flow velocity and subsequent deposition of sediment (Costa, 1984). However, the range over which alluvial fan gradients have been observed implies that variation in debris flow composition, which is typically controlled by the underlying lithology and regolith in a catchment, may be a controlling factor upon fan gradient by influencing flow mobility, and therefore the runout distance of an event (Costa, 1984; Innes, 1983).

Debris flow velocity can have a significant impact upon flow characteristics, most notably flow depth (Chow, 1959). Mangeney *et al.* (2010) and Davies (1990) noted that as flow velocity increases, a decrease in flow depth is observed, a process known as

‘debris flow thinning’. Similarly, Muñoz-Salinas *et al.* (2007) found an inverse correlation between flow depth and velocity with lahars. Stock and Dietrich (2006) comment on a similar relationship, and discussed the possible impact of this upon flow processes and erosion. Significantly, they suggested that the thinning of a flow event may lessen erosion as the reduction of flow depth reduces the shear stress at the bed, in addition to lowering the height at the head of the flow and thus reducing impact forces on the bed. However, flow thinning will impact on the rheology of the mass, thus the reduction in basal shear stress may not be solely attributed to a reduction in flow depth.

### **1.5. Effect of channel geometry on debris flow dynamics**

Debris flow velocity is controlled primarily by two factors: channel gradient and the viscosity of the debris flow mixture itself. However, secondary factors, such as channel geometry, have not yet been investigated in great detail (Davies, 1990; Iverson, 1997; Iverson *et al.*, 2010).

The radius of curvature of a bend is an important component of channel form controlling the magnitude of superelevation that may occur. Superelevation arises due to the flow travelling at a higher velocity at the outside of the bend, than at the inside bank (Chow, 1959; Muñoz-Salinas *et al.*, 2007). Apmann (1973) and Pierson (1985) explained that this characteristic of debris flow motion is due to the deformation of the free surface in a bend as a result of the action of centrifugal force, whilst Muñoz-Salinas *et al.* (2007) further described this relationship with reference to Newton’s second law of motion acting in a curve. Apmann (1973) stated that the magnitude of superelevation varies with angular distance through the bend, related to the acceleration of the fluid at the entrance and exit of the curve and of the variation of curvature through the bend. Consequently, as radius of curvature decreases, i.e. as a bend becomes sharper, the magnitude of superelevation should increase due to a greater centrifugal force. Thus, for the experimental debris flows studied in the present research it is hypothesised that superelevation will increase as the radius of curvature decreases, under conditions of fixed slope, and therefore constant velocity.

The superelevation equation used to back-calculate velocity estimates from debris flow deposits is:

$$v = \left[ \frac{g R_c \Delta h}{k b} \right]^{0.5} \quad \text{Equation 1}$$

where:

- $\Delta h$  = Height of superelevation (m)
- $k$  = Correction factor for viscosity and vertical sorting (dimensionless)  
(discussed in Section 2.2.)
- $b$  = Flow top width (m)
- $v$  = Mean flow velocity ( $\text{m s}^{-1}$ )
- $R_c$  = Centreline radius of curvature (m)
- $g$  = Acceleration due to gravity ( $\text{m s}^{-2}$ )

## 1.6. Thesis structure

This chapter has introduced debris flows as a powerful geomorphic agent in the global landscape, demonstrated the hazard they pose to the environment (a threat that increases significantly with channel breakout) and the lack of current knowledge surrounding debris flow superelevation. This provides the foundation for conducting this research and justified the aims and objectives. In the remainder of this thesis, the theory behind the superelevation equation (Eq. 1) and the importance of particle size distribution in a debris flow will be discussed (Chapter 2), followed by a description of the flume facility and methodologies (Chapter 3). Then the results will be presented (Chapter 4) before their discussion and interpretation (Chapter 5). It will be of particular interest to explore the applicability of the superelevation equation (Eq. 1) when comparing predicted and observed results, which will be of importance for future studies as this is the most commonly used method for back-calculating debris flow velocity estimates.

## Chapter 2: Theoretical and Experimental Background

This brief chapter will discuss the theory behind the superelevation equation and the correction factor  $k$ , as well as providing an overview of the superelevation equation and its potential limitations. Second, the importance of determining sediment properties of the debris flow mix will be discussed. This includes a consideration of the grain size of the sediment, bulk density, influence of temperature upon debris flow mobility and the suitability of rheological models for this research.

### 2.1. Derivation of the superelevation equation

The superelevation equation (Eq. 1) is a fluid pressure equation, derived by applying Newton's second law of motion in a curve (Eq. 2) (Tipler and Mosca, 2004). This assumes that a flow has uniform velocity ( $v$ ) and that centreline radius of curvature ( $R_c$ ) is constant throughout the entire bend (Muñoz-Salinas *et al.*, 2007; Prochaska *et al.*, 2008a; Tipler and Mosca, 2004):

$$a_c = \frac{v^2}{R_c} \quad \text{Equation 2}$$

where:

- $a_c$  = Centrifugal acceleration ( $\text{m s}^{-2}$ )
- $v$  = Velocity ( $\text{m s}^{-1}$ )
- $R_c$  = Radius of curvature (m)

Equation 2 is a development of the forced vortex equation (Eq. 3) (Tipler and Mosca, 2004), which describes the flow of a perfect fluid in a curved channel. However, given the different rheology and viscosity of a debris flow compared to that of water, an additional parameter,  $k$ , is introduced to Equation 1 which compensates for this (Chow, 1959; Prochaska *et al.*, 2008a; Whipple, 1997):

$$v_{\theta} = \omega r \quad \text{Equation 3}$$

where:

- $v_{\theta}$  = Tangential velocity ( $\text{m s}^{-1}$ )  
 $\omega$  = Angular velocity ( $\text{radians s}^{-1}$ )  
 $r$  = Radial distance from the centre of the vortex (m)

## 2.2. Derivation of $k$

The superelevation equation is derived from the forced vortex equation for free flowing Newtonian fluids, and so consequently it contains a crucial parameter,  $k$ . In Equation 1,  $k$  is a dimensionless number that corrects for viscosity and vertical sorting within the flow, and is related to the vertical velocity distribution within the flow and therefore to ‘Reynolds’ number’ and the ‘momentum correction coefficient’. The Reynolds’ number is a non-dimensional parameter and describes the degree of turbulence in the flow (Eq. 4) (Chow, 1959; Davies, 1986; Enos, 1977; Henderson, 1966; Webber, 1965):

$$Re = \frac{\bar{v} d \rho}{\mu} \quad \text{Equation 4}$$

where:

- $Re$  = Reynolds’ number (dimensionless)  
 $\bar{v}$  = Mean velocity ( $\text{m s}^{-1}$ )  
 $d$  = Depth (m)  
 $\rho$  = Density of fluid ( $\text{kg m}^{-3}$ )  
 $\mu$  = Kinematic viscosity of fluid ( $\text{kg m}^2$ )

In this expression, Davies (1986) stated that if  $Re$  is greater than 1500 for open channel flow then flow will be turbulent, whilst Enos (1977) was of the belief that turbulent flow occurred where  $Re$  is greater than 2000. Flow is classified as laminar if

$Re$  is in the region of 500-600 or less, whilst flow between the  $Re$  values for laminar and turbulent flow is identified as transitional (Davies 1987; Enos, 1977).

The velocity distribution within a flow is important because this has a controlling influence upon  $k$ . Laminar flow has a parabolic velocity profile (Figure 2.1A), whilst a steeper profile (often close to a uniform distribution) occurs in turbulent flow (Figure 2.1B). For ease of computation in calculations, the mean flow velocity,  $\bar{v}$ , is typically applied to all real fluids. In a turbulent flow, where velocity profile can be almost uniform, the position of mean flow velocity is only slightly departed from the maximum flow velocity, whereas in laminar flows the mean velocity is somewhat reduced from the maximum flow velocity.

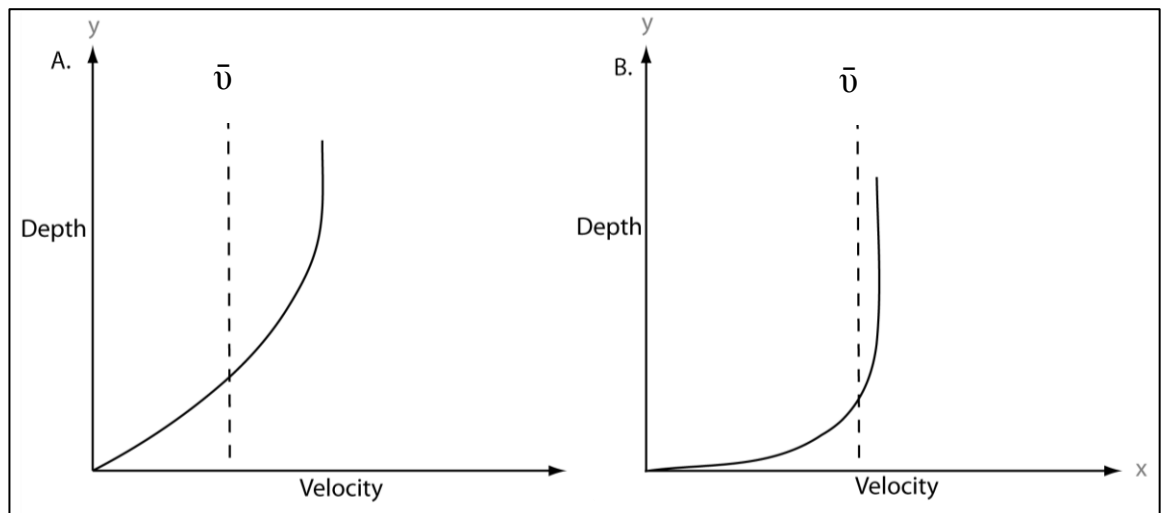


**Figure 2.1:** Example of the velocity profile in **A.** laminar flow, **B.** turbulent flow. The dashed line indicates the position of mean flow velocity,  $\bar{v}$ .

$k$  is not clearly defined by Prochaska *et al.* (2008a), Hungr *et al.* (1984) or Lorenzini and Mazza (2004). Since superelevation is related to the force exerted on the curved channel by the flow, and vice versa,  $k$  is likely to relate closely to the momentum correction coefficient,  $\beta$ , [Force = rate of change of momentum].

The momentum correction coefficient (Eq. 5) is a correction factor applied to the mean velocity of a flow to account for the non-uniform distribution of velocity which occurs (Chow, 1959; Henderson, 1966; Webber, 1965). When the velocity distribution is uniform, the momentum correction coefficient has a value of unity. However, in

reality the mean velocity profile in open channel flow is not uniform. Therefore as the mean velocity profile deviates further from uniformity, the momentum correction coefficient assumes a greater value to account for this deviation, typically slightly greater than 1 (Henderson, 1966).

$$\beta = \frac{1}{\bar{v} Q} \int v d Q = \frac{1}{\bar{v}^2 A} \int v^2 d A \quad \text{Equation 5}$$

where:

- $\beta$  = Momentum coefficient (dimensionless)
- $\bar{v}$  = Mean velocity ( $\text{m s}^{-1}$ )
- $Q$  = Discharge ( $\text{m}^3 \text{s}^{-1}$ )
- $d$  = Flow depth (m)
- $v$  = Filament velocity ( $\text{m s}^{-1}$ )
- $A$  = Cross sectional area of flow ( $\text{m}^2$ )

Therefore, the value for  $k$  in a turbulent flow ought to be 1, reflecting the superelevation equation's (Eq.1) derivation from the forced vortex equation (Eq. 3), whilst theoretically  $k$  for a laminar flow should be greater than 1 owing to the significant deviation of the position of mean flow velocity from the location of maximum flow velocity (Davies, T.R.H., *pers. comms., August 2011*) (Figure 2.1). However, in several sources, there is little consistency for the value of  $k$  with some authors assigning  $k$  a value as low as 0.1 (Bulmer, 2002), whilst others have said that it could be as high as 10 (Chen, 1987), demonstrating a variation by as much as two orders of magnitude (Figure 2.2; Figure 2.3). However,  $\beta$  cannot be less than 1, so  $k$  values of  $< 1$  indicate some additional influence. In the literature,  $k$  has most commonly been assigned a value close to 1, which corresponds to observations from debris flows and deposits suggesting that flow is laminar (Davies, 1986; Enos, 1977). In fact,  $k$  could appear to be adjustable, which may seem logical as debris flow composition can vary from very fluid to granular, and thus the viscosity, vertical sorting and velocity distribution will differ from one event to another. Therefore, in this research  $k$  will be treated as a dependent parameter and compared with previous studies, although more work is required to better assess the factors that influence  $k$ .

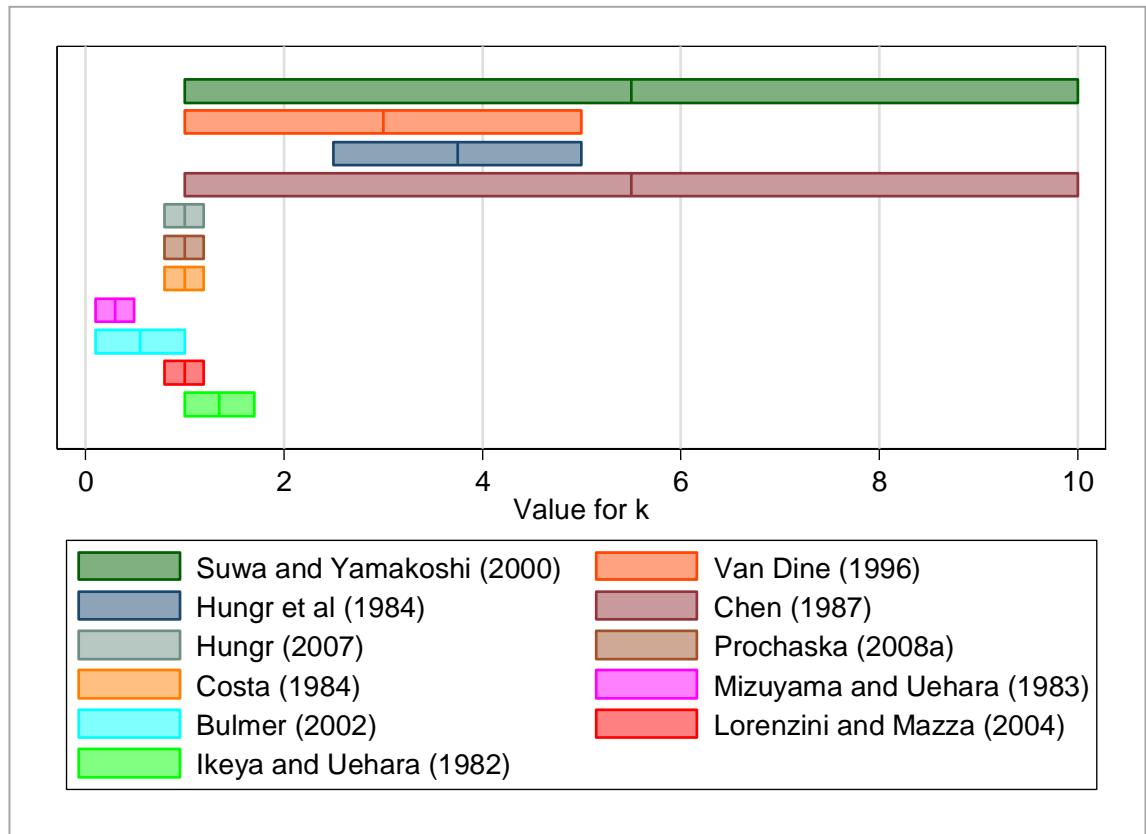


**Figure 2.2:** Variation in values assigned to  $k$  by various authors. Note, that although the values assigned for  $k$  in different studies are wide ranging, there does seem to be a consensus among many authors for a value of  $k = 1$ .

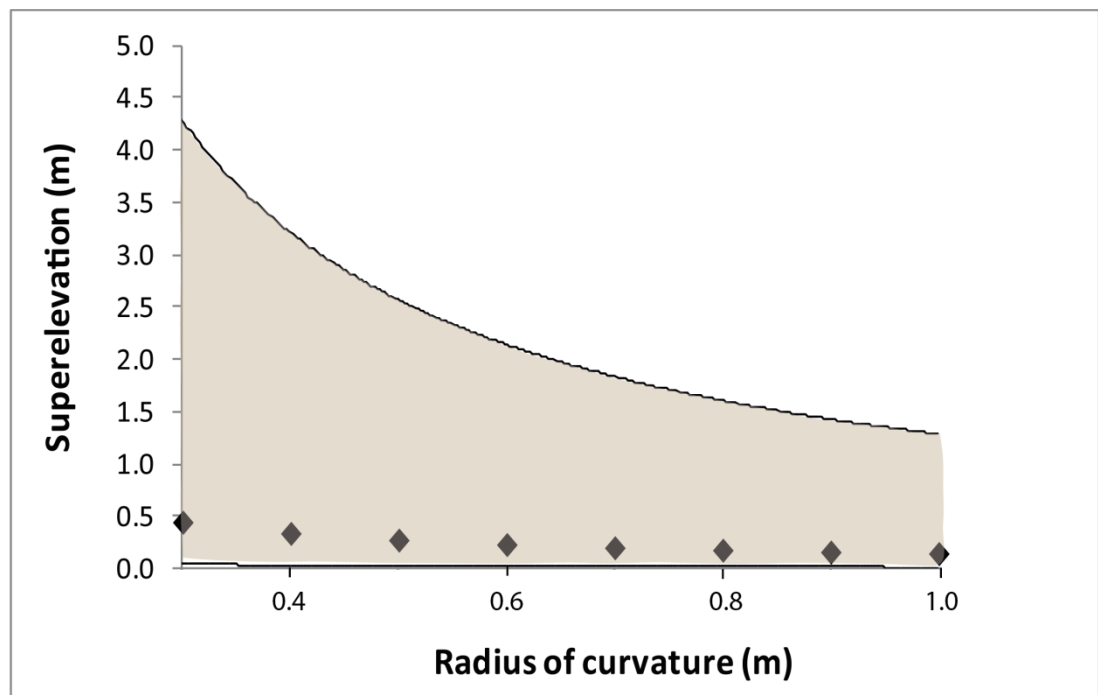


**Figure 2.3:** Sensitivity analysis for  $k$ . Data points represent superelevation for  $k = 1$ , shaded area demonstrates superelevation range for  $k$  values from 0.1-10, where:  $b = 0.14\text{m}$ ,  $v = 3\text{ m s}^{-1}$

However, a single value for  $k$  is perhaps a little misleading because  $k$  will vary in space, time and location within a debris flow. This is expected owing to the morphological and rheological evolution of debris flows (Iverson, 2003) discussed in Section 1.1.

### 2.2.1. Superelevation equation review

Equation 1 utilises lateral deposits around a curve in a channel to estimate the minimum velocity of a flow event at one time in one location. Apmann (1973) and Prochaska *et al.* (2008a) explained that the use of lateral deposits in a bend for back-calculating estimates of velocity is based on the principle that the height of the deposit is related to the velocity of the flow and the geometry of the bend in question. It assumes that, if repeated, the flow would be similar under most conditions to a reasonable accuracy (Apmann, 1973).

As mentioned, Equation 1 is typically used to back-calculate velocity estimates. However, by rearranging Equation 1 and using an estimated velocity value, it is possible to predict the magnitude of superelevation in a bend with a given radius of curvature. This will enable an analysis of the accuracy of the superelevation equation by comparing predicted and observed values against one another, thus investigating the third and fourth objectives: ‘To explore the relationship between velocity and superelevation in curved channels’; and ‘To test the applicability of the ‘superelevation method’ in predicting debris-flow velocity in curved channels’. Therefore, to predict the height of superelevation for this research, Equation 1 is rearranged (Chen, 1987; Hungr *et al.*, 1984; Van Dine, 1996):

$$\Delta h = \frac{k b v^2}{R_c g} \quad \text{Equation 6}$$

Using this expression, the predicted values of superelevation can be assessed for artificial flume experiments with a flow width of 0.2 m (Figure 2.4). When the radius of curvature is halved from 1 m to 0.5 m, the magnitude of superelevation doubles, suggesting an inversely proportional relationship. However, there is a lack of published literature documenting these variations.

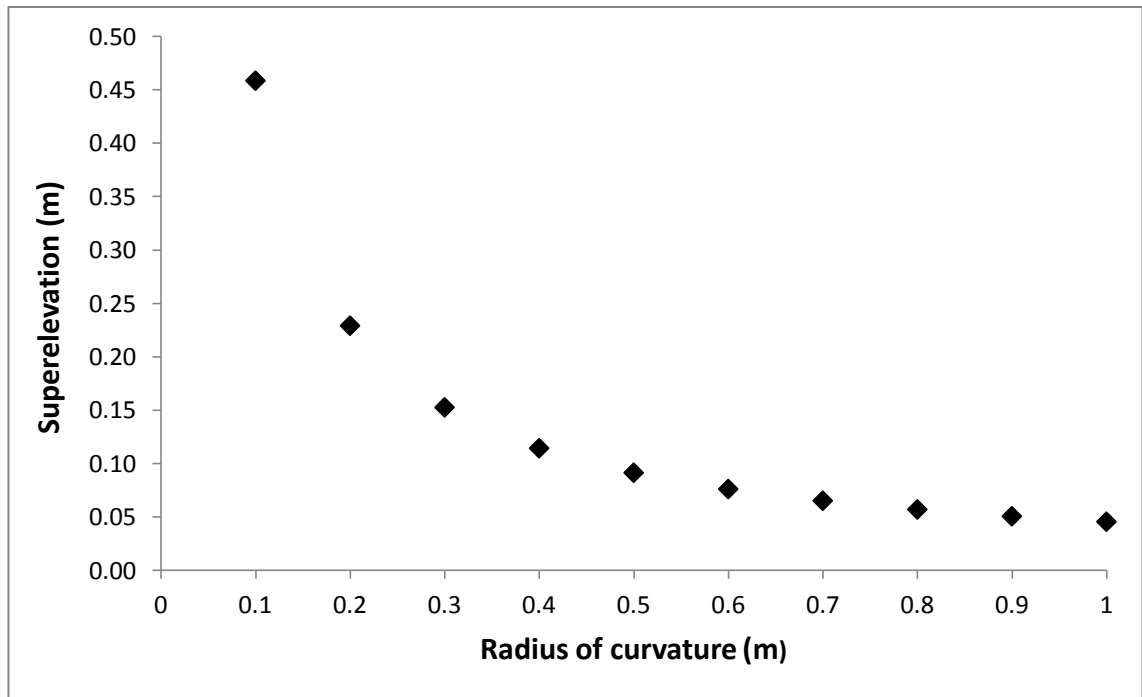


**Figure 2.4:** Predicted magnitudes of superelevation against varying radius of curvature where:  $k = 1$ ,  $b = 0.2 \text{ m}$ ,  $v = 1.5 \text{ m s}^{-1}$ .

The accuracy of the superelevation method for calculating velocity has not been fully evaluated, but discrepancies have been noted ranging from 15-30% between observed and estimated velocities, with the equation often underestimating the true velocity (Evans *et al.*, 2001; Iverson *et al.*, 1994; Muñoz-Salinas *et al.*, 2007; Pierson, 1985). Consequently, Evans *et al.* (2001) amended the radius of curvature parameter slightly, suggesting that rather than using the centreline radius of curvature of the bend itself, the centreline of the flow path through the bend should be measured instead. Unpublished experimental test data has subsequently shown this adoption results in better estimates of velocity and superelevation on observed flows (Evans *et al.*, 2001). However, there are several drawbacks with the use of Equation 1 (Pierson, 1985): (1) it assumes that there are no frictional losses from the channel bed and banks; (2) splash marks above the flow line can exaggerate the apparent superelevation in a bend; (3) errors are also encountered from unsteady flow with the passage of the frontal bore; and (4) flow is assumed to be a perfect fluid which is unsuitable for all known flow types and compositions. In particular, the assumption that there is no loss of energy to

friction from the channel boundary will have significant implications upon calculations. These losses have not been calculated in this investigation. (5) Equation 1 is also known to overestimate superelevation in tight bends; this is because a tight bend acts more as a direct obstacle in the path of a debris flow rather than a curve. Therefore, because the angle of incidence of the debris flow on the channel walls is not taken into account in Equation 1, superelevation is often over-estimated. (6) Furthermore, Prochaska *et al.* (2008a) evaluated the radius of curvature for a number of channel bends using maps, aerial photographs and field observations and found that radius of curvature was very difficult to measure accurately and consistently. Consequently, an inability to accurately judge the radius of curvature of a channel bend could impact significantly on calculations using Equation 1.

Hence, the planned experiments are important because they will be able to assess the accuracy of the superelevation method in a controlled environment.

### **2.3. Material properties**

Prior to experiments in the artificial flume a series of tests were performed to characterise the materials used in the experimental debris flow mix. These included grain size, experimental composition and bulk density analyses.

#### **2.3.1. Grain size analysis**

Debris flows consist of a mass of cohesionless, poorly sorted sediment and water (e.g. Berger *et al.*, 2011; Hampton, 1975; Pierson, 1995; Rickenmann and Zimmermann, 1993). The wide range of grain sizes which exist in a debris flow mass, from clay to boulders, is necessary for debris flow formation. As the various sizes of material are sheared in a moving flow, the larger grains rise to the surface and then migrate towards the flow front where they accumulate, due partly to a process known as ‘kinetic sieving’, producing a distinctive granular front which precedes a more fluid tail (Davies 1990; Iverson, 1997; Iverson and Vallance, 2001; Johnson, 1970). It is this process of grain size segregation, and the ensuing creation of a dense, slow flowing granular front, which leads to the destructive, erosive and powerful nature of debris flows.

Consequently, it is important to understand the grain size distributions of the clay, sand and gravel fractions in order to recognise how this may impact upon the behaviour of the debris flow.

### **2.3.1.1. Clay**

The importance of the fine sediment fraction (less than 62.5  $\mu\text{m}$ ) for debris flow motion has been noted on several occasions (Costa, 1984; Coussot and Piau, 1994; Deangeli, 2009; Iverson *et al.*, 2010; Pierson, 1981; Whipple, 1997). Studies of naturally occurring debris flows have shown that the silt and clay content rarely exceeds 10% by weight (Berti *et al.*, 1999; Costa, 1984; Johnson, 1970; Whipple, 1997) but is significant in maintaining a high pore water pressure. Even values as low as 1-2% for fine grained material can greatly enhance debris flow mobility (Costa, 1984). The influence of silt and clay upon mobility has been highlighted by Iverson *et al.* (2010) where experiments have been carried out at the 90 m USGS flume with several compositions of debris flow mixtures, including silt and clay rich mixtures (fines content 7%), and fine-poor (fines less than 1%) sediment textures. Comparison of the results from these experiments shows how important the silt and clay content can be for debris flow motion, being associated with significantly greater runout distance, higher pore water pressure and, most importantly, the persistence of elevated pore water pressure when slurries contain a relatively large quantity of silt and clay particles.

The ability of the fine sediment fraction to enhance debris flow motion is thought to be due to the variation in size of the grains in the matrix. Pierson (1981) suggests that, because the mixture is poorly sorted, the pores in between individual grains of various sizes are very small. Consequently, the fines are able to block the pores and prevent the fluid fraction from dissipating, thus retaining the fluid under pressure in the interstitial space. Therefore, because the hydraulic diffusivity is lowered, it aids in the development and persistence of high pore water pressure, reducing friction between particles and enhancing flow mobility (Costa, 1984; Iverson, 2003; Iverson *et al.* 2010; Pierson, 1981).

### **2.3.1.2. Sand**

The sand fraction (0.0625-2 mm) can also contribute notably to debris flow motion, although it is less influential upon debris flow motion than the fine sediment fraction. Whipple (1997) states that the macroscopic behaviour of a debris flow is controlled by matrix deformation, where the matrix is constituted by all particles less than 2 mm in diameter, and thus sand is an integral part of this matrix. Pierson (1981) notes how the addition of sand to a slurry can aid debris flow motion. In laboratory experiments, Pierson (1981) observed a temporary increase in pore water pressure when sand was

added to a static slurry of water and clay, prior to the sand settling from suspension. However, a debris flow in motion would be able to maintain the sand in suspension, and so pore water pressure would remain high for longer. Similarly, experiments involving sand and water mixtures in an artificial flume have demonstrated the persistence of pore water pressure in the presence of sand (Deangeli, 2008). As described earlier, the preservation of high pore water pressure will enhance flow mobility by reducing friction between the individual grains.

### **2.3.1.3. Gravel**

A characteristic trait of debris flows is their ability to transport gravel and large boulders, which enhance the destructive and erosive power significantly. The solid volume concentration can range from 25-80% (Davies *et al.*, 1992; Takahashi, 1981), with one sample from a fresh debris flow deposit in Acquabona, northeast Italy, demonstrating that approximately 75% of the sediment mass transported was larger than 20 mm (Berti, 1999). It is this grain size fraction that appears to be important for the provision of pore water pressure by providing a structural framework within which pore fluid may be retained (Pierson, 1981). Subsequently, the granular front exhibits negative pore pressures, whilst the body and tail of a flow experience positive pore pressures (Denlinger and Iverson, 2001; Iverson and Vallance, 2001). Pierson (1981) additionally proposed that the structural framework is able to support a share of the load's weight through grain-to-grain contact and thus facilitate transport of large clasts. However, if the concentration of coarse grains is too high, motion can be resisted and even cease due to the increased internal friction which would develop within a flow (Hampton, 1975; Pierson, 1981). The accumulation of gravel and large boulders at the front of a flow can greatly enhance an event's erosional capability (Davies *et al.*, 1992). Studies by Berger *et al.* (2011a) and Stock and Dietrich (2006) have demonstrated that the passing of the frontal bore of a debris flow contributes to a significant proportion of the channel bed erosion which occurs. In addition, the bulking (increase in volume) of debris flows with eroded saturated sediment can enhance the runout distance considerably (Berger *et al.*, 2011a).

It is apparent that each sediment size fraction plays an influential role in debris flow behaviour, and indeed the wide distribution of particle sizes is what gives debris flows their characteristic form and their destructive, powerful nature. Consequently, it will be

important to perform grain size analyses upon the individual sediment classifications to be incorporated into the debris flow mix.

### **2.3.2. Experimental mixture composition and bulk density**

Debris flow composition can vary greatly from one flow event to another, and within a single surge, producing mixtures of a very granular nature when a high proportion of large, coarse grained solids are present (as at the front) or very fluid flows when there is a high water content and a significant quantity of fine material (as in the tail), whilst many intermediate conditions exist between these extremes (Costa, 1984; Coussot and Meunier, 1996; Iverson, 2003; Whipple, 1997). The grain size distribution and water content of a mixture can have a significant bearing upon the behaviour of the resultant debris flow, such as mobility, runout distance and velocity (Iverson, 2003; Pierson, 1981; Takahashi, 1981; Whipple, 1997). Further, Whipple (1997) suggests that differences in grain size distribution may explain the global variation in debris flow behaviour and the similarity of local flow events. Therefore, to understand the behaviour of the debris flows in the present research, a particle size analysis of the mixture itself will be performed to establish its grain size distribution.

Additionally, dry and wet bulk density analyses of the mixture will be conducted whilst the water content within the flow mixture will be controlled throughout the experiments. These will enable comparison with samples taken from naturally occurring debris flow deposits.

## **2.4. Influence of temperature**

The effect of temperature upon the viscosity of a fluid is relevant for this study, due to the outdoor setting, and thus variable climatic conditions, for the experiments.

It is logical to assume that the temperature of a fluid influences its viscosity (Hampton, 1975; Massoudi and Phuoc, 2004). The effect of this is readily seen with lava flows; as the lava begins to cool, its viscosity increases and thus the flow becomes less mobile and more 'sticky' in nature (Coussot and Piau, 1994; Nichols, 1939). However, the temperature range over which this change occurs is relatively large, often over several hundred degrees Celsius.

In contrast, the most relevant temperature range for debris flow slurries is between 0-20 °C (Coussot and Piau, 1994). Coussot and Piau (1994) performed experiments on natural debris flow mixtures over this temperature range to produce a flow curve. The

results obtained from these demonstrate that there is no distinguishable pattern of debris flow viscosity with temperature. Similarly, Van Steijn (1989) was unable to conclude a definitive link between flow temperature and mobility from experimental data.

Massoudi and Phuoc (2004) attempted to model the viscosity of non-Newtonian fluids. This study acknowledged the influence of temperature upon the viscosity of a fluid within their model, but also concluded that sediment concentration and, most importantly, shear rate are more prominent in dictating the viscosity of a fluid.

Consequently, for this investigation the influence of temperature upon the viscosity of the debris flow mixture will be assumed to be negligible, although for experimental consistency an attempt will be made to use a steady water temperature throughout all mixtures.

## **2.5. Rheology and rheological models**

When modelling or working with debris flows, a rheological model is often characterised to define the behaviour of the flow. Commonly used rheologies include Bingham, Herschel-Bulkley and Dilatant models (Figure 1.1) which tend to describe viscoplastic behaviour (Contreras and Davies, 2000; Coussot *et al.*, 1998; Iverson, 2003; Johnson, 1970; Rodine and Johnson, 1976).

A Bingham fluid debris flow has an inherent shear strength resulting from cohesion, internal friction and viscosity which must be overcome before permanent deformation (movement) occurs. This is known as the yield strength, or yield stress. Once the yield stress is exceeded the fluid behaves as if it were Newtonian, i.e. stress and strain rate increase proportionately to one another (Johnson, 1970; Takahashi, 2007). Similarly, a Herschel-Bulkley fluid is assumed to have a yield stress, but its mobility increases with increasing shear stress in a complex, non-linear relationship (Takahashi, 2007). Conversely, the mobility of a Dilatant fluid decreases non-linearly with increasing shear stress (Takahashi, 2007).

There is a large and complex literature describing each of these models and others, although a thorough examination of these is beyond the scope of this research.

However, more recently an increasingly sceptical approach has been adopted towards the use of rheological models to define debris flow motion (Contreras and Davies, 2000; Iverson, 2003; Johnson, 1970; Rodine and Johnson, 1976). For example, the Bingham model classifies a material as viscoplastic, i.e. a material has a yield stress which must be overcome before permanent deformation occurs. Once deformation

occurs, the model assumes that the material still has strength. However, when contextualised for debris flows, this situation is clearly not applicable, for if the yield stress in a block of sediment has been exceeded, motion will be initiated and thus, the flowing mass no longer has strength (Iverson, 2003).

Furthermore, the suitability of using a single rheology to classify debris flow characteristics is questionable. As discussed previously, debris flows do not exhibit uniform distribution of their components. The front of a debris flow is very granular, with a preponderance of large, coarse particles and is relatively dry, whilst the tail is more fluid, being dominated by water and fine sediment in suspension (Iverson, 1997; Iverson and Vallance, 2001; Lorenzini and Mazza, 2004). Considering this disparity within debris flows and how there are essentially two or three different flow regimes present at any one time, it is perhaps inaccurate to apply a single rheology to debris flow models (Contreras and Davies, 2000; Iverson, 2003; Phillips and Davies, 1991).

## Chapter 3: Research Methods

This chapter will outline the methods used to study the objectives of this research. Several techniques will be used for the research including preliminary tests to determine properties of each sediment type and the debris flow mixture, construction of the channel curves, experimental set up and channel configuration, and the procedure for recording data.

### 3.1. Flume facility

The flume constitutes a section of channel mounted upon a frame. The channel is comprised of a segment of PVCu storm gutter, 8 m in length, with a width of ~0.2 m and a depth of ~0.12 m (width-depth ratio, 5:3) (Figure 3.1). The cross section morphology of the channel is parabolic (Figure 3.2). The channel width-depth ratio is important because if it is too narrow, flow will be concentrated in a confined space, increasing the friction at the head of the flow, whilst if the channel was too wide the flow could quickly lose momentum due to a reduction in flow depth and spreading of the flow. The channel has been roughened by gluing fine sand (mean grain size ~300  $\mu\text{m}$ ) to the bed to more accurately resemble a natural channel and increase friction between the base of the debris flow and the bed (Mangeney *et al.*, 2010). This reduces basal sliding and encourages shear in the flowing debris which is an essential component of debris flow behaviour. The fine sand used to roughen the bed has a median grain size distribution of 250  $\mu\text{m}$ , which is significantly below the  $d_{50}$  of the experimental debris flow mixture of ~500  $\mu\text{m}$ . Owing to the rigid boundary conditions and relatively low channel roughness in comparison to natural channels, very little deposition is expected to occur within the channel. To assist with measurement of flow velocity from image analysis, wooden markers were used as reference points and were attached to the flume, straddling the channel perpendicularly at regular 0.5 m intervals.

The aluminium frame upon which the channel is emplaced is 8 m in length, with a width of approximately 1 m, and is split into four sections, each of which is ~2 m long. At the top of the frame is a vertical headgate and containment tank used to store the debris flow mixture before it is released. The headgate is released manually by means of a lever arm (Figure 3.3). The containment tank has an angled base plate (~25°) to ensure rapid and complete debouching of the mix into the channel, whilst the walls of the

containment tank are aligned with the width of the headgate to ensure smooth transition of flow into the flume, thus aiding flow development (Akhtari *et al.*, 2009). The headgate and containment tank have been designed for rapid release of debris slurries to best mimic dam-break conditions which occur in natural debris flows (Iverson *et al.*, 2010).

The slope of the channel is uniform across the entire length (Figure 3.4), although the overall gradient can be readily adjusted. At the head of the flume, a set of stilts can be mounted onto the frame which, when operated, will enable the gradient of the channel to be adjusted between 15-25° (Figure 3.5). In addition, due to the apparatus being constructed in sections, it is possible to alter the channel morphology by inserting purpose-made curves into the flume with an array of bend geometries. The versatility of the flume facility enables multiple experiments to be performed in a controlled environment and under a range of boundary conditions.

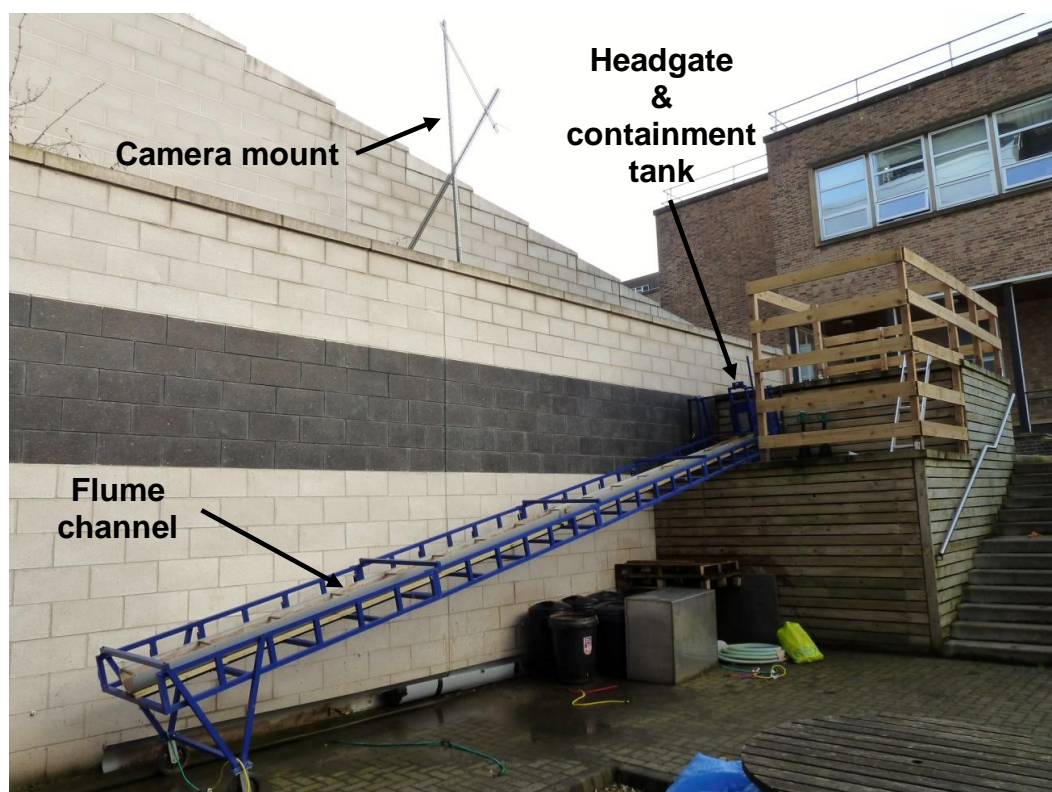


**Figure 3.1:** Visualisation of the experimental flume setup, with the overhead camera frame.



**Figure 3.2:** A cross section of the channel, demonstrating the parabolic shape. Note, wooden marker is 0.2 m across.

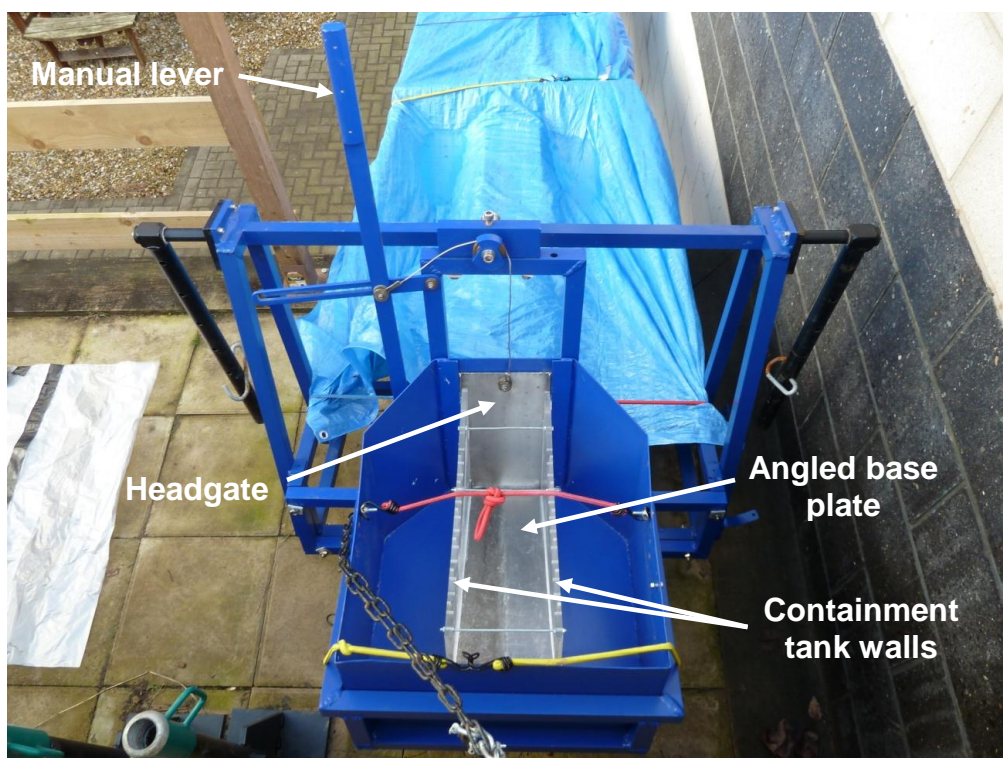


**Figure 3.3:** Headgate configuration, showing the alignment of the walls with the gate and the lever-arm release mechanism.

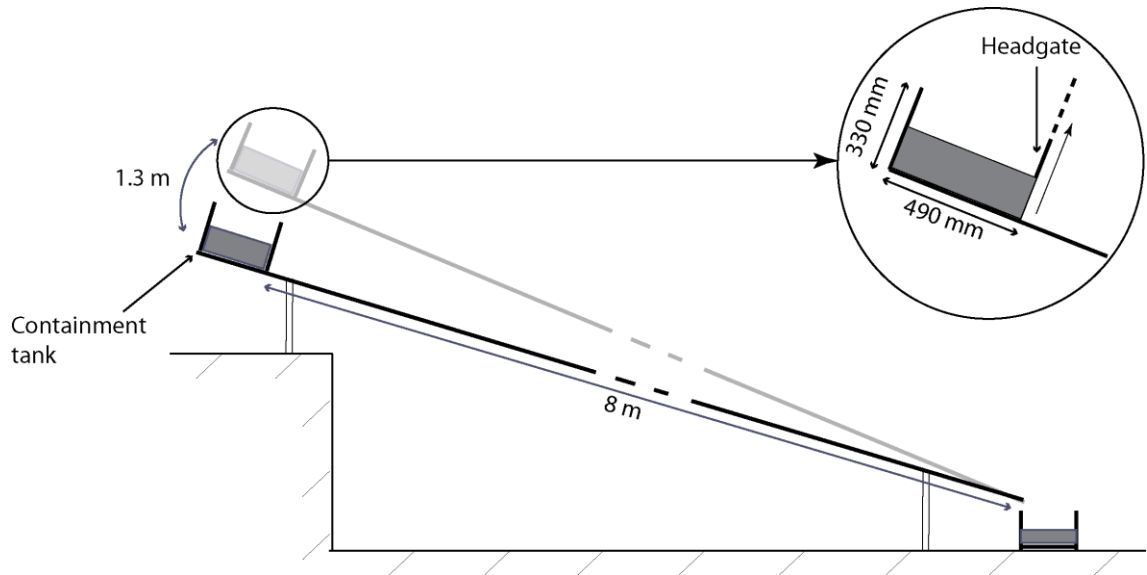


**Figure 3.4:** A schematic representation of the experimental setup, including the variation in channel gradient and the headgate configuration.

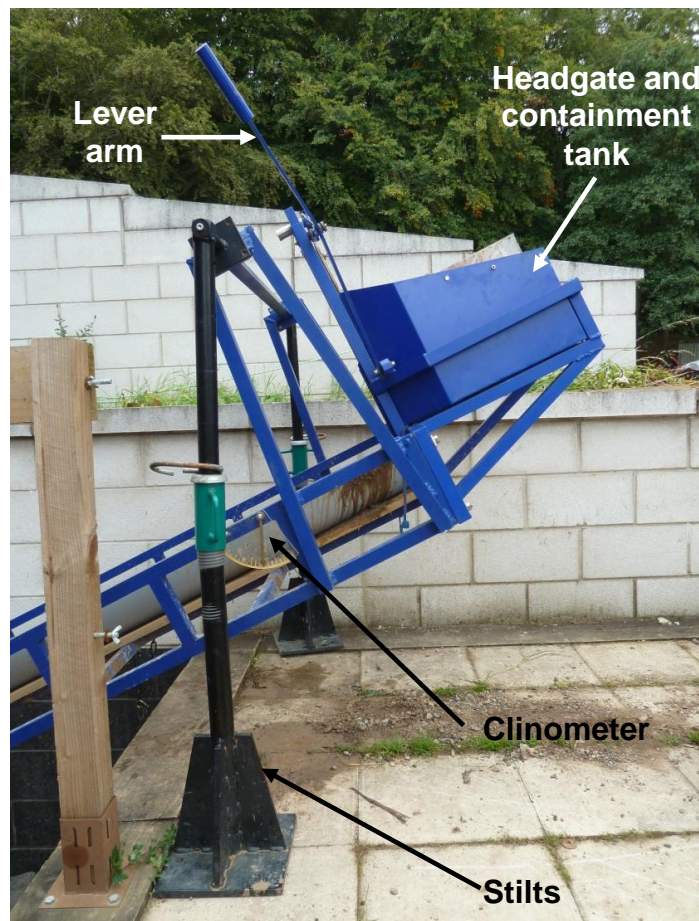


**Figure 3.5:** Visualisation of the artificial flume mounted on the stilts. Here, the flume has been raised to obtain a slope angle of  $25^\circ$

### 3.1.1. Bend construction

In order to observe debris flow behaviour in a curved channel (see objectives in Section 1.3.) modification of the straight flume channel was necessary. Due to a lack of commercially available curved sections of guttering, a mould and cast approach was adopted with Buffin-Bélanger *et al.* (2003) used as a guide, who used a similar procedure to form a facsimile of a natural river bed.

Prior to fabrication of the channel curves, a range of possible bend geometries were calculated and evaluated based on the workable horizontal dimensions of the flume facility (0.9 m) and the length of the polyurethane foam section (1.8 m). There were no examples of similar work in the literature for which to use as guidance or comparison. Four differing bend geometries would be used; three curves with radii of curvature ( $R_c$ ) of 0.4 m, 0.55 m and 0.7 m with a constant bend angle ( $\theta$ ) of  $40^\circ$ , and an additional bend of  $R_c = 0.7$  m and  $\theta = 20^\circ$  (Figure 3.6). This range was selected to enable exploration of the influence of bend angle upon superelevation for the third objective (Section 1.3.).

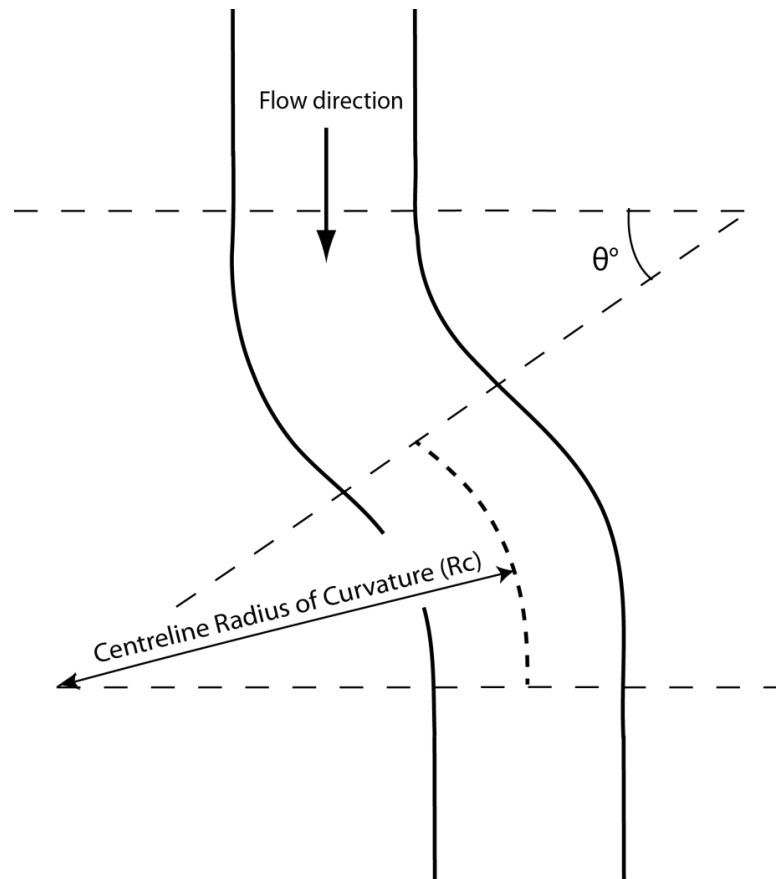


**Figure 3.6:** An illustration of radius of curvature ( $R_c$ ) and bend angle ( $\theta$ ) in the bend complex

To perform the moulding process, first a flexible cast of the channel was required, from which the desired geometries of channel bends could be shaped. The product chosen for this was self-skinning polyurethane foam due to its flexibility and strength. The self-skinning nature of the product enhanced durability by minimising deterioration of the foam from general use.

Prior to the application of the polyurethane resins, a continuous 4 m section of channel was cleaned thoroughly and dried. A wooden cover was fashioned for the moulding procedure which sealed the top and one end of the channel segment, whilst outlets in the lid enabled excess air to escape from the enclosed channel section to avoid accumulation of large air pockets which would weaken the foam. Petroleum jelly was applied to the channel and the cover to prevent the expanding foam from adhering to either surface, thus facilitating separation of the cover and channel from the mould. The cover was then secured to the channel with tape, and silicone sealant was administered at the junction of the two components to minimise loss of the foam from the channel. The channel section was raised to an angle of approximately  $45^\circ$  to ensure complete reproduction of the channel form was achieved once the foam was administered (Figure 3.7). The polyurethane foam was produced by reacting two unspecified chemicals in a ratio of 2:1, as was provided. The chemicals were reacted in a container and mixed together thoroughly before being poured into the covered channel within 1.5 minutes. The resultant cast was left to cure overnight, before being carefully separated from the channel and cover.



**Figure 3.7:** *Channel arrangement for the moulding process*

In order to construct the desired bends from the channel mould, the geometry of the channel walls was measured and drawn out onto a board, with metal nails hammered onto the board at this geometry to ensure the foam remained in position. ModRoc Plaster of Paris was used to create a cast of the foam as it was readily available and easy to manipulate when wet but dried hard, thus producing an accurate and usable reproduction of a channel curve.

In preparation for the application of ModRoc, a coating of petroleum jelly was administered onto the surface of the foam section to prevent adhesion of the two materials. To use the ModRoc bandages, they were briefly immersed in a bucket of luke warm water and applied when wet in strips down the length of the foam section, forming a continuous covering. 3 layers of ModRoc were administered in order to provide required strength and the cast was left overnight at room temperature to cure (Figure 3.8). Further, to reinforce the cast a metal mesh framework was laid over the mould and a further application of ModRoc was added. Once more, this was left to set for 24 hours at room temperature.

The finished mould was then separated from the foam section, sealed with waterproof masonry paint and roughened in the same manner as the main channel by affixing a layer of fine sand to the surface (Figure 3.9). Finally, each section was secured to a wooden board, supports emplaced around the sides and then mounted upon the experimental flume 4 m from the headgate (Figure 3.10).



**Figure 3.8:** *Manufacturing a channel bend. Here, the ModRoc layers have been applied to the foam mould, which is pinned for a curve of  $R_c = 0.7$  m and  $\theta = 20^\circ$*



**Figure 3.9:** A completed bend having been reinforced, painted and a sand coating applied. Bend is  $R_c = 0.55 \text{ m}$ ,  $\theta = 40^\circ$



**Figure 3.10:** Channel bend inserted into the flume structure. The geometry of the channel bend is  $R_c = 0.7 \text{ m}$ ,  $\theta = 40^\circ$

### **3.2. Determining sediment mix properties**

Prior to experimentation in the artificial flume a series of material tests were performed to establish information about the material properties of the sediment mixture and thus enable scaling and comparisons with similar studies and natural debris flows. In designing the debris flow mixture it was important that the constituents were based on locally available commercial raw materials. Thus materials could be readily obtained to given quality standards so that the debris flow mixtures could be reconstituted in a consistent and controlled manner.

#### **3.2.1. Grain size analysis**

The behaviour of a debris flow is influenced significantly by its grain size distribution. For example, an event with a relatively high percentage of fines (less than 62.5  $\mu\text{m}$ ) may often achieve greater runout distances than those with a much lower proportion of these grains (Costa, 1984; Iverson *et al.*, 2010; Johnson, 1970; Whipple, 1997). Therefore, it is important to understand the distribution of particle size within each sediment fraction and of the final mixture itself. For experimental consistency, a constant grain size distribution shall be used across the entire investigation.

##### **3.2.1.1. Clay sized fraction**

For the experiments, the clay used constituted 10.5% of the flow mixture by mass. To obtain a grain size distribution for the clay, a Beckman Coulter LS230 was used, which operates by means of laser diffraction analysis. This process uses a series of detectors to record the extent of diffraction from a single laser beam (with a wavelength of 750 nm), and thus measure particles ranging from 0.4-2000  $\mu\text{m}$  (Blott and Pye, 2006; Eshel *et al.*, 2004).

Blott and Pye (2006) performed a detailed analysis of this technique using various materials, determining an accuracy of 0.03% for mean particle size of latex and glass spheres. Upon carrying out repeat testing with moderately to poorly sorted sands, the grain size measurements were accurate to within 1.5%. Although there are some uncertainties with this method, notably the distribution of material within a size classification and the influence of particle shape upon results, these previous experiments illustrate that laser diffraction techniques provide a high accuracy for grain size measurements (Blott and Pye, 2006).

In order to obtain an average grain size profile for the clay, correct preparation of these samples is necessary prior to analysis with the LS230. 10 samples of clay were collected and with each one then divided into a further three sub samples to act as replicates for analysis, between 0.3-0.4 g in mass, as specified by the British Standards Institution (1999; Mora *et al.*, 1998). To digest organic matter, Hydrogen Peroxide ( $H_2O_2$ ) was added in excess to each of the sample containers in a fume cupboard. Samples were then placed into a boiling water bath and left overnight. The samples were checked and if any organic matter remained, the sample having a brown appearance rather than being colourless, further  $H_2O_2$  was added and the sample was replaced in the water bath. The samples were then centrifuged at 4000 revolutions per minute (rpm) for 4 minutes, before decanting off the liquid and rinsing with deionised water. This process of centrifuging and decanting was then repeated to remove traces of  $H_2O_2$ . Finally, 20 ml of deionised water was supplemented to the sample tubes in addition to 2 ml of Sodium Hexametaphosphate solution which acts as a deflocculating agent, separating the particles from one another and thus facilitating measurement in the LS230.

The results from the LS230 on the 30 clay samples demonstrate the consistency of the material used (Figure 3.11; Figure 3.12). Of the 30 samples which were tested, particle size exceeded that of silt (less than  $62.5 \mu m$ ) in 8 samples; 5 of these had nominal quantities of particles larger than silt (less than 0.1% by volume), whilst the remaining 3 samples contained higher quantities of fine sand, albeit still at relatively insignificant volumes of 1.5%, 2.2% and 5.2%. This fine sand content could be attributed to minor imperfections or inconsistencies within the clay.

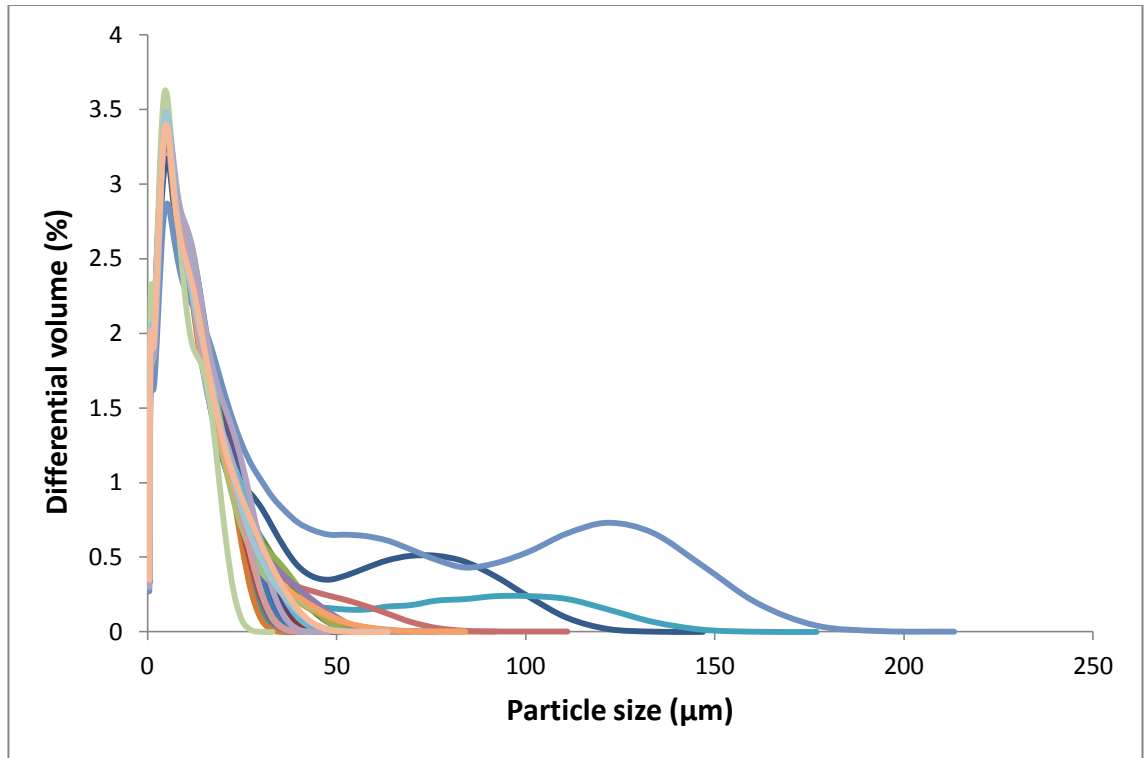


**Figure 3.11:** Particle size distribution of clay samples tested using the Beckman Coulter LS230. Differing line colours represent individual samples. Differential volume is the relative percentage quantity per size classification.

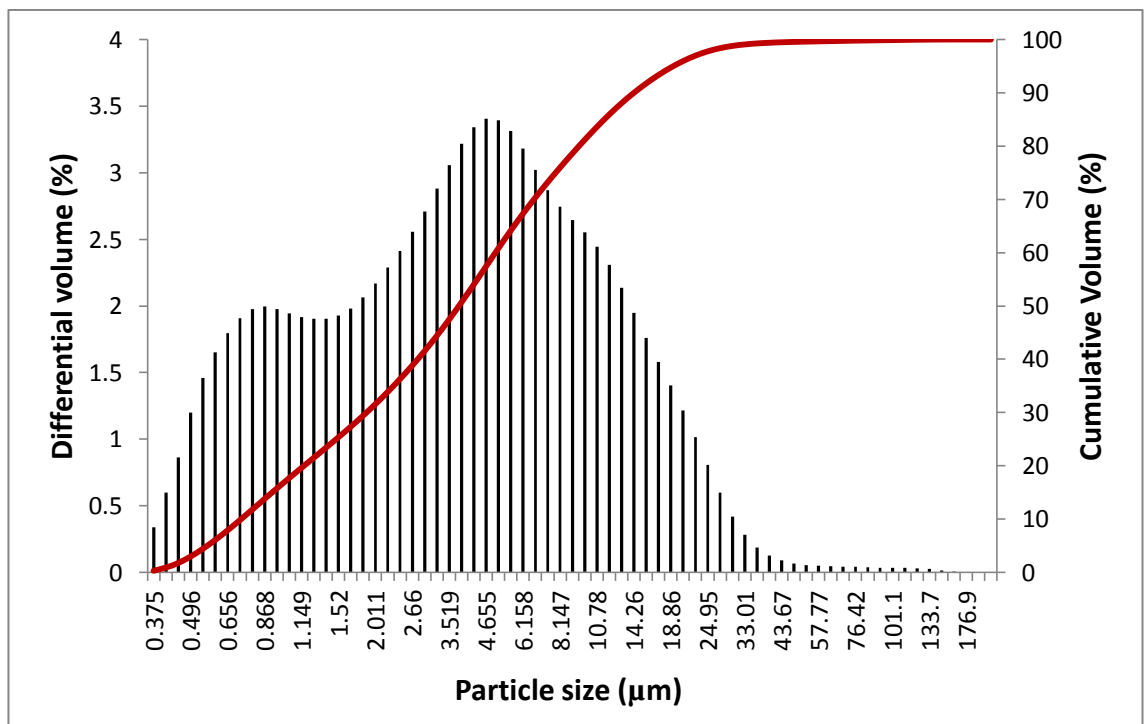


**Figure 3.12:** Mean particle size distribution of the clay samples ( $n = 30$ ) using the Beckman Coulter LS230

### 3.2.1.2. Sand sized fraction

Kiln dried sand was chosen for the sand fraction as it was readily available. Three samples of sand were analysed, each approximately 1 g in mass using the Beckman Coulter LS230. The method of preparation and analysis used for the clay (described in Section 3.2.1.1.) was also adopted for the sand. Grain size analysis of the kiln dried sand demonstrates that on average it comprised mainly fine (35% by volume) (0.125-0.25 mm) and medium (41%) sand (0.25-0.5 mm), with a minor peak (7%) in the coarse sand fraction (0.5-1.0 mm) (Figure 3.13).

An additional variety of coarser sand (referred to from here on as ‘sharp sand’) was also used to increase the spread of particle sizes within the mix. Visual inspection of this material indicated that the grain size distribution of this sharp sand exceeded 2 mm in some instances, greater than the upper threshold of detection for the Beckman Coulter LS230. Therefore, a single analysis was performed using a half phi graded sieve set, ranging from 0.063-2.8 mm, with a minimum mass of 2 kg of sediment, as stipulated by the British Standards Institution (1989; Mora *et al.*, 1998). The graded sieves and a receiving pan were secured onto an electronic sieve shaker and set for 4 minutes at an appropriate amplitude. Each sieve was weighed before and after the sieving process to determine the mass of sediment retained at each size class, and using this, a percentage of the total composition for every grade could be calculated. The sharp sand illustrated a much wider spread of grain sizes, consisting of 32% small gravels by mass and a relatively even spread throughout the fine and medium sand fractions (approximately 11%), with some coarse (2%) and very coarse (4%) sand (1000-2000  $\mu\text{m}$ ) present also (Figure 3.14).

For the debris flow mixture used, kiln dried sand constituted 10.5% of the flow by mass, whilst 28% by mass was sharp sand.

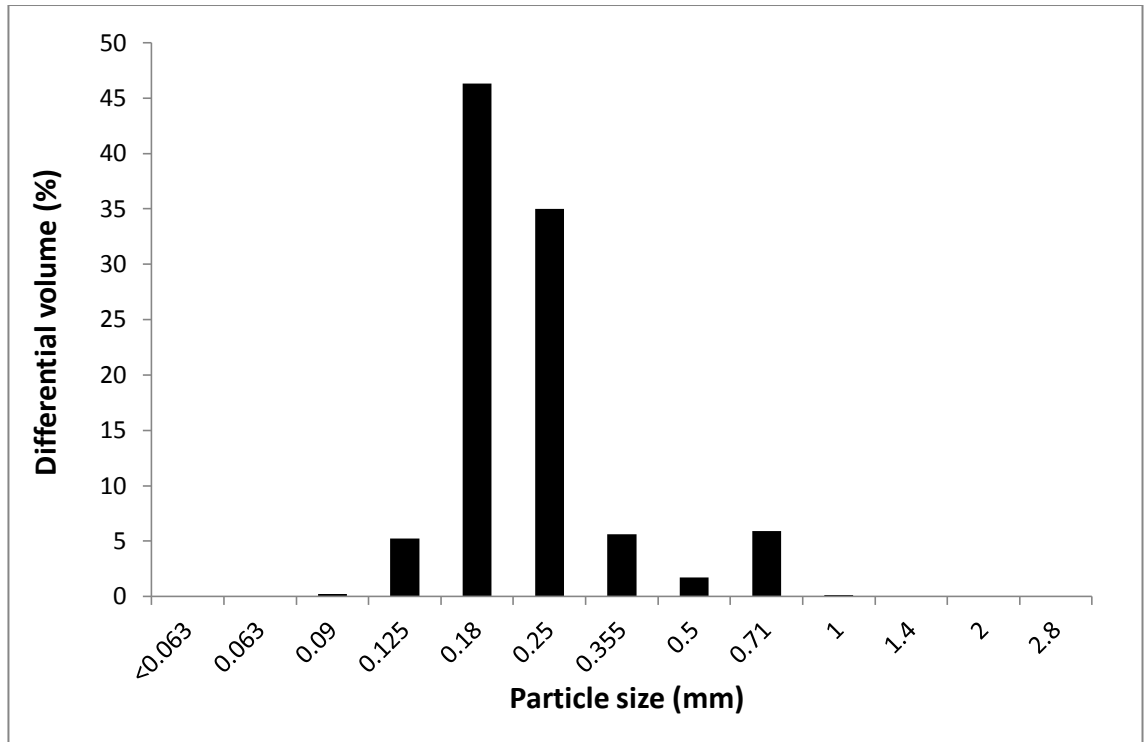


**Figure 3.13:** Average particle size analysis of kiln dried sand samples.

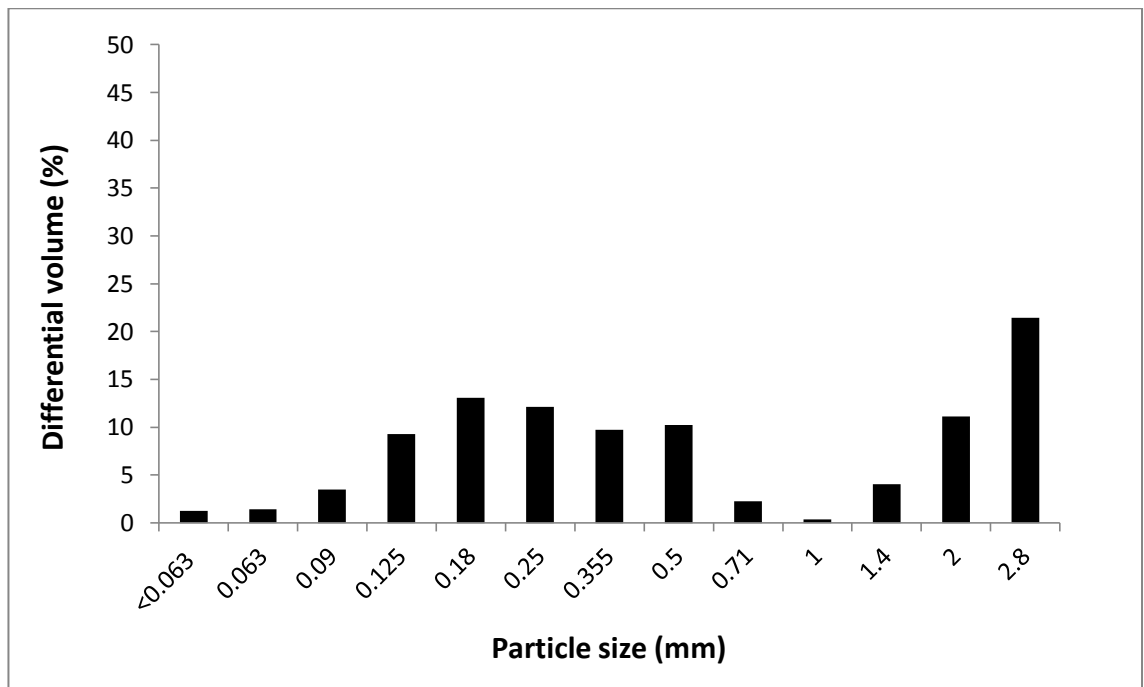


**Figure 3.14:** Grain size distribution of sharp sand.

### 3.2.1.3. Gravel sized fraction

A combination of gravel sizes, both 10 mm and 20 mm gravels, and a mixed aggregate which contained a broad mixture of sediment classes, were used to acquire a wide spread of particle distribution in the overall mixture.

Particle size distribution was determined by sieving. A half-phi graded sieve set, ranging from 1-22.6 mm, was selected to attain a detailed sediment profile. For the mixed aggregate, the sieve sizes were extended to 0.063 mm. A single sample, with a minimum mass of 2 kg, was analysed for each of the three sediment types using an electronic sieve shaker (BSI, 1989; Mora *et al.*, 1998).

The 10 mm gravel demonstrated a narrow spread of particles, with 82.5% of grains by mass contained within the 5.6 mm and 8 mm sieves, and some additional contribution from the 4 mm (11%) and 11.2 mm (3%) classes (Figure 3.15, grey).

Grain size analysis for the 20 mm gravel illustrated a similarly narrow spread of grain sizes, with 99.1% of particles by mass constrained between 8-16 mm, and 91.4% of grains falling within the 11.2 mm and 16 mm sieve classes (Figure 3.15, black) and negligible contribution from the smaller sieve classes.

The grain size profile of the mixed aggregate was much broader in comparison, with 48.9% of all particles by mass in the 8-16 mm range, whilst the remainder is relatively evenly distributed between 0.125-5.6 mm with an average of 4% contained in each sieve class (Figure 3.16).

In the experimental mixtures, both 10 mm and 20 mm gravels constituted 8.5% of the flow by mass, whilst 17% of mixed aggregate was used.

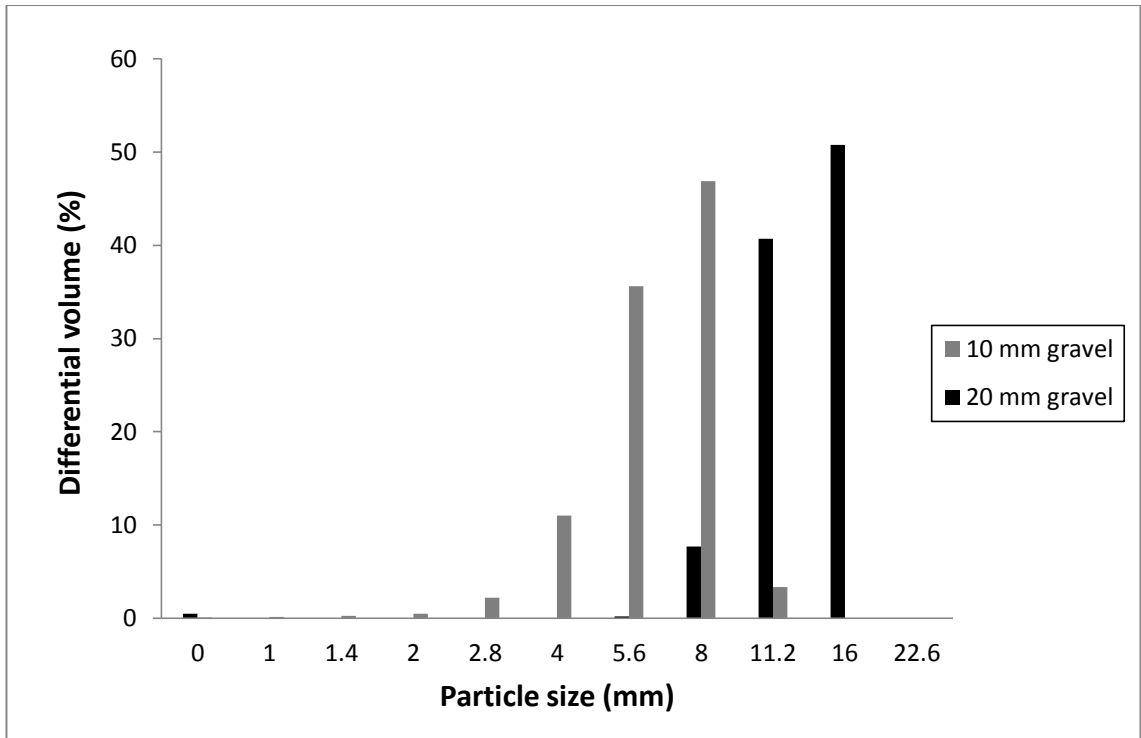


**Figure 3.15:** Grain size profile of 10 mm and 20 mm gravels.

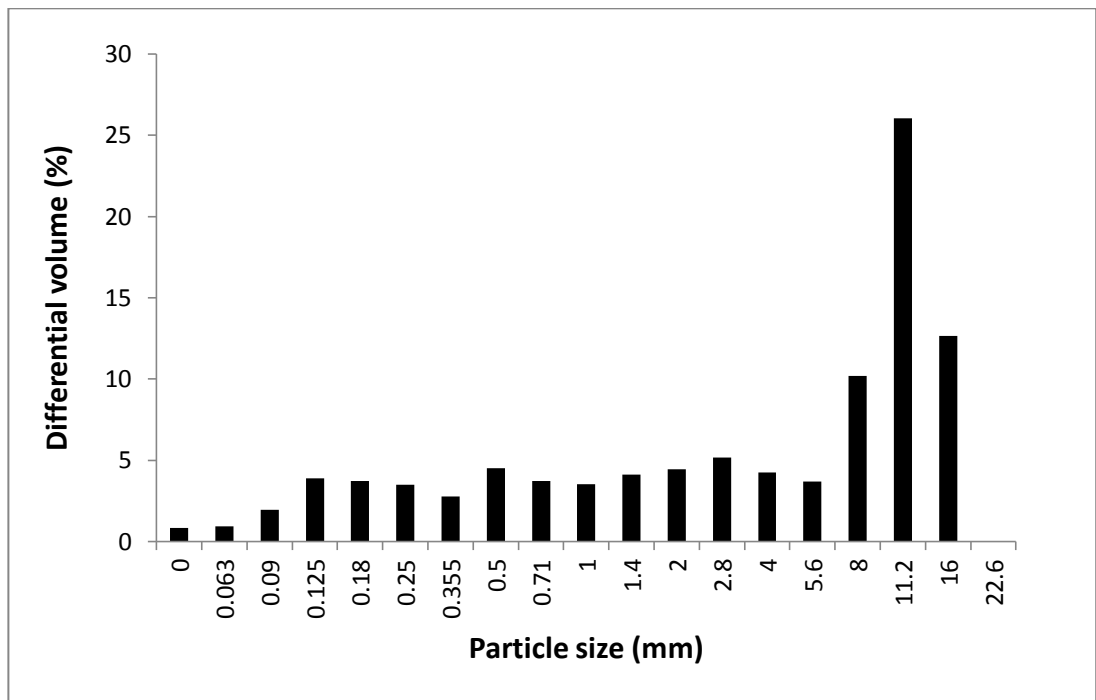


**Figure 3.16:** Grain size distribution of the mixed aggregate.

### 3.2.2. Experimental mixture composition and bulk density

The composition of the debris flow mix was finalised using prior experimental work on the same flume apparatus as guidance (Fairfield, 2011; J Warburton, *pers. comms.*, April 2011). Previously, the mixture used was composed of 50% gravel, 25% sand, 10% clay and 15% water by mass (Mixture 1) (Fairfield, 2011). However, grain size analysis of this showed an uneven distribution of particle sizes (Figure 3.17, grey). Significantly, the gravel fraction overwhelmingly dominates the mix, while little or no sediment spans between coarse sand and very fine gravel (0.5-4 mm). This large gravel component is known to dominate flow behaviour by increasing friction at the head of the debris flow (Hampton, 1975), while grains less than 2 mm in size are important for the retention of a high pore water pressure (Deangeli, 2008; Pierson, 1981; Whipple, 1999). Therefore it was desirable to adjust the mixture to achieve a more uniform grain size distribution, particularly by reducing the high gravel content and increasing sediment composition in the range of 0.1-4 mm.

Mixture 2 was developed with these requirements in mind and therefore has a much broader spread of particle sizes, with no sediment class entirely dominating within the mixture (Figure 3.17, black). The composition of Mixture 2 is: 8.5% 20 mm gravel, 8.5% 10 mm gravel, 17% mixed aggregate, 28% sharp sand, 10.5% kiln dried sand, 10.5% clay and 17% water by mass. For experimental consistency, it is assumed that all the sediment types used are dry, and therefore no additional water is introduced to the mixture. The mass of mixture used for each straight channelled experimental run was 18 kg, but varied between 9 kg and 13 kg for curved channel experiments to prevent channel overtopping and sediment loss.

Bulk density, both dry and wet, was analysed for Mixture 2. A 2 kg sample of Mixture 2 was prepared using each sediment type in the proportions listed above in the absence of water. The sediment was deposited into a roasting tray and placed in an oven at 105 °C until all residual moisture had evaporated and then transferred to a measuring cylinder where its mass and volume were recorded.

To obtain the wet bulk density of the debris flow mixture, the appropriate volume of water was added to the sediment in the measuring cylinder. This was then weighed and the volume recorded.

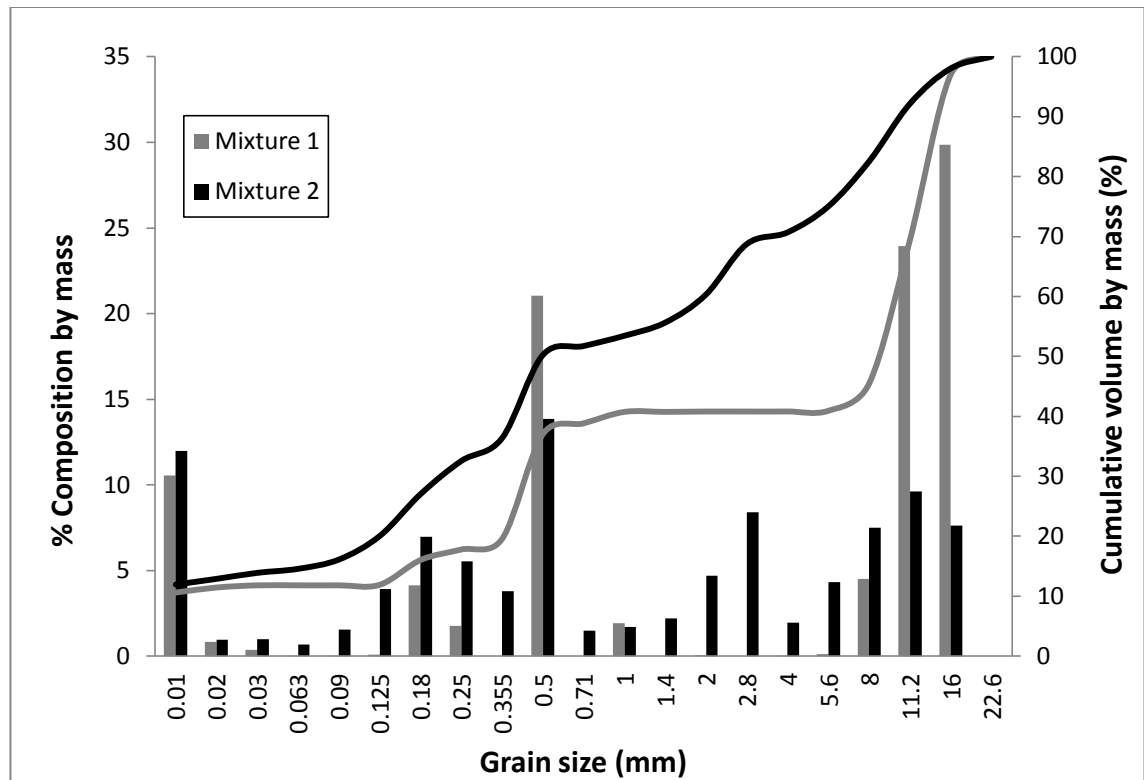


**Figure 3.17:** Graph to compare grain size distribution from the previous (Mixture 1) (Fairfield, 2011) and current (Mixture 2) composition.

The bulk density was calculated by dividing the mass of sediment (kg) with the volume it occupies ( $\text{m}^3$ ). This yielded a value of  $1570 \text{ kg m}^{-3}$  for dry bulk density, and  $1880 \text{ kg m}^{-3}$  for wet bulk density. As discussed previously, naturally occurring debris flows typically have a wet bulk density of between  $1800\text{-}2500 \text{ kg m}^{-3}$ , which results from this research comply with.

### 3.3. Experimental configuration

In order to study the objectives set out previously, an array of experimental configurations were required (Table 3.1). For objective 1 (Section 1.3), a total of twelve experiments were performed in a straight channel, with three repeat runs at each of the four different inclinations of  $15^\circ$ ,  $17^\circ$ ,  $23^\circ$  and  $25^\circ$  inclusive.

Experiments using the curved channel involved four differing bend geometries: radii of curvature 0.4 m, 0.55 m and 0.7 m with a bend angle of  $40^\circ$ ; in addition to a single geometry with a radius of curvature ( $R_c$ ) of 0.7 m and a bend angle ( $\theta$ ) of  $20^\circ$ , at gradients of  $15^\circ$ ,  $17^\circ$ ,  $23^\circ$  and  $25^\circ$ . Debris flows were repeated three times for each experiment configuration to ensure repeatability. This totalled in 48 curved runs overall.

	<b>Straight flume</b>	<b>Curved Channel</b>
<b>Channel Gradients</b>	4 x ; (15°, 17°, 23° and 25°)	4 x ; (15°, 17°, 23° and 25°)
<b>Radius of curvature – 40°</b>	N/A	0.4, 0.55, 0.7 m
<b>Radius of curvature – 20°</b>	N/A	0.7 m
<b>Repetitions</b>	3	3
<b>TOTAL EXPERIMENTS</b>	12	48

**Table 3.1:** *Experimental configuration combinations.*

### 3.3.1. Release of sediment mixture

The debris flow mix was made by combining the quantities of each sediment type (listed in Section 3.2.2.) in a cement mixer. The most important aspect of this process was to ensure that the clay had homogenised fully with the water to form a fine suspension, and that there were no lumps of clay remaining to be mixed. This was then transferred into the closed headgate, which had previously been shut and petroleum jelly applied to the seals to minimise leakage of the intergranular fluid from the containment tank. Due care was taken not to compact the sediment, although some disturbance and grain size segregation of the mixture was inevitable during the transfer from the bucket to the containment tank.

When ready, the manual lever was released to open the headgate and discharge the debris flow mixture into the channel. A camera was suspended overhead to record each experiment, and a receiving tank was placed at the end of the channel length to collect the mixture. Between each run, the headgate and flume were rinsed with water to prevent deposition of material in the channel and ensure the same conditions for each run.

### 3.3.2. Image analysis

For the purpose of monitoring debris flow characteristics in this investigation, a digital camera was suspended above the flume facility. Video footage has been widely used to quantify flow characteristics of debris flows (Arratano and Marchi, 2000; Genevois *et al.*, 2001; Hürlimann *et al.*, 2003; Uddin *et al.*, 1998). The selected camera was a Panasonic Lumix DMC-TZ8, with a wide-angle 25 mm (35 mm equivalent) lens. This particular make and model of camera had been used for a similar project on the

same debris flow flume (Fairfield, 2011), and therefore was known to be suitable for the various requirements. A camera with a wide-angle lens was necessary to accommodate the entire length of the flume in one field of view, whilst the 12.1 mega pixels produced an image with clarity and sharpness. The camera was mounted onto an overhead frame with a bracket and suspended at sufficient height above the flume for filming. When filming each debris flow, video footage was recorded at 30 frames per second.

Velocity at the flow front was calculated frame-by-frame with use of video footage together with the wooden markers attached to the channel, spaced at 0.5 m intervals. Furthermore, the wooden markers had horizontal reference points upon them at 20 mm intervals which could be used to estimate flow width.

Average velocity between the reference markers was calculated by combining the length of time taken for the flow front to travel between markers. The length of time required for the flow front to travel between two markers was calculated by counting the number of frames of video footage, starting when the flow front arrived at the first marker and stopped upon its arrival at the following reference point, and multiplying this number by the time between frames (0.033 seconds). Then, the distance in metres between the reference markers (0.5 m) was divided by the time in seconds for the flow to travel this distance, to thus obtain an average velocity estimate ( $\text{m s}^{-1}$ ). This velocity is that quoted, but is then averaged again using the repeat runs at each channel gradient which will be used in the experimental analysis.

Therefore, by adopting this technique it is possible to estimate debris flow velocity at various sections throughout each experiment's transit down the artificial channel, and thus plot how velocity changes as a flow accelerates and then reaches its terminal velocity. Comparison of the results for velocity across the range of boundary conditions used will enable assessment of the first objective (Section 1.3.). Further, the calculated velocities formed the foundations for the analysis of the following three objectives.

To quantify the magnitude of superelevation around a channel bend, vertical measurements were marked on both the inside and outside banks of the channel to enable visualisation of the flow surface as it progressed through the curve. The markings were spaced at  $5^\circ$  intervals for ease of comparison between bends (Figure 3.18). The extent of superelevation was recorded with the use of the graded markings and tide marks left by the passage of the frontal bore. The depth of flow upstream from the bend (where the flow had reached terminal velocity) was noted, and superelevation was recorded relative to this value.

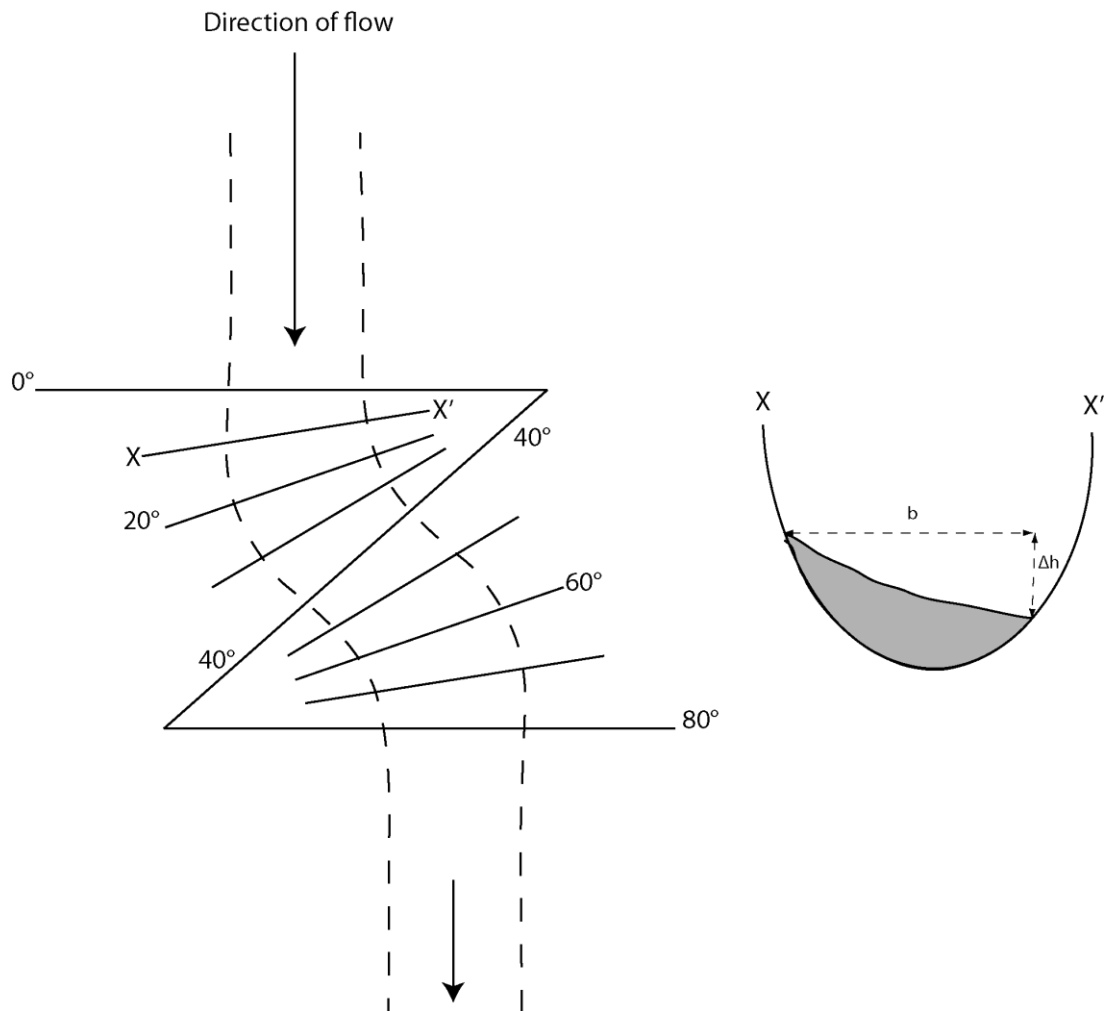


**Figure 3.18:** *Demonstration of the recording of superelevation at the inside and outside walls of the channel. In practise, superelevation was recorded at 5° intervals, rather than the 10° intervals pictured here.*

### 3.4. Experimental precision and statistical analysis

The superelevation recordings are precise to  $\pm 0.5$  cm ( $\sigma$ ), ascertained from duplicate measurements performed on a single experimental test. Velocity values are precise to within  $\pm 0.3$  m s<sup>-1</sup>, based on repeat measurements from video footage. Pixel distortion was not directly tested, although image clarity in the video footage was consistently excellent.

For analysis of the velocity and superelevation data, a power-law trendline will be applied to each set of data, and an  $R^2$  value will be fit to this to demonstrate the degree

of variance of the data from a straight line, with a value of '1' being linear and '0' showing no linearity. Similarly, a Pearson Correlation Coefficient,  $r$ -value, will be performed to establish the degree of linearity between two variables, where a value of '1' indicates a positive relationship, '-1' represents a negative relationship and '0' implies that no linear relationship is exhibited. Finally, a ' $p$ -value' will be given to determine the statistical significance of the datasets, to a confidence level of 95%. For example, a value of '1' represents no correlation, while a value of  $< 0.05$  suggests that the relationship is statistically significant.

### 3.5. Summary

Prior to flume investigations, tests of material characteristics were undertaken on the gravel, sand and clay components to be used in the experiments. In addition, dry and wet bulk densities of the debris flow mixture were measured, while detailed grain size distributions of the individual sediment components and of the debris flow mixture itself were performed using a Beckman Coulter LS230 and a half-phi graded sieve set. These tests enabled an experimental mixture to be developed, and concluded that the mixture used herein is consistent with other experimental mixtures.

Four channel curves were constructed using polyurethane foam mould and ModRoc Plaster of Paris, and in turn were inserted into the flume in order to study superelevation of debris flows.

Analysis of flow events was primarily performed using digital imaging software, utilising both still and video footage (Arratano and Marchi, 2000; Genevois *et al.*, 2001; Hurlimann *et al.*, 2003; Uddin *et al.*, 1998). A digital camera suspended above the flume recorded the flow from release of the headgate to runout at the flume exit. These videos were used in conjunction with fixed reference markers positioned at a set distance to enable velocity estimates to be calculated for each flow. To quantify the extent of superelevation, graded markings were positioned at regular intervals to the sides of the flume, thus providing the means to track the magnitude of banking around a bend.

## Chapter 4: Results

This chapter discusses the results obtained from the debris flow flume experiments, using the methodology developed and described in Chapter 3. First, the results for the straight channel experiments are presented, demonstrating the relationship between channel gradient and velocity. Second, the results from the curved channel experiments are outlined. These show the influence of velocity upon the magnitude of superelevation, and the extent to which radius of curvature and bend angle control superelevation. Furthermore, the spatial pattern of superelevation around each bend will be assessed and described.

Before discussing the results it is important to outline the terminology to be used in this and later chapters:

<b>Terminology</b>	<b>Measurement</b>	<b>Error</b>
<b>Average velocity (AV)</b>	The average velocity calculated from release of the headgate to runout at the end of the flume.	$\pm 0.3 \text{ m s}^{-1}$
<b>Average terminal velocity (ATV)</b>	Average velocity once the flow was deemed to have reached maximum velocity, calculated by averaging the velocity values once the flow was deemed to have reached a stable phase (acceleration = 0).	$\pm 0.3 \text{ m s}^{-1}$
<b>Bend entry velocity (BEV)</b>	The calculated velocity at which the experimental debris flow enters the first curve of the bend complex.	$\pm 0.3 \text{ m s}^{-1}$
<b>Radius of curvature (Rc)</b>	A measure of bend curvature relative to the equivalent radius of a circular arc.	$\pm 0.02 \text{ m}$
<b>Bend angle (<math>\theta</math>)</b>	The measurement, in degrees, of a channel bend following a circular arc.	$\pm 2^\circ$
<b>Experimental precision (<math>\sigma</math>)</b>	Error encountered when recording superelevation.	$\pm 0.5 \text{ cm}$

**Table 4.1:** *Summary of terminology, measurements and experimental error associated with each component.*

#### 4.1. Straight channel results

In total, 12 experiments were carried out in a straight channel, with three repeat experiments performed at each of the four channel gradients of  $15^\circ$ ,  $17^\circ$ ,  $23^\circ$  and  $25^\circ$ .

For a low angle debris flow channel of  $15^\circ$ , the flow accelerated for the first 3.5 m, reaching a stable velocity between 3.5-5.5 m down flume. Flow then decelerated after 5.5 m down the channel (Figure 4.1A). This deceleration phase will be discussed in Section 5.1.1. The AV for the three experiments at a channel gradient of  $15^\circ$  was  $2.31 \text{ m s}^{-1}$ , with a standard error of  $\pm 0.03 \text{ m s}^{-1}$ , whereas the ATV for the same experimental runs was slightly higher at  $2.86 \text{ m s}^{-1} \pm 0.01 \text{ m s}^{-1}$  ( $\pm 0.3\%$ ). The standard error for most of the averaged points fell within  $\pm 10\%$  of the average velocity at that location, with the exception of recordings at 6.5 m ( $\pm 16.4\%$ ), 7 m ( $\pm 11.5\%$ ) and 7.5 m ( $\pm 11.1\%$ ).

At a channel gradient of  $17^\circ$ , the flow was in an accelerating phase from 0-3 m, with velocity stable between 3-5.5 m and deceleration of flow beginning at 5.5 m (Figure 4.1B). This is a similar trend to that displayed for a channel gradient of  $15^\circ$ . The AV for the three debris flows was  $2.37 \text{ m s}^{-1} \pm 0.02 \text{ m s}^{-1}$  ( $\pm 0.9\%$ ), and ATV was greater at  $3.08 \text{ m s}^{-1} \pm 0.03 \text{ m s}^{-1}$  ( $\pm 1.2\%$ ). The standard error for all of the points fell within  $\pm 8\%$  of the average velocity for that location.

For a channel gradient of  $23^\circ$ , the flow was in an accelerating phase from 0-3.5 m, with a longer period of stable velocity from 3.5-7 m. A slight deceleration phase was present from 7 m until runout at the end of the flume, although this is less pronounced than the deceleration observed at channel gradients of  $15^\circ$  and  $17^\circ$  (Figure 4.1C). The three experimental debris flows achieved an AV of  $2.91 \text{ m s}^{-1} \pm 0.08 \text{ m s}^{-1}$  ( $\pm 2.8\%$ ). The ATV reached during these experiments was  $3.55 \text{ m s}^{-1} \pm 0.12 \text{ m s}^{-1}$  ( $\pm 3.5\%$ ). The standard error for most of the points fell within  $\pm 10\%$  of the average velocity at that location, with the exception of measurements at 7.5 m ( $\pm 13.2\%$ ) and 8 m ( $\pm 12.2\%$ ).

At the steepest debris flow channel of  $25^\circ$ , the flow was accelerating from 0-3.5 m, with an approximate period of stable velocity from 3.5 m until runout at the end of the channel; there was no deceleration phase present (Figure 4.1D). The changing position of the terminal velocity phase will be discussed in Section 5.1.1. Three experimental tests returned an AV of  $3.17 \text{ m s}^{-1} \pm 0.13 \text{ m s}^{-1}$  ( $\pm 2.4\%$ ) and an ATV for the same experiments of  $3.92 \text{ m s}^{-1} \pm 0.21 \text{ m s}^{-1}$  ( $\pm 3.2\%$ ). The AV and ATV exceeded all those recorded at the three previous channel gradients. The standard error for most of the data

points was less than  $\pm 10\%$  of the average velocity value at that location; the 2 points that fall outside of this were at 5.5 m ( $\pm 10.6\%$ ) and 7 m ( $\pm 10.5\%$ ).

<b>Channel gradient</b>	<b>AV <math>\pm</math> Standard Error ( m s<sup>-1</sup>)</b>	<b>ATV <math>\pm</math> Standard Error ( m s<sup>-1</sup>)</b>	<b>Average Experimental Precision (%)</b>
15°	2.31 $\pm$ 0.03	2.84 $\pm$ 0.01	$\pm$ 6.2
17°	2.37 $\pm$ 0.02	3.08 $\pm$ 0.04	$\pm$ 2.8
23°	2.91 $\pm$ 0.08	3.55 $\pm$ 0.12	$\pm$ 5.4
25°	3.17 $\pm$ 0.08	3.92 $\pm$ 0.13	$\pm$ 5.7

**Table 4.2:** *Summary of straight channel results at each channel gradient, calculated from video footage of the debris flow experiments.*

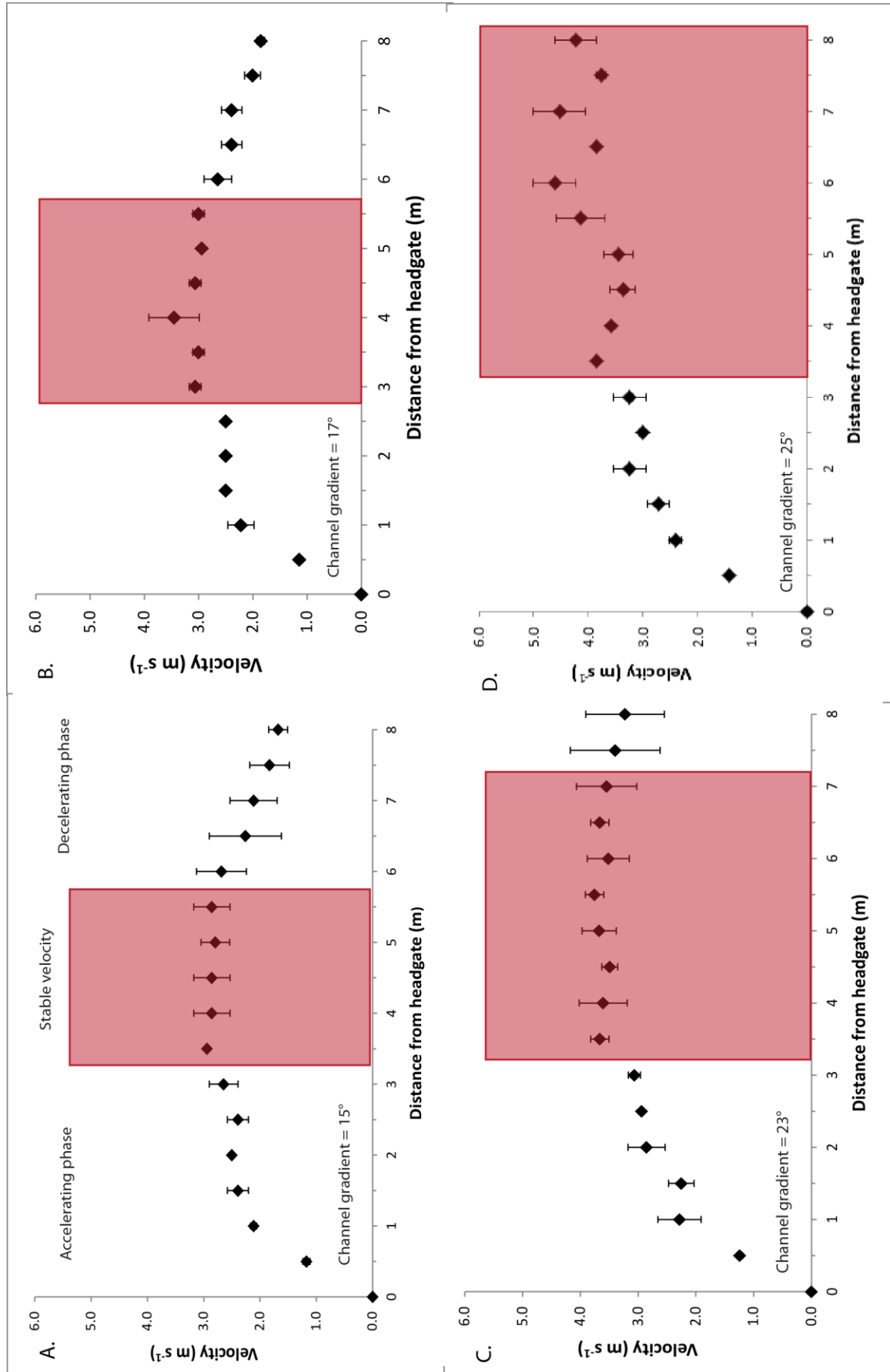


**Figure 4.1:** Average velocity profile for straight channel experiments at **A.** channel gradient = 15°; **B.** channel gradient = 17°; **C.** channel gradient = 23°; and **D.** channel gradient = 25°. **Bars** show  $\pm$  standard error of the mean ( $n = 3$  at each slope). The red boxes highlight the regions where flow is judged to have reached terminal velocity (acceleration = 0).

#### 4.2. Channel gradient versus velocity

The straight channel data presented in Section 4.1 illustrates that at channel gradients of 15°, 17°, 23° and 25° terminal velocity was achieved by 3.5 m from the headgate, with deceleration of flow down channel for the three shallower channel gradient (Figure 4.1). This provided a constraint on where to place the channel curves because it was important for the flow to be entering the bend complex at terminal velocity with any deceleration occurring after the position of the curve complex.

A strong, positive linear relationship exists between AV and channel gradient ( $R^2 = 0.98$ ;  $r = 0.99$ ;  $p = 0.01$ ; Figure 4.2). ATV is also significantly related to channel gradient ( $R^2 = 0.98$ ;  $r = 0.99$ ;  $p = 0.01$ ; Figure 4.2). This linear relationship between velocity and slope is consistent with the theory of laminar flow (Chaudhry, 2008; Chow, 1959).

The slope of the linear trendline for AV is 0.09, and intercepts the y axis at 0.95 (equation  $y = 0.09x + 0.95$ ). ATV has a similar linear gradient of 0.10, and intercepts the y axis at 1.41 (equation  $y = 0.10x + 1.41$ ). The lower intercept for AV reflects the inclusion of acceleration and deceleration phases, while the similar slope demonstrates consistency between the findings.

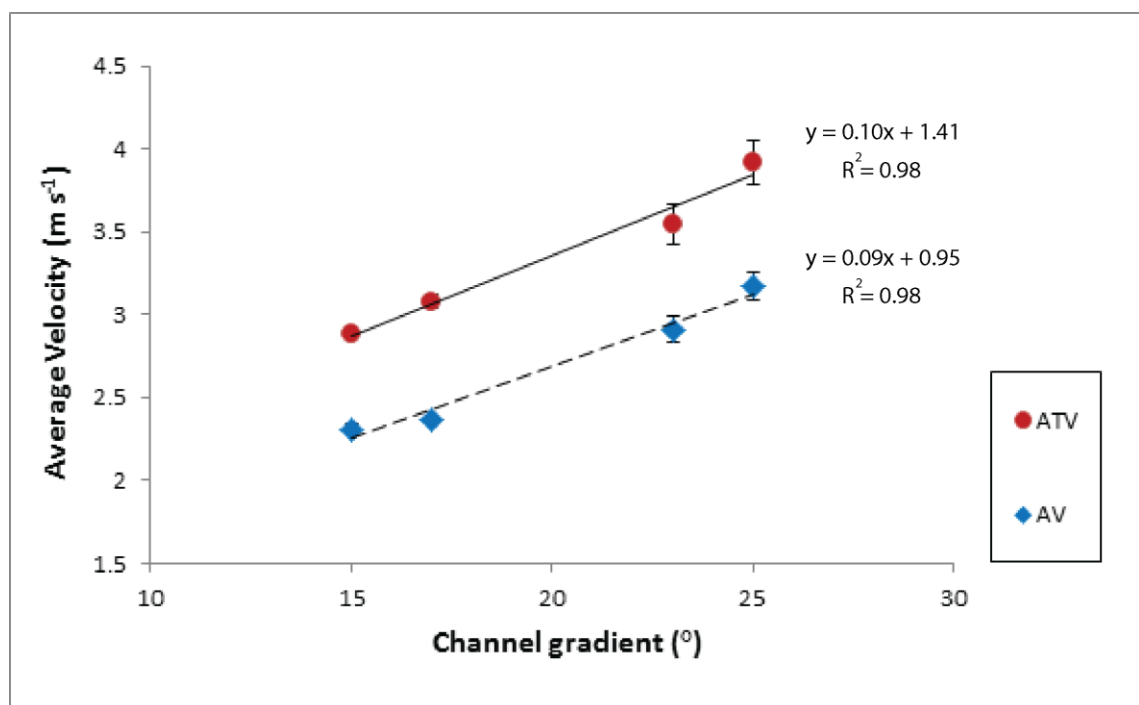


**Figure 4.2:** Average terminal velocity (ATV) and average velocity (AV) at each channel gradient. Trendlines have been applied and the  $R^2$  value displayed for both data sets. Bars show  $\pm$  standard error of the mean where applicable ( $n = 3$ ).

### 4.3. Curved channel results

In total, 48 experiments were performed across four different bend geometries:  $R_c = 0.7$  m, 0.55 m and 0.4 m where  $\theta = 40^\circ$ ; and a single bend at  $\theta = 20^\circ$  with  $R_c = 0.7$  m. Each bend configuration had twelve experiments, where three debris flow runs were performed at each of the four channel gradients. All the superelevation data reported in this section have been recorded from the first bend in the complex. On no occasion did superelevation at the second bend exceed that at the first.

#### 4.3.1. Superelevation versus velocity

In this section, the measured value for superelevation is the maximum change in debris mark elevation between the inside and outside of the bend, recorded at one or more locations in the curved channel (Figure 3.19). The value for debris flow velocity is determined by the flow velocity measured prior to entry to the curves (BEV), i.e. between 3.5-4m from the headgate.

##### 4.3.1.1. Bend geometry: $R_c = 0.7$ m, $\theta = 20^\circ$

For this bend configuration, a slight positive linear relationship is shown between channel gradient and average superelevation ( $R^2 = 0.32$ ;  $r = 0.56$ ; Figure 4.3), although this is not suggested at the 95% confidence level ( $p = 0.44$ ). Standard error for average superelevation varied between  $\pm 0.0\%$  and  $\pm 14.3\%$ . Perhaps significantly, average superelevation observed at a channel gradient of  $17^\circ$  exceeded that recorded at  $23^\circ$ , and was equal to that for a  $25^\circ$  slope. This is contrary to the expected trend where superelevation should increase with increasing channel slope.

A weak power law relationship exists between debris flow BEV and maximum superelevation for this bend configuration ( $R^2 = 0.19$ ;  $r = 0.43$ ;  $p = 0.17$ ; Figure 4.4). It is of interest to note that in several circumstances superelevation does not increase with increased velocity as predicted it would for a given channel, for example experiments for a channel gradient of  $15^\circ$  where superelevation remained at 6 cm, with velocity ranging from 2.5-3.1  $\text{m s}^{-1}$ .

The power law relationship between the average BEV for a given channel slope and the average maximum superelevation is stronger, although  $p > 0.05$  suggests this is not significant at the 95% confidence level ( $R^2 = 0.45$ ;  $r = 0.65$ ;  $p = 0.35$ ; Figure 4.5). The standard error for mean BEV was less than  $\pm 7\%$  across all 4 gradients.

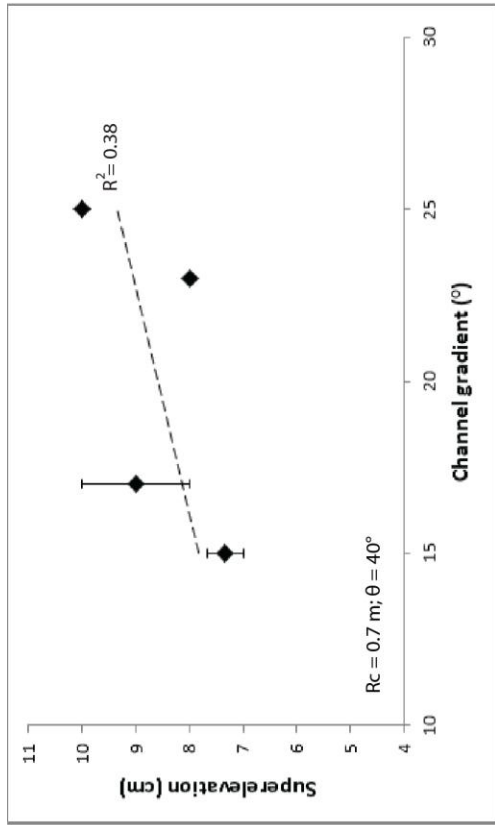


**Figure 4.3:** Average superlevation at each channel gradient, with respective standard error shown as bars. A linear trendline and  $R^2$  value are displayed.

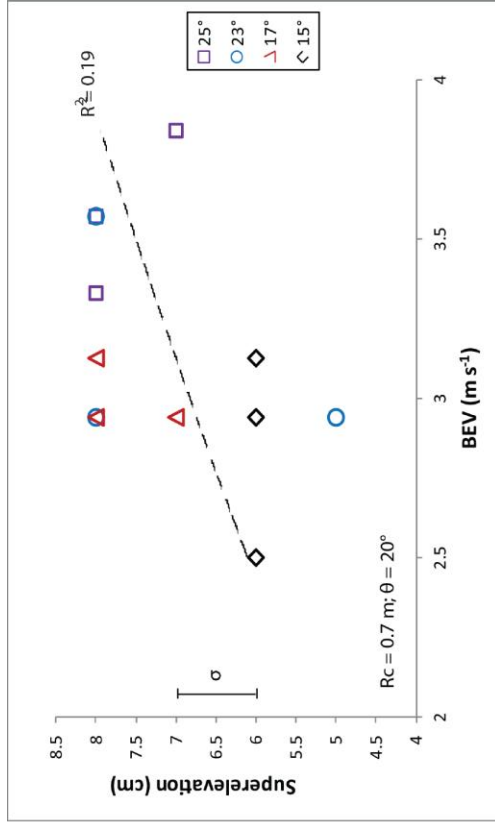


**Figure 4.4:** BEV of each debris flow with the respective maximum recorded superlevation. A power law trendline and an  $R^2$  value have been applied to the data.

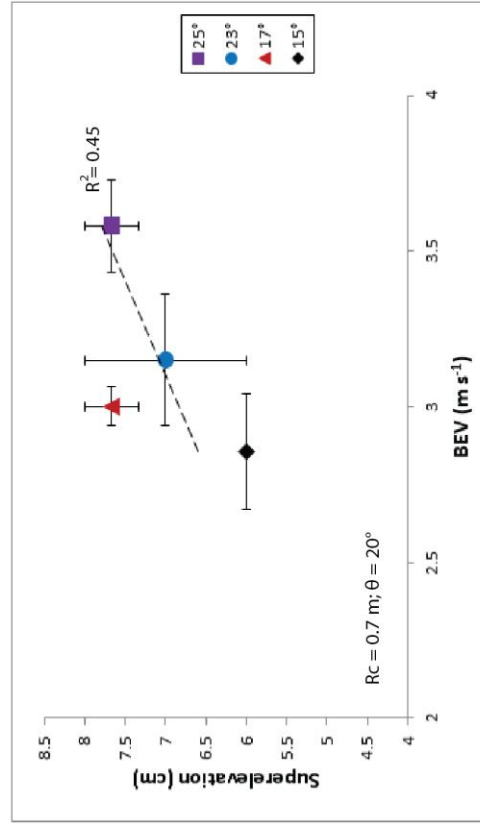


**Figure 4.5:** Average debris flow BEV for each channel gradient and the respective average maximum recorded superlevation, with a power law trendline and an  $R^2$  value applied. Regression equation:  $y = 2.84 * x^{0.80}$ . Standard error is shown as bars.

Relationship	R <sup>2</sup> value	r-value	p-value
Average superelevation versus channel gradient	0.32	0.56	0.44
BEV versus maximum superelevation	0.19	0.43	0.17
Average BEV versus average maximum superelevation	0.45	0.65	0.35

**Table 4.3:** Summary of statistical results for  $R_c = 0.7$  m,  $\theta = 20^\circ$  calculated from the experimental data.

Channel slope	Mean BEV $\pm$ standard error (m s <sup>-1</sup> )	Precision (%)	Mean superelevation $\pm$ standard error (cm)	Precision (%)
15°	2.86 $\pm$ 0.19	6.5	6.0 $\pm$ 0.0	0.0
17°	3.00 $\pm$ 0.06	2.1	7.7 $\pm$ 0.3	4.3
23°	3.15 $\pm$ 0.21	6.7	7.0 $\pm$ 1.0	14.3
25°	3.58 $\pm$ 0.15	4.1	7.7 $\pm$ 0.3	4.3

**Table 4.4:** Summary of statistical results for  $R_c = 0.7$  m,  $\theta = 20^\circ$ . Mean BEV was calculated from video footage of the debris flow experiments.

#### 4.3.1.2. Bend geometry: $R_c = 0.7$ m, $\theta = 40^\circ$

A weak linear relationship is displayed between channel gradient and average maximum superelevation ( $R^2 = 0.38$ ;  $r = 0.62$ ; Figure 4.6) though this is not statistically significant at a 95% confidence interval ( $p = 0.38$ ). Standard error for average superelevation varied between  $\pm 0.0\%$  and  $\pm 11.1\%$  of the respective value.

The power law relationship between superelevation and debris flow BEV is reasonably weak ( $R^2 = 0.40$ ;  $r = 0.65$ ; Figure 4.7), although a returned  $p$ -value of 0.03 suggests a statistically significant relationship at the 95% confidence level.

For the relationship between average BEV and average superelevation at each channel gradient, an  $R^2$  value of 0.52 demonstrates a reasonable power law association between the two data sets ( $r = 0.74$ ; Figure 4.8), although this is not statistically significant ( $p = 0.25$ ). The standard error for mean BEV does not exceed  $\pm 6\%$  of the relative velocity at any given gradient. Perhaps significantly, average BEV for a channel gradient of  $23^\circ$  exceeded the average BEV recorded on a channel slope of  $17^\circ$ , although observed average superelevation was lower at  $23^\circ$ .

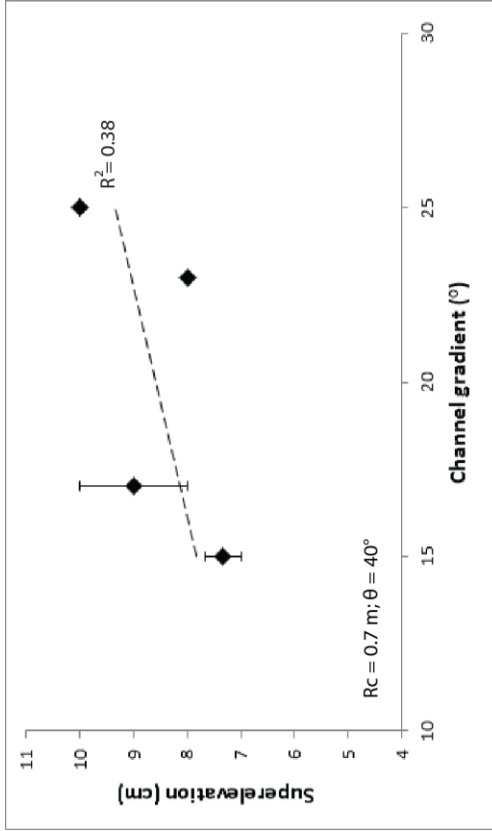


**Figure 4.6:** Average superlevation at each channel gradient  
As per Figure 4.3.

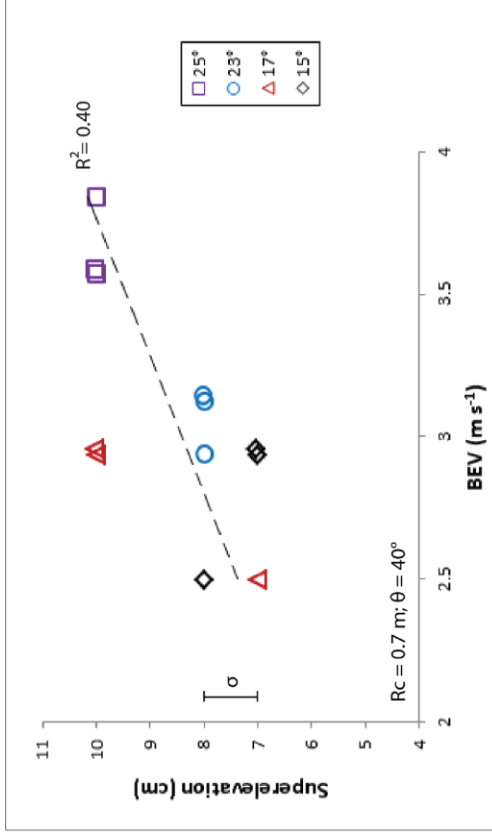


**Figure 4.7:** BEV of each debris flow with the respective maximum recorded superlevation. As per Figure 4.4.

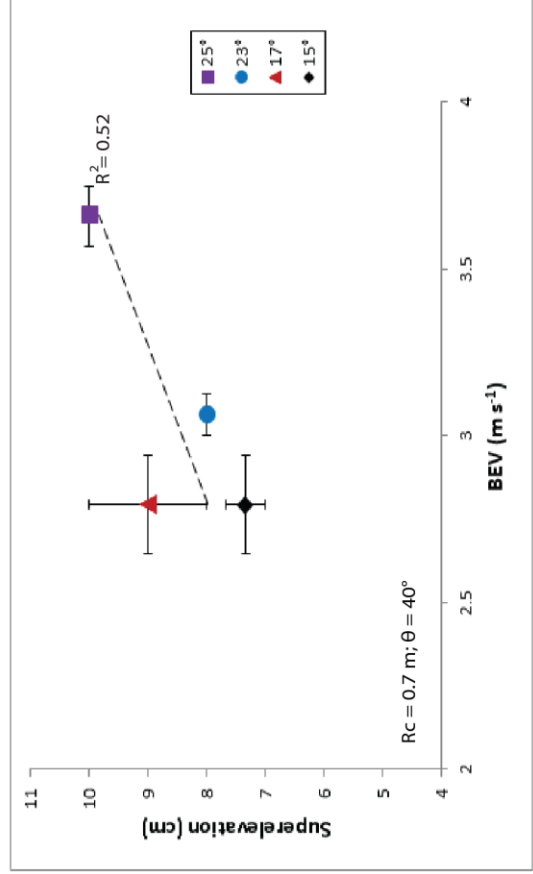


**Figure 4.8:** Average debris flow BEV for each channel gradient and the respective average maximum recorded superlevation. Regression equation:  $y = 3.62 * x^{0.77}$ .  
As per Figure 4.5.

Relationship	R <sup>2</sup> value	r-value	p-value
Average superelevation versus channel gradient	0.38	0.63	0.38
BEV versus maximum superelevation	0.40	0.65	0.03
Average BEV versus average maximum superelevation	0.52	0.74	0.25

**Table 4.5:** Summary of statistical results for  $R_c = 0.7$  m,  $\theta = 40^\circ$ . As per Table 4.3.

Channel slope	Mean BEV $\pm$ standard error (m s <sup>-1</sup> )	Precision (%)	Mean superelevation $\pm$ standard error (cm)	Precision (%)
15°	2.79 $\pm$ 0.15	5.3	7.3 $\pm$ 0.3	4.5
17°	2.79 $\pm$ 0.15	5.3	9.0 $\pm$ 1.0	11.1
23°	3.06 $\pm$ 0.06	2.0	8.0 $\pm$ 0.0	0.0
25°	3.66 $\pm$ 0.09	2.5	10.0 $\pm$ 0.0	0.0

**Table 4.6:** Summary of statistical results for  $R_c = 0.7$  m,  $\theta = 40$ . As per Table 4.4.

#### 4.3.1.3. Bend geometry: $R_c = 0.55$ m, $\theta = 40^\circ$

A statistically significant, positive linear relationship is observed between channel gradient and average maximum superelevation ( $R^2 = 0.79$ ;  $r = 0.89$ ;  $p = 0.11$ ; Figure 4.9). Standard error for mean superelevation varied between  $\pm 0.0\%$  and  $\pm 6.5\%$  of the respective value.

The power law relationship exhibited between debris flow BEV and superelevation is strong, illustrated by an  $R^2$  value of 0.92 ( $r = 0.96$ ; Figure 4.10), and a  $p$ -value of  $< 0.0001$  suggests that this is statistically significant. This is in stark contrast to the results from bend geometries  $R_c = 0.7$  m.

Average BEV and average maximum superelevation has a similarly strong linear relationship, ( $R^2 = 0.97$ ;  $r = 0.98$ ;  $p = 0.02$ ; Figure 4.11). Standard error for mean BEV does not exceed  $\pm 6\%$  at any of the 4 gradients.

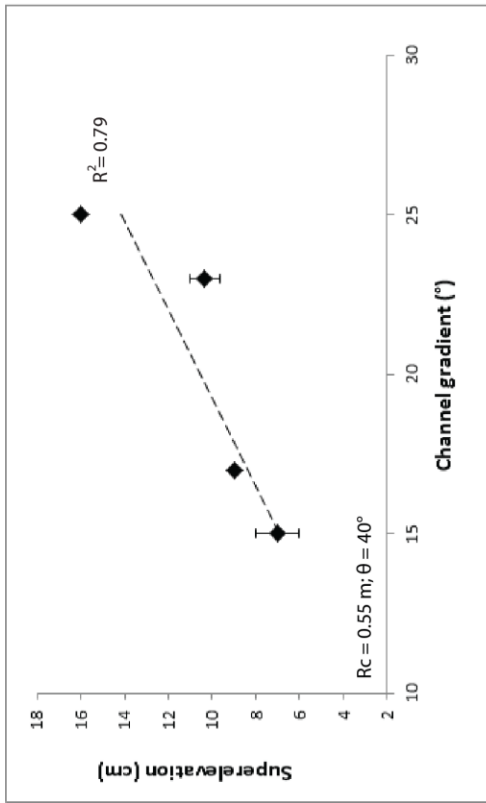


**Figure 4.9:** Average superlevation at each channel gradient As per Figure 4.3.

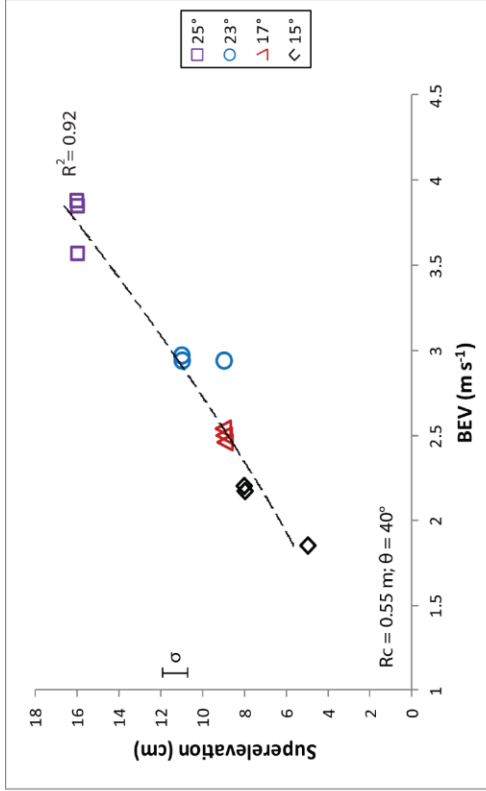


**Figure 4.10:** BEV of each debris flow with the respective maximum recorded superlevation. As per Figure 4.4.

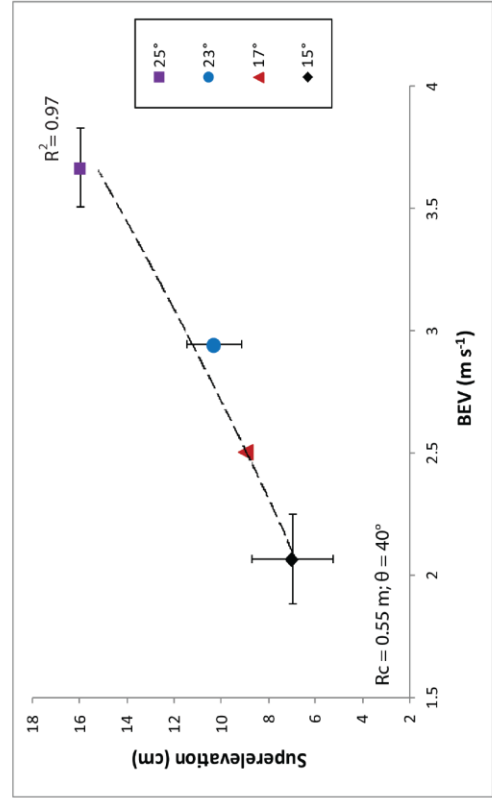


**Figure 4.11:** Average debris flow BEV for each channel gradient and the respective average maximum recorded superlevation. Regression equation:  $y = 2.47 * x^{1.40}$ . As per Figure 4.5.

Relationship	R <sup>2</sup> value	r-value	p-value
Average superelevation versus channel gradient	0.79	0.89	0.11
BEV versus maximum superelevation	0.92	0.96	< 0.0001
Average BEV versus average maximum superelevation	0.97	0.98	0.02

**Table 4.7:** Summary of statistical results for  $R_c = 0.55$  m,  $\theta = 40^\circ$ . As per Table 4.3.

Channel slope	Mean BEV $\pm$ standard error (m s <sup>-1</sup> )	Precision (%)	Mean superelevation $\pm$ standard error (cm)	Precision (%)
15°	2.06 $\pm$ 0.11	5.2	7.0 $\pm$ 1.0	4.5
17°	2.79 $\pm$ 0.15	0.0	9.0 $\pm$ 0.0	0.0
23°	3.06 $\pm$ 0.06	0.0	10.3 $\pm$ 0.7	6.5
25°	3.66 $\pm$ 0.09	2.5	16.0 $\pm$ 0.0	0.0

**Table 4.8:** Summary of statistical results for  $R_c = 0.55$  m,  $\theta = 40^\circ$ . As per Table 4.4.

#### 4.3.1.4. Bend geometry: $R_c = 0.4$ m, $\theta = 40^\circ$

A strong, positive linear relationship is exhibited between channel gradient and average maximum superelevation ( $R^2 = 0.95$ ;  $r = 0.97$ ;  $p = 0.03$ ; Figure 12). Standard error for mean superelevation varied from  $\pm 2.9\%$  to  $\pm 10.6\%$  of the relative values.

A statistically significant power law relationship is displayed between the data for debris flow BEV and maximum recorded superelevation ( $R^2 = 0.64$ ;  $r = 0.80$ ;  $p = 0.002$ ; Figure 4.13). This is similar to the result obtained for  $R_c = 0.55$  m,  $\theta = 40^\circ$ , in contrast to the results from bend configurations  $R_c = 0.7$  m.

The power law relationship exhibited between average maximum superelevation and average BEV is very strong ( $R^2 = 0.97$ ;  $r = 0.98$ ; Figure 4.14) and a  $p$ -value of 0.02 suggests that this is statistically significant at a 95% confidence level. The standard error for mean BEV is less than  $\pm 7\%$  of the respective value for all points. It is of interest to note that average BEV for a channel gradient of  $17^\circ$  is slightly lower than that observed for a channel gradient of  $15^\circ$ , contrary to expectations.

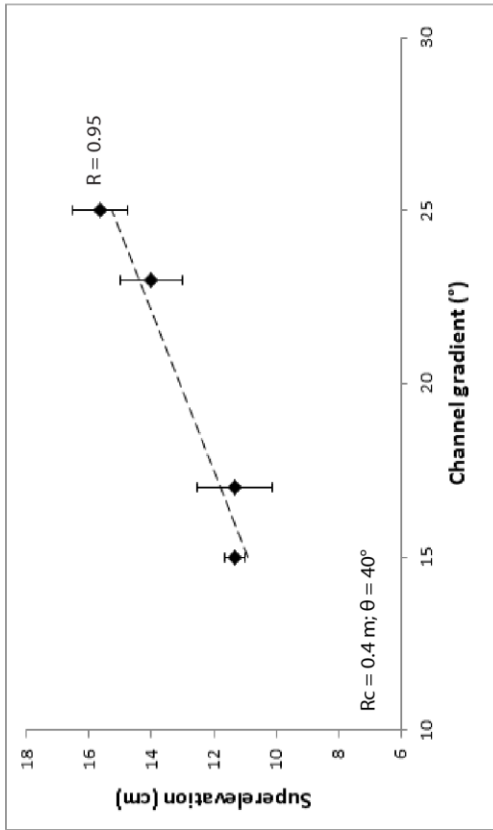


**Figure 4.12:** Average superlevation at each channel gradient  
As per Figure 4.3.

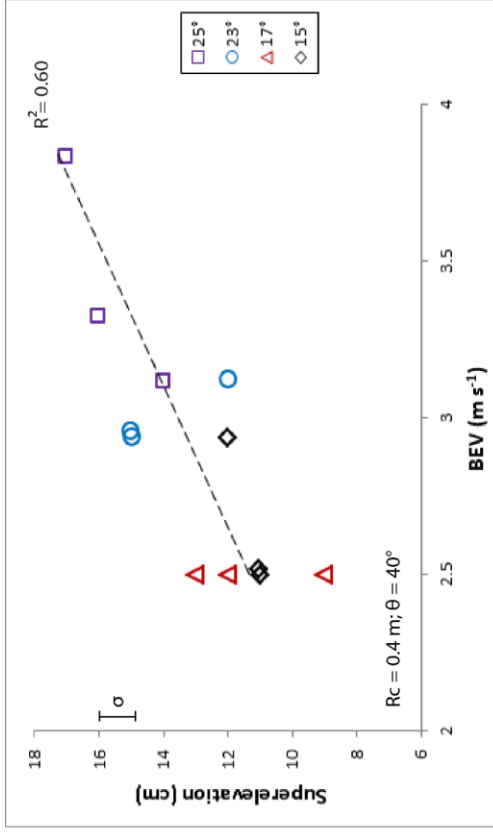


**Figure 4.13:** BEV of each debris flow with the respective maximum recorded superlevation. As per Figure 4.4.

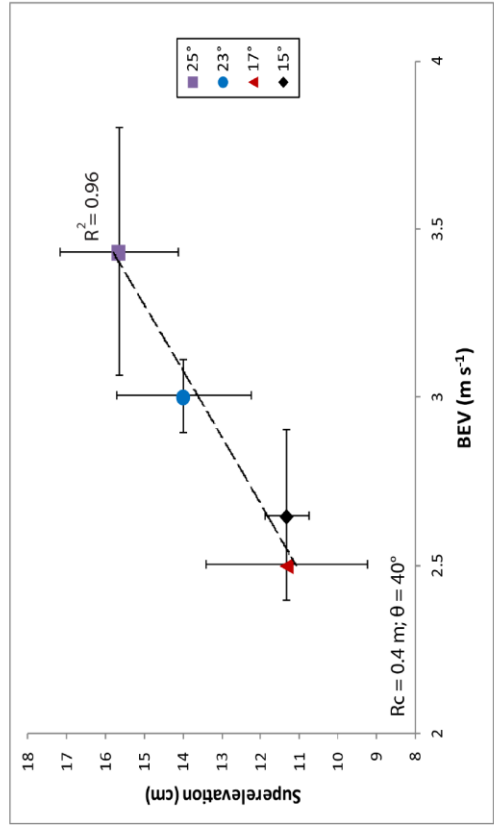


**Figure 4.14:** Average debris flow BEV for each channel gradient and the respective average maximum recorded superlevation. Regression equation:  $y = 3.97 * x^{1.12}$ .  
As per Figure 4.5.

Relationship	R <sup>2</sup> value	r-value	p-value
Average superelevation versus channel gradient	0.95	0.97	0.03
BEV versus maximum superelevation	0.60	0.80	0.002
Average BEV versus average maximum superelevation	0.96	0.98	0.02

**Table 4.9:** Summary of statistical results for  $R_c = 0.4$  m,  $\theta = 40^\circ$ . As per Table 4.3.

Channel slope	Mean BEV $\pm$ standard error (m s <sup>-1</sup> )	Precision (%)	Mean superelevation $\pm$ standard error (cm)	Precision (%)
15°	2.65 $\pm$ 0.15	5.5	11.3 $\pm$ 0.3	2.9
17°	2.50 $\pm$ 0.00	0.0	11.3 $\pm$ 1.2	10.6
23°	3.00 $\pm$ 0.06	2.1	14.0 $\pm$ 1.0	7.1
25°	3.43 $\pm$ 0.21	6.2	15.7 $\pm$ 0.9	5.6

**Table 4.10:** Summary of statistical results for  $R_c = 0.4$  m,  $\theta = 40^\circ$ . As per Table 4.4.

Velocity recordings obtained from curved channel experiments demonstrate that mean BEV was lower than ATV for 15 of the 16 results displayed (Tables 4.3, 4.5, 4.7 and 4.9), and on 9 occasions was in excess of 10% lower than the equivalent ATV result. Potential reasons for this will be discussed in Section 5.1.1.

### 4.3.2. Spatial pattern of superelevation around bends

For all of the channel configurations, the maximum superelevation value observed in the second bend never exceeded that recorded in the first. Of the 48 experiments performed, maximum superelevation was observed exclusively in the first bend on 40 occasions, while in the remaining 8 cases, all for a bend configuration  $R_c = 0.55$  m,  $\theta = 40^\circ$ , superelevation in the second bend was equal to that observed in the first.

In some circumstances, maximum superelevation was recorded at just one location in the curve complex, while at other times maximum superelevation was maintained for up to  $15^\circ$  through the bends.

Of the twelve experiments performed for a bend geometry of  $R_c = 0.7$  m,  $\theta = 20^\circ$ , maximum superelevation was recorded at an angular distance of  $25^\circ$  eight times, and was twice measured to have peaked at  $20^\circ$  and between  $20$ - $25^\circ$ . For this bend geometry, the maximum recorded superelevation was 8 cm, with standard deviation of the mean of  $7.1 \text{ cm} \pm 1.1 \text{ cm}$  (Figure 4.15A).

For the twelve experiments performed at a bend geometry of  $R_c = 0.7$  m,  $\theta = 40^\circ$ , maximum superelevation was recorded on three occasions between  $30$ - $40^\circ$ ,  $35$ - $40^\circ$  and  $30$ - $45^\circ$  angular distance through the curves; twice recorded peaking between  $25$ - $40^\circ$  and once between  $25$ - $35^\circ$ . The maximum recorded superelevation was 10 cm, with standard deviation of the mean value of  $8.6 \text{ cm} \pm 1.3 \text{ cm}$  (Figure 4.15B).

For the twelve experiments carried out with a channel configuration  $R_c = 0.55$  m,  $\theta = 40^\circ$ , maximum superelevation was recorded on three occasions between  $35$ - $40^\circ$  and  $35$ - $45^\circ$ , twice at  $40^\circ$  alone and  $30$ - $35^\circ$ , and once at both  $30$ - $45^\circ$  and  $40$ - $50^\circ$ . Maximum superelevation was observed at 16 cm, with a mean standard deviation of  $10.6 \text{ cm} \pm 3.6 \text{ cm}$  (Figure 4.15C).

On four of the twelve occasions, maximum superelevation was observed at an angular distance of  $45^\circ$  alone and  $45$ - $50^\circ$  for a bend with  $R_c = 0.4$  m and  $\theta = 40^\circ$ . In a further two experiments, maximum superelevation was measured between  $40$ - $45^\circ$ , and once at both  $40^\circ$  and  $50^\circ$  individually. Maximum superelevation was measured at 17 cm, with a mean value of  $13.1 \text{ cm} \pm 2.3 \text{ cm}$  (Figure 4.15D).

As radius of curvature decreases, the location in the curve complex where maximum superelevation is observed is further into the curves, i.e. the debris flows are peaking at an increased angular distance through the bends (Figure 4.16). This observation is related to the incidence angle at which the centreline of the debris flow comes into contact with the outside wall of the channel and will be discussed in Section 5.2.3.

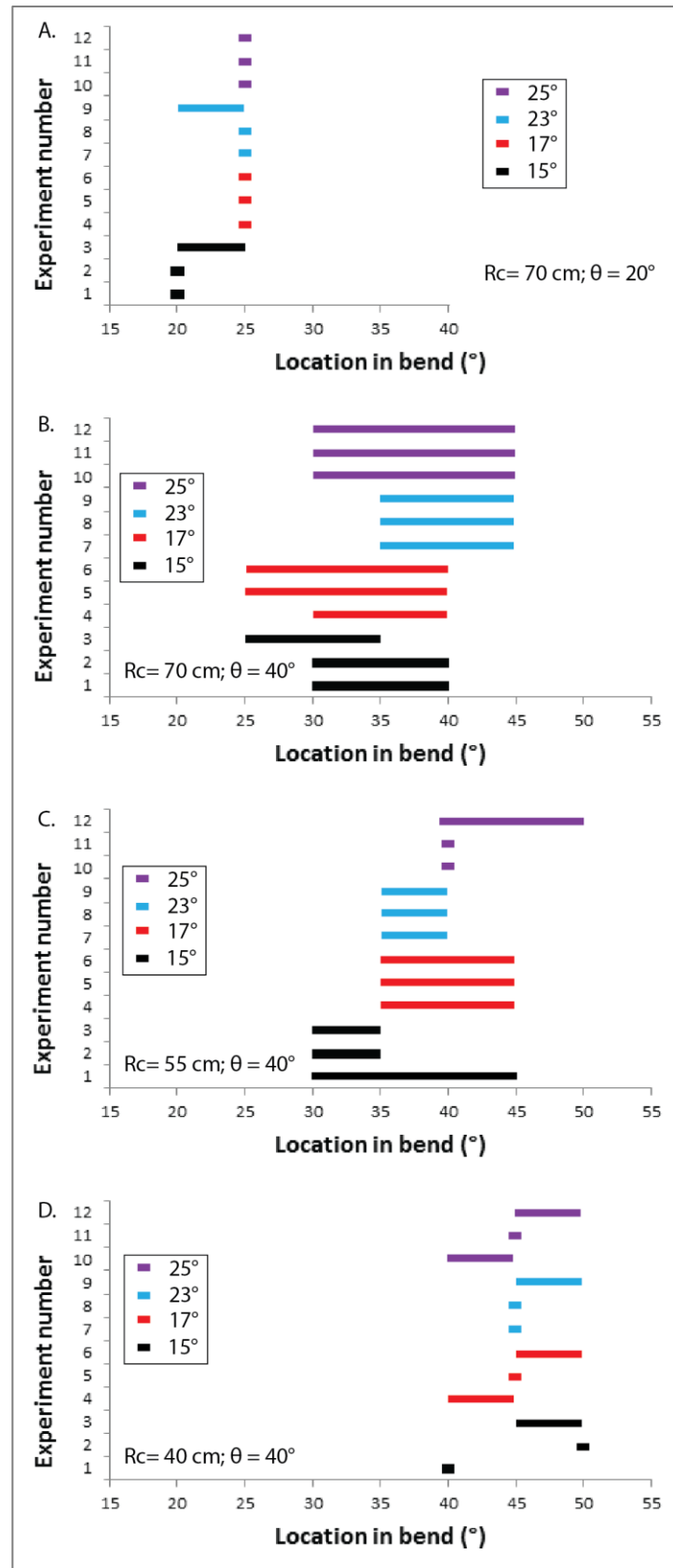


**Figure 4.15:** A schematic representation demonstrating the varying location in the bend complex where maximum superelevation was observed for channel geometry:  
**A.**  $R_c = 0.7 \text{ m}, \theta = 20^\circ$ ; **B.**  $R_c = 0.7 \text{ m}; \theta = 40^\circ$ ; **C.**  $R_c = 0.55 \text{ m}; \theta = 40^\circ$ ;  
**D.**  $R_c = 0.4 \text{ m}; \theta = 40^\circ$

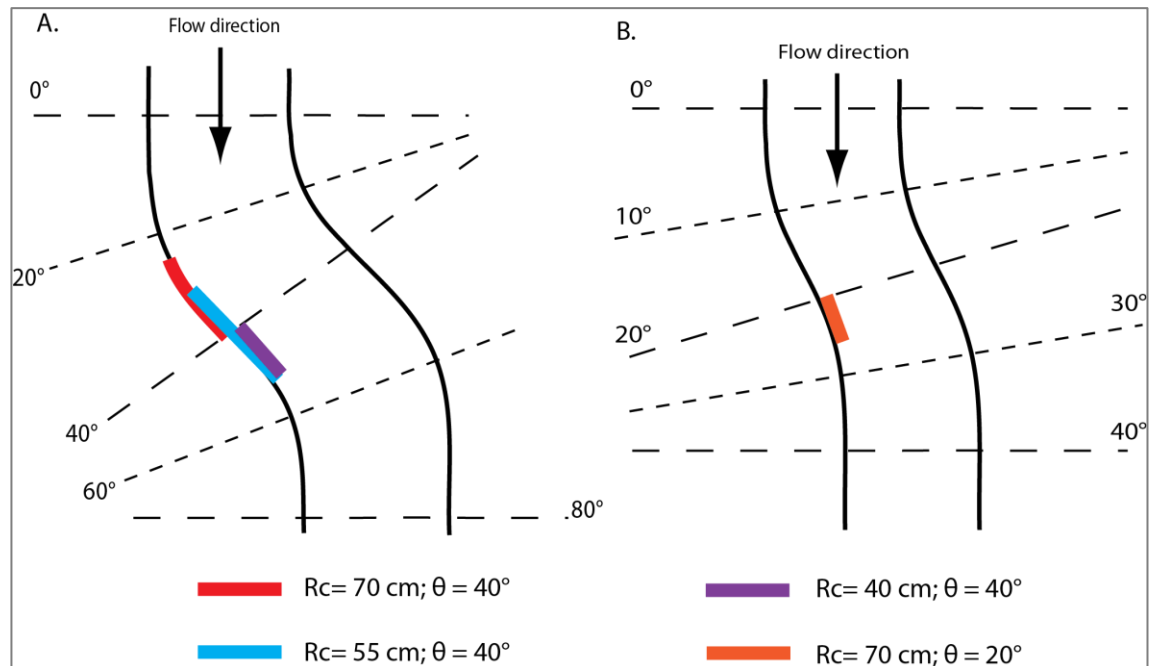


**Figure 4.16:** Location of maximum superlevation in curves: **A.** where  $\theta = 40^\circ$ , and **B.** where  $\theta = 20^\circ$

### 4.3.3. Superlevation versus radius of curvature

The results presented in Section 4.3.1. demonstrate that as radius of curvature decreases the magnitude of observed superlevation increases. The superlevation data obtained from channel configurations with a bend angle of  $40^\circ$  has been collated and is displayed in Figure 4.17. These results illustrate how superlevation increases with decreasing radius of curvature, and with increasing BEV.

Of the five velocity bands displayed, it was possible to calculate an average superlevation at three of these, with results for each radii of curvature (Figure 4.18). Velocity bands  $2\text{-}2.5 \text{ m s}^{-1}$  and  $2.51\text{-}3 \text{ m s}^{-1}$  demonstrate the relationship clearly, exhibiting very strong power law relationships ( $R^2 = 0.99$  and  $1.00$  respectively). This is also strong, albeit less pronounced for  $3.5\text{-}4 \text{ m s}^{-1}$  ( $R^2 = 0.77$ ). However, it is not possible to assess the statistical significance of these relationships with only three data points available.

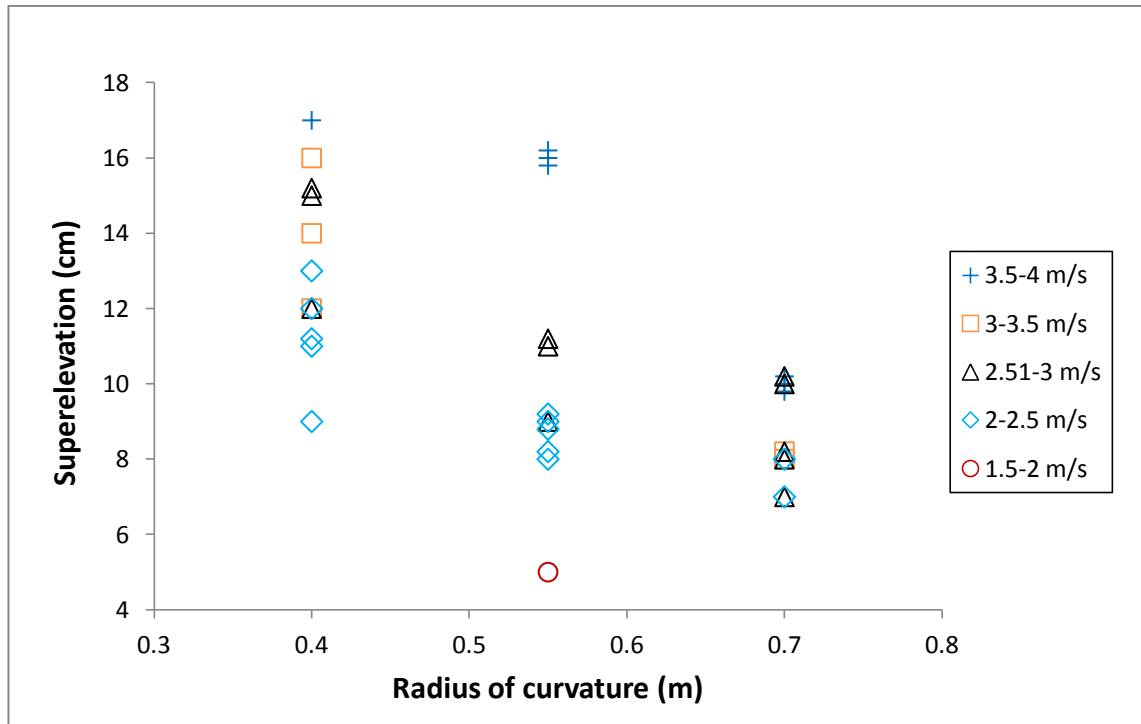


**Figure 4.17:** Superlevation across varying radii of curvature with differing BEVs ( $n = 36$ ).

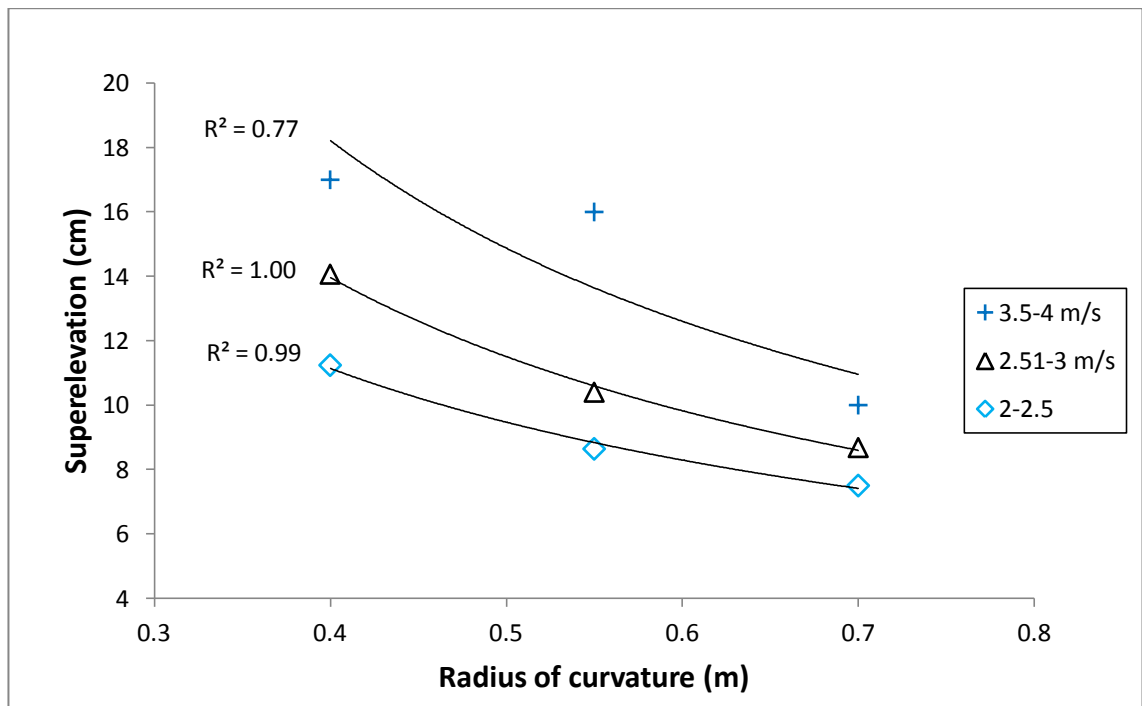


**Figure 4.18:** Average superlevation at each radius of curvature across 3 complete BEV bands. Standard errors are shown as bars and power law trendlines have been fitted to the data with an  $R^2$  value.

#### 4.3.4. Superelevation versus bend angle

To investigate how bend angle influences superelevation, radius of curvature remained constant at 0.7 m while bend angle was varied between  $20^\circ$  and  $40^\circ$ . From the results presented in Sections 4.3.1.1 and 4.3.1.2, it is evident at each channel gradient that superelevation is greatest for a bend angle of  $40^\circ$ , although there is a minor overlap between the data (Figure 4.19). Average superelevation at each channel gradient was 6 cm, 7.6 cm, 7 cm and 7.6 cm where  $\theta = 20^\circ$  at channel gradients of  $15^\circ$ ,  $17^\circ$ ,  $23^\circ$  and  $25^\circ$  respectively, while for  $\theta = 40^\circ$  average superelevation was recorded at 7.3 cm, 9 cm, 8 cm and 10 cm across the same gradient range.

However, upon analysis of the spatial pattern of superelevation within each curve, there was less consistency. For example, superelevation peaked between  $20$ - $25^\circ$  for a bend geometry of  $R_c = 0.7$  m,  $\theta = 20^\circ$ . However, on five occasions the magnitude of superelevation recorded at this location was greater than that observed for the same location where  $R_c = 0.7$  m,  $\theta = 40^\circ$ : twice for a channel gradient of  $15^\circ$ , once at  $17^\circ$  and twice more at  $23^\circ$ .

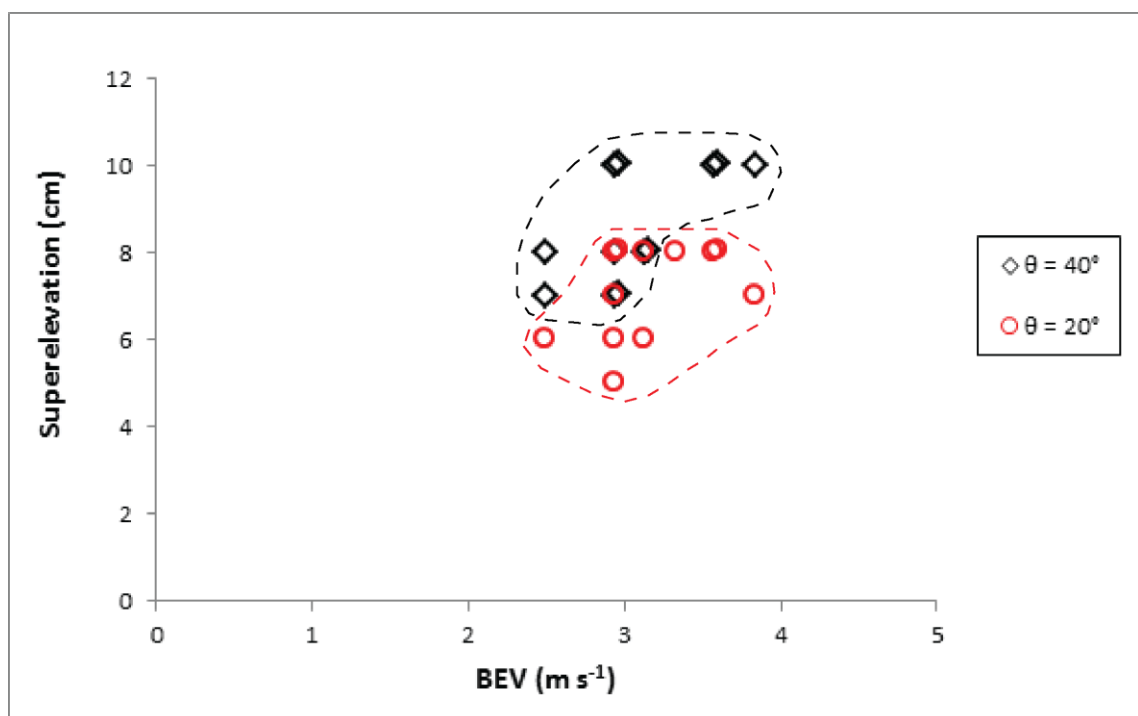


**Figure 4.19:** Superelevation at differing BEVs for  $\theta = 20^\circ$  and  $\theta = 40^\circ$  at  $R_c = 0.7$  m. Note, overlapping data points indicates repetition of the result.

This dataset demonstrates the role of bend angle upon the resulting magnitude of superelevation. However, the results obtained from the two differing bend configurations where  $R_c = 0.7$  m had the weakest relationship with BEV, and therefore it is perhaps not plausible to discern or quantify the extent to which bend angle influence superelevation.

#### 4.4. Summary of results

The results presented in this chapter have been collected with a mixture of video-based and direct observations. In the straight channel experiments, a distinct flow velocity pattern was evident, with an initial acceleration phase followed by a period of stable velocity. At channel gradients of  $15^\circ$  and  $17^\circ$ , this was succeeded by a pronounced deceleration stage, although this was reduced at a channel slope of  $23^\circ$ , and not evident at  $25^\circ$ . A very strong and statistically significant relationship was exhibited between channel gradient and AV, and ATV.

A strong positive, power law trend was observed between debris flow velocity and superelevation across the four differing bend geometries.

The spatial pattern of superelevation in the channel curves was seen to vary across the bend geometries. Maximum superelevation was observed to occur further through the bend complex as radius of curvature decreased, i.e. as the bends became tighter. Furthermore, when bend angle was varied between  $20^\circ$  and  $40^\circ$ , on occasion superelevation was distinctly different between the two differing geometries, even at the same angular location in the curves.

The power law relationship exhibited between radius of curvature and superelevation was strong, demonstrating an increase in superelevation as radius of curvature decreased which is consistent with the theory of Equation 6. The observed superelevation results presented in this chapter will be compared with predicted values and discussed in Chapter 5 for an analysis of the superelevation equation (Eq. 6).

A general trend was evident between superelevation and bend angle, with observed superelevation for a bend angle of  $40^\circ$  exceeding that recorded for a  $20^\circ$  curve, although there was a minor overlap in the data.

## Chapter 5: Discussion

This chapter provides a synthesis of the main results presented in Chapter 4 and how the results achieve the overarching aim and the four research objectives specified in Chapter 1. Where possible, results will be compared with previous investigations; and the superelevation equation (Eq. 6) will be critiqued using observed and predicted values to better inform whether the equation is a reliable description of debris flow dynamics in curved channels.

$$v = \left[ \frac{g R_c \Delta h}{k b} \right]^{0.5} \quad \text{Equation 1}$$

### 5.1. Effect of channel gradient upon debris flow velocity

The straight channel experiments performed in this investigation fulfil the first research objective. The results help improve understanding of the relationship between debris flow velocity and channel gradient.

#### 5.1.1. Velocity results

The average velocity profiles for the straight channel experiments show phases where velocity appears to fluctuate during the ‘quasi-stable velocity’ period. This is most significant for a channel gradient of 25° (Figure 4.1D). Similarly, for the majority of the curved channel experiments mean BEV was lower than the equivalent ATV for the same channel gradient. These occurrences suggest that some internal processes are operating within the flow, such as small-scale debris flow deceleration and surging (Davies, 1986; Davies, 1990; Davies, 1992). Alternatively, this variation could be due to the method of velocity recording, where velocity was calculated by monitoring the number of frames taken for the flow to travel a set distance; a time increment fixed distance method (Section 3.3.2.). However, using this method the velocity was not recorded if the position of the flow front was just before a reference marker (Figure 5.1, fine dotted line), and so ultimately in the following frame when the time could be recorded the position of the flow front may have been significantly beyond the reference marker. Consequently, this would impact upon the velocity of the flow at that location. The error associated with this is estimated to be  $\pm 0.3 \text{ m s}^{-1}$ , equating to approximately  $\pm 10\%$  depending on the relative velocity where this occurs.

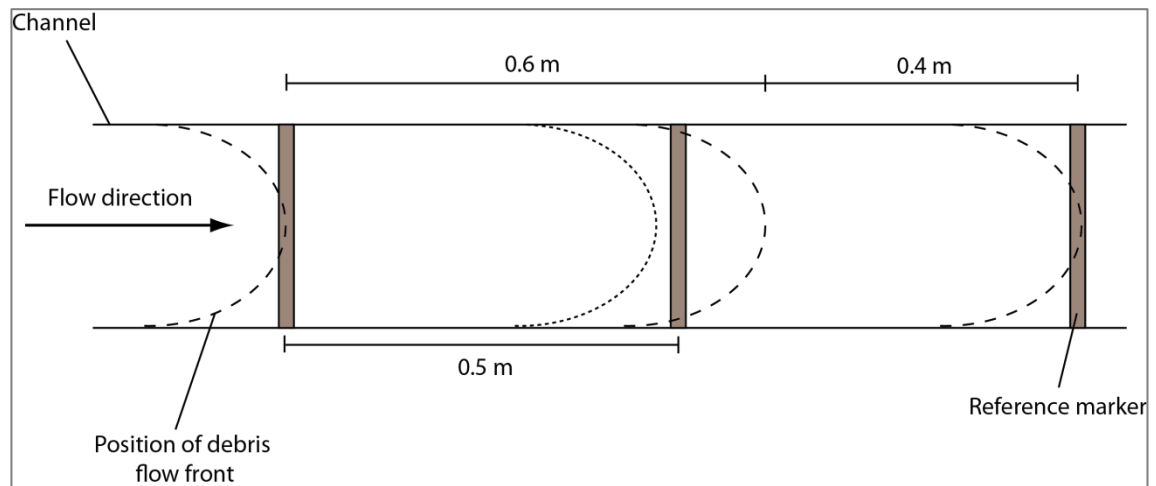


**Figure 5.1:** *Demonstration of debris flow front position in video analysis.*

Therefore, a recommendation to improve the resolution of the method in future investigations would be to calculate velocity for each time frame by recording the variable distances travelled, i.e. using a distance-by-frame method, rather than frame-by-distance.

In the straight channel experiments, a deceleration phase was observed at slope angles of  $15^\circ$ ,  $17^\circ$  and  $23^\circ$ . For channel gradients of  $15^\circ$  and  $17^\circ$ , the deceleration of flow began after 5.5 m; while at  $23^\circ$  this phase was less pronounced, occurring after 7 m from the headgate. It is hypothesised that this deceleration was brought about through formation of a granular debris flow front, thus increasing friction at the head of the debris flow. The granular front was observed to have formed between 1-1.5 m from the headgate, and flow continued to accelerate until velocity was stable. However, upon formation of the characteristic debris flow head, friction increased due to the direct interaction of large, coarse particles with one another (Costa, 1984; Davies, 1986; Davies, 1990; Iverson, 1997; Lorenzini and Mazza, 2004). Consequently, at channel gradients of  $15^\circ$ ,  $17^\circ$  and  $23^\circ$ , the slope of the channel was insufficient to enable velocity to increase to such an extent that it would dominate over the frictional forces within the debris flow head (Hampton, 1975).

Although the deceleration phase observed at such high channel gradients is unexpected, it is not uncommon for naturally occurring debris flows to stop in a steep channel (Costa, 1984; Davies, 1986; Innes, 1983). Moreover, as debris flow motion ceases in a channel, it forms a dam, blocking the channel and causing further material to build up behind the dam until sufficient material has accumulated to bring about remobilisation of the sediment. It is this process that gives debris flows their

characteristic surge-like behaviour (Costa 1984, Davies, 1986; Innes, 1983). Therefore, if the artificial channel was extended in this investigation, with a sustained supply of debris flow material flowing down the channel, it is possible that this behaviour would be observed.

### 5.1.2. Comparison with previous investigations and theory

The results collected from the straight channel experiments appear to produce a strong linear relationship between channel gradient and velocity. This is generally consistent with the theory of laminar flow in open channel flow (Davies, 1986; Enos, 1977).

Further analysis of the debris flow hydraulics was performed by applying a Newtonian laminar flow model and Manning-Strickler's Newtonian turbulent flow model (Eq. 7) (Lorenzini and Mazza, 2004; Rickenmann, 1999) to approximate the flow:

$$V = C_r H^\alpha S^\beta \quad \text{Equation 7}$$

Where:

- $V$  = Mean flow velocity ( $\text{m s}^{-1}$ )
- $C_r$  = An empirical constant dependent upon the values of  $\alpha$  and  $\beta$
- $H$  = Flow depth (m)
- $\alpha$  = Exponent of  $H$
- $S$  = Channel slope ( $^\circ$ )
- $\beta$  = Exponent of  $S$  (Radians)

Although debris flow hydraulics are not strictly comparable with those of water flows due to high sediment concentrations and solid particle interactions, empirical evidence has shown that conventional resistance laws (Eq. 7) can be used to approximate the bulk flow. Here, the mean flow velocity is modelled as a function of flow depth ( $H$ ), slope, ( $S$ ) and a coefficient of overall resistance ( $C_r$ ). Exponents in Equation 7 used in the Newtonian laminar flow model and Manning-Strickler's Newtonian turbulent flow model are given in Lorenzini and Mazza (2004, Table 5.7) and are used to construct the theoretical relationships shown in Figure 5.2.

Three of the four average terminal velocity (ATV) results lie directly on the turbulent flow line, which suggests that flow is turbulent rather than laminar, and that velocity has a power-law relationship with channel slope (Figure 5.2). This result is expected because the debris flow mixture used has a relatively low viscosity. Debris flow viscosity is strongly dictated by sediment composition of the mixture, which in turn may control the 'n' value in the Manning-Strickler equation, thus influencing the flow regime in a debris flow (Lorenzini and Mazza, 2004; Rickenmann, 1999). Similar relationships have also been found from previous research which supports these findings (Julien and Paris, 2010; Rickenmann, 1993). Additionally, the ATV results provide a better fit with turbulent flow than average velocity (AV) results because flow resistance (friction) was measured indirectly, and therefore is probably underestimated.

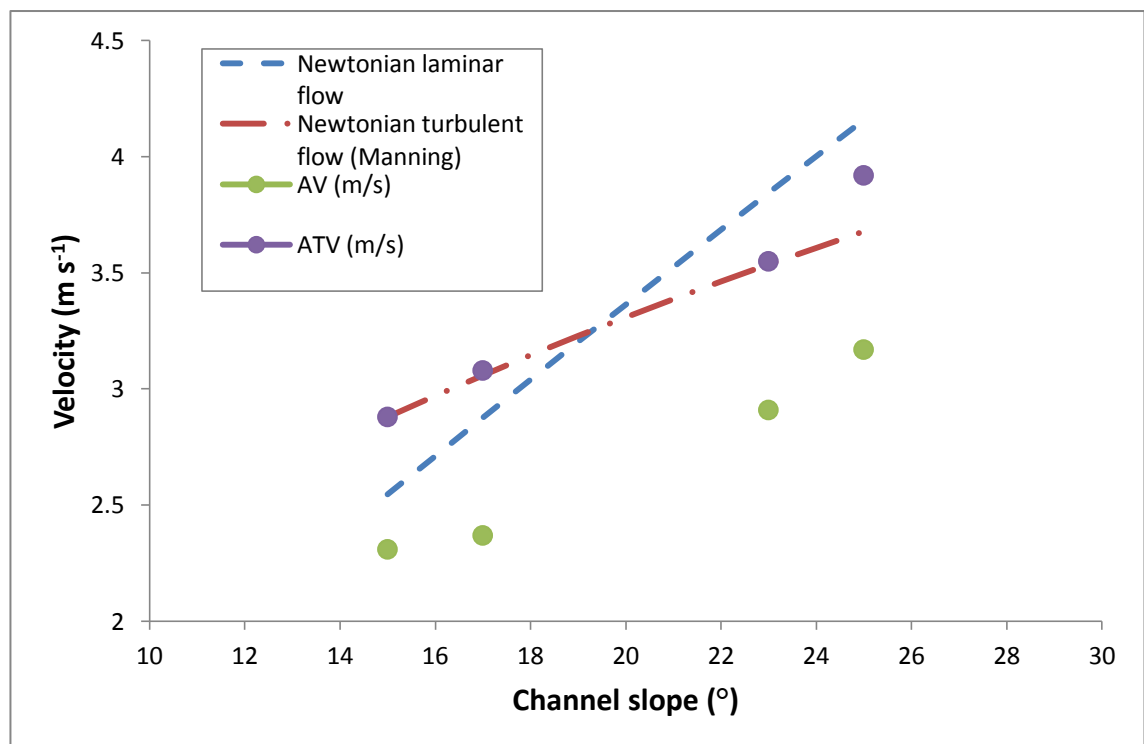


**Figure 5.2:** Demonstration of debris flow hydraulics using experimental and literature-based data. Note, dashed lines do not follow a linear relationship, although this appears to be the case owing to the relatively small range in values across which the data is displayed.

Consequently, it is hypothesised that if the viscosity of the mixture was increased, for example by increasing the fine, cohesive sediment content, the trend exhibited by velocity and channel slope should rotate counter-clockwise, and align more closely with the laminar flow line.

## 5.2. Curved channel experiments

The results obtained from the curved channel experiments allow the exploration of the second and third objectives: to study the influence of velocity and radius of curvature respectively upon superelevation, and form the basis for investigating the fourth objective: to test the accuracy of the superelevation equation for estimating debris flow velocity.

### 5.2.1. Velocity and superelevation

The curved channel experiments produced results which demonstrate a power law relationship between superelevation and bend entry velocity (BEV). For a bend configuration of  $R_c = 0.7$  m,  $\theta = 20^\circ$ , the relationship between average superelevation and average BEV had a  $p$ -value of 0.35, while for bend geometry  $R_c = 0.7$  m,  $\theta = 40^\circ$  exhibited a  $p$ -value of 0.25, both of which suggest a lack of a statistically significant relationship (Table 4.2; Table 4.4). Despite this, at tighter bend geometries of  $R_c = 0.55$  m,  $\theta = 40^\circ$  and  $R_c = 0.4$  m,  $\theta = 40^\circ$  the power law relationship between superelevation and BEV is statistically significant, as illustrated by  $p$ -values of 0.02 at both configurations (Table 4.6; Table 4.8). This suggests that a radius of curvature of 0.7 m is too subtle for debris flow superelevation to be reliably observed.

Furthermore, this power law relationship is consistent with the theorised relationship between velocity and superelevation demonstrated in Equation 6.

Additionally, there were some data points where superelevation did not change despite increased velocity or vice versa, such as those at  $15^\circ$  in Figure 4.4. This is unusual and could be attributed to experimental error or signify some internal processes operating within the flow.

However, the datasets used to analyse these relationships are relatively small, with only 12 experiments performed for each of the four bend geometries. Additionally, due to constraints with the experimental flume, there is a hiatus in the data spanning between channel gradients of  $17^\circ$  and  $23^\circ$  which prevents more detailed observations over this range of slopes.

Unfortunately, there are no previous work observations of this aspect of debris flow behaviour in the literature, so this remains a hypothesis for further testing.

### 5.2.2. Role of radius of curvature

The results presented in Section 4.3.3. demonstrate how superelevation increases as radius of curvature decreases. However, as illustrated in Figure 4.18, there are few data points which have a consistent BEV, and occur at each of the three radii of curvature where  $\theta = 40^\circ$ . Therefore, to explore this trend more closely the relationship will be examined for a constant BEV at each radii of curvature (using the regression equation for each power law trendline between superelevation and BEV, from Figures 4.8, 4.11 and 4.14). For this simulation, a consistent BEV of  $3 \text{ m s}^{-1}$  will be used in conjunction with the regression equations to predict the approximate magnitude of superelevation at each of the three bend geometries where  $\theta = 40$ . Using this technique produces superelevation estimations of 8.4 cm for  $R_c = 0.7 \text{ m}$ , 11.5 cm for  $R_c = 0.55 \text{ m}$ , and 13.6 cm for  $R_c = 0.4 \text{ m}$  (Figure 5.3). However, it is not sensible to apply a trendline or statistical analysis to this data with only three data points available.

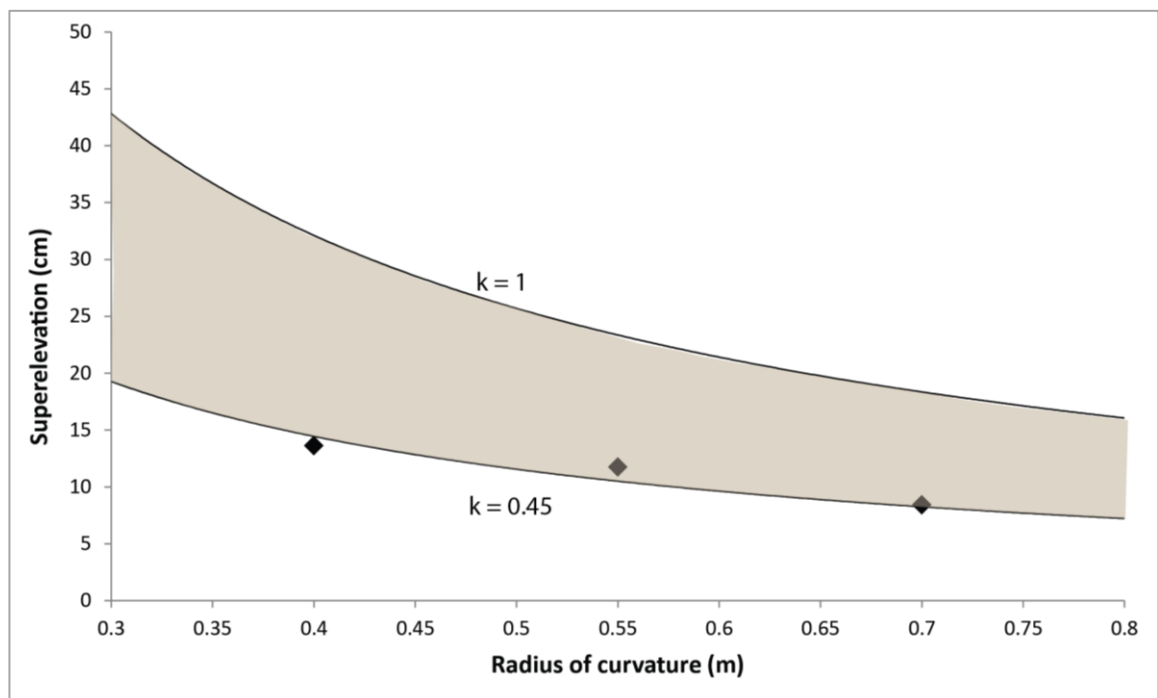


**Figure 5.3:** Predicted superelevation using power law trendline gradients for a constant BEV of  $3 \text{ m s}^{-1}$ . Shaded area represents the range in predicted superelevation for a range of 'k' values. Equation parameters:  $b = 0.14$ ,  $v = 3 \text{ m s}^{-1}$ .

It is apparent that a value for  $k$  of 1, commonly applied in much of the literature (Section 2.2), considerably overestimates predicted superelevation (18.3 cm, 23.4 cm and 32.1 cm) by over 100% in comparison to the magnitude of estimated superelevation above. Therefore an approximate value of  $k = 0.45$ , calculated using Equation 8 (Section 5.3.3.), fits the observed data from this investigation much more accurately (Figure 5.3). However, it would be inappropriate to assign a value for  $k$  of 0.45 for all future investigations, especially those studying natural debris flows without further, more detailed analysis of this coefficient.

### 5.2.3. Role of bend angle

Observations from the curved channel experiments reveal that as radius of curvature decreases, superelevation peaks at an increased angular distance through the bend. This result is linked to the incidence angle at which the centreline of the debris flow strikes the outside wall of the channel (J Warburton, *pers. comms.*, November 2011). The calculated incidence angle is approximately  $28^\circ$  for a bend geometry  $R_c = 0.7$  m,  $\theta = 40^\circ$ , whereas for  $R_c = 0.55$  m,  $\theta = 40^\circ$  this angle is  $32^\circ$ . Furthermore, for a bend geometry  $R_c = 0.4$  m,  $\theta = 40^\circ$  the incidence angle is greater still at  $36^\circ$ .

For a bend configuration  $R_c = 0.7$  m,  $\theta = 20^\circ$ , less than 50% of the debris flow width comes into contact with the outside wall of the curve. This significantly reduces the extent to which superelevation occurs because the main body of the flow is less influenced by the bend geometry. Therefore, this may explain why a clear trend of superelevation is not visible for this bend geometry. However, the two differing bend geometries ( $R_c = 0.7$  m) used for analysing the influence of bend angle had relatively weak relationships with superelevation in comparison to experiments with  $R_c = 0.55$  m,  $\theta = 40^\circ$  and  $R_c = 0.4$  m,  $\theta = 40^\circ$ , therefore a clear and quantifiable relationship is not established.

For the first time, it has been clearly established that both radius of curvature and bend angle play an influential role in dictating the magnitude of superelevation. However, discerning the relative importance of one parameter over the other is not feasible without further experiments across greater ranges of radii of curvature and bend angles.

### 5.3. Testing the superelevation equation

The superelevation equation is commonly used to estimate debris flow velocity reconstructed from debris flow deposits preserved around channel bends (Section 1.5). Here, the predicted magnitudes of superelevation will be compared to those recorded in the debris flow experiments.

#### 5.3.1. Observed vs. predicted superelevation

Predicted values of superelevation (Eq. 6) were compared with observed superelevation data from experimental tests where  $\theta = 40^\circ$ . In the equation, a default value for  $k$  of 1 was used, as this was the general consensus used in the literature (Section 2.2), and an approximate flow width ( $b$ ) of 0.14 m was input, as observed in the experiments.

It is apparent that there is a disparity between the observed and predicted superelevation values. In all instances where  $k = 1$ , observed values for superelevation are always less than the predicted values (Figure 5.4). However, as the value for  $k$  is adjusted to less than 1, the correlation between observed and predicted superelevation becomes much closer to a 1:1 ( $y = x$ ) relationship. This is demonstrated in the gradient of the trendlines for each data series. The predicted and observed superelevation results for  $k = 1$  has a slope of 0.45, while a gradient of 0.64 exists where  $k = 0.7$ . Further, the results for a  $k$  value of 0.45 have a trendline gradient of 1.0. In each instance where  $k$  is varied, the linear trendlines intercept the y-axis at 0 cm.

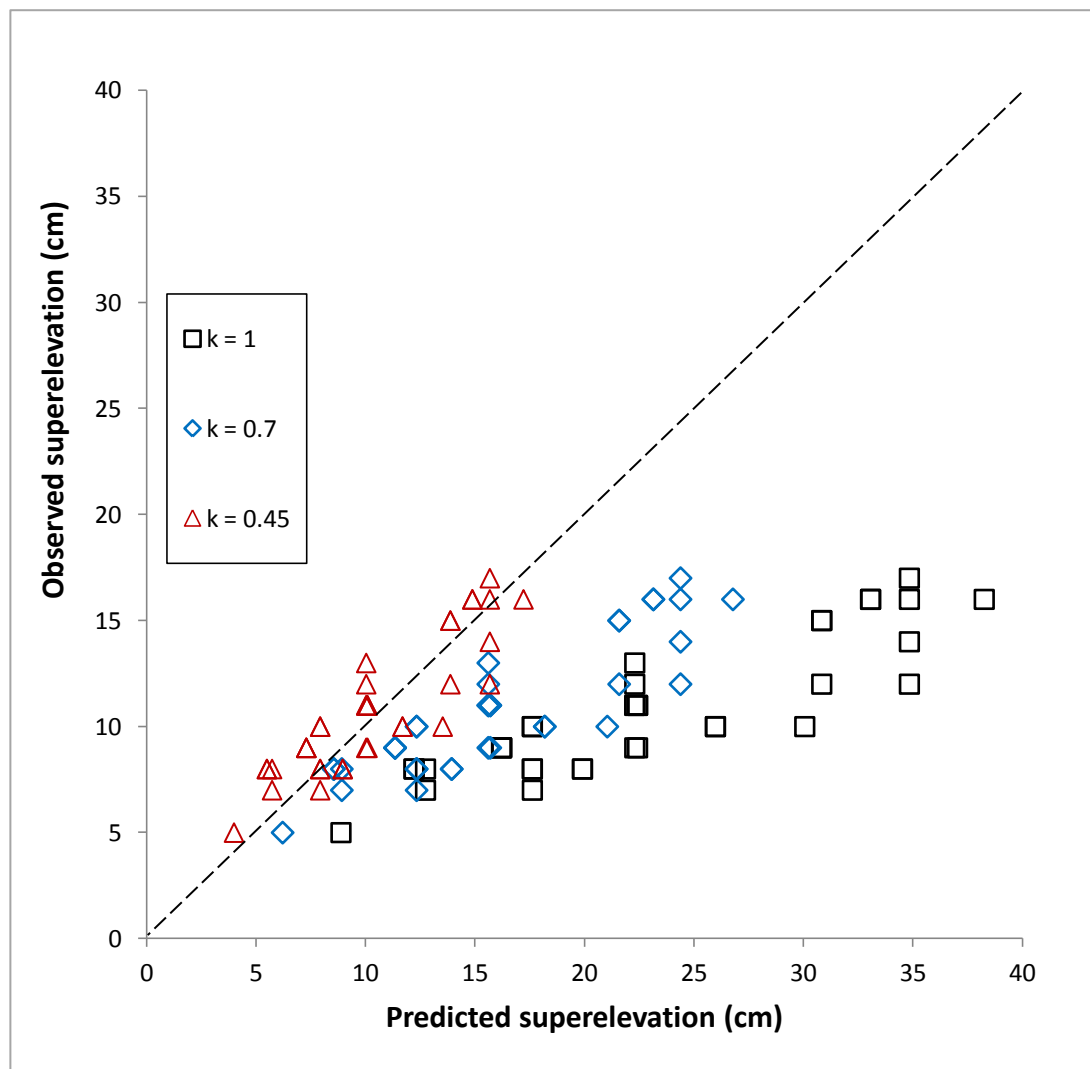


**Figure 5.4:** Discrepancy between predicted and observed superelevation values, with varying 'k'. Dashed line indicates 1:1 relationship.

Analysis of the experimental and theoretical results shows that predicted superelevation consistently exceeds the observed values (Table 5.1), although the extent to which this occurs is variable. The most accurate result revealed by this technique was an overestimation by 50.0%, recorded for an observed superelevation of 8 cm, and a predicted value of 12 cm (Table 5.1). In some cases, the predicted superelevation was three times greater (30 cm; 53 cm) than the actual observed figure (10 cm; 17 cm; Table 5.1).

However, when this method was applied to the experimental tests for  $R_c = 0.7$  m,  $\theta = 20^\circ$ , the difference between the predicted and observed superelevation values became even greater (Table 5.2). This is because the superelevation equation does not take into account the influence of bend angle upon the resulting magnitude of

superelevation, and so therefore does not differentiate between a curve with bend angle of  $20^\circ$  and another of  $40^\circ$ . Consequently, predicted superelevation is the same for both bend configurations where  $R_c = 0.7$  m.

It is apparent that this discrepancy is a significant drawback to the superelevation equation, and thus further work should concentrate on the introduction of a parameter to account for the influence of bend angle.

Radius of curvature (m)	Observed velocity ( $\text{m s}^{-1}$ )	Observed average superelevation (cm)	Predicted superelevation (cm)	Overestimation (%)
0.7	2.5	7.5	13	73.3
0.7	2.94	8.6	18	109.3
0.7	3.13	8.0	20	150.0
0.7	3.57	10.0	26	160.0
0.7	3.84	10.0	30	200.0
0.55	1.85	5.0	9	80.0
0.55	2.17	8.0	12	50.0
0.55	2.5	9.0	16	77.8
0.55	2.94	10.3	22	112.9
0.55	3.57	16.0	33	106.3
0.55	3.84	16.0	38	137.5
0.4	2.5	11.2	22	96.4
0.4	2.94	14.0	31	121.4
0.4	3.13	13.0	35	169.2
0.4	3.33	16.0	40	150.0
0.4	3.84	17.0	53	211.8

**Table 5.1:** Summary of predicted and average observed superelevation from experiments where  $\theta = 40^\circ$ , with overestimation included. Equation parameters:  $k = 1$ ,  $b = 0.14$  m.

Radius of curvature (m)	Observed velocity ( $\text{m s}^{-1}$ )	Observed average superelevation (cm)	Predicted superelevation (cm)	Overestimation (%)
0.7	2.5	5.0	13.0	160.0
0.7	2.94	7.0	18.0	157.1
0.7	3.13	7.0	20.0	185.7
0.7	3.33	8.0	23.0	187.5
0.7	3.57	8.0	26.0	225.0
0.7	3.84	7.0	30.0	328.6

**Table 5.2:** Summary of predicted and average observed superelevation from experiments where  $\theta = 20^\circ$ , with overestimation included. Equation parameters:  $k = 1$ ,  $b = 0.14 \text{ m}$ .

### 5.3.2. Comparison with previous studies of superelevation

Scaling results from this investigation with back-calculated estimates in previous studies is difficult due to the number of parameters involved. Four independent variables: flow width, flow velocity, flow depth and radius of curvature; and one dependent variable: superelevation, need to be known. Additionally, a lack of available field data in the literature increases this difficulty further. For example, Muñoz-Salinas *et al.* (2007) document a comprehensive dataset back-calculating velocity for lahars, but because these have a volcanic origin and differ slightly from debris flows comparisons cannot be easily made (Innes, 1983). Consequently, in the absence of comparable data a scaling comparison with naturally occurring debris flows has not been performed.

In previous studies, the velocity estimation produced from the superelevation equation has been found to be within 30% of the actual velocity recorded at that location (Berti *et al.*, 1999; Bovis and Jakob, 1999; Iverson *et al.*, 1994; Muñoz-Salinas *et al.*, 2007; Pierson, 1985; Webb *et al.*, 1988). However, there appears to be some disagreement within the literature, with some sources believing these velocity estimates should be regarded as maxima (Bovis and Jakob, 1999; Costa, 1984; Johnson and Rodine, 1984) because the unstable flow in the passage of the frontal bore can cause the presence of splash marks which exaggerate the apparent superelevation. On the contrary, other investigations have concluded that the estimated velocities produced

from the equation should be viewed as minima (Crudden and Lu, 1992; Pierson, 1985; Webb *et al.*, 1988) because the equation does not take into account any loss of energy through friction and other sources.

Of the two circumstances above, experimental results from this investigation support the view that the values for predicted superelevation should be regarded as maxima. However, discrepancies between predicted and observed results (discussed in Section 5.3.1.) show distinctly different results even when using the same channel and debris flow parameters. For example, in one instance observed superelevation was 17.0 cm, while the predicted value for the same parameters and channel morphology was 53.0 cm; a significant overestimation.

### 5.3.3. Variability and impact of 'k' factor

As discussed in Section 2.2,  $k$  is a dimensionless number accounting for viscosity and vertical sorting within a flow, although the value assigned to this has been noted to vary from 0.1-10 in previous publications (Bulmer, 2002; Chen, 1987), a discrepancy of two orders of magnitude.

However, by rearranging the superelevation equation to make  $k$  the subject (Eq. 8), it is possible to calculate the value of  $k$  for experimental data:

$$k = \frac{R_c g \Delta h}{b v^2} \quad \text{Equation 8}$$

The minimum value of  $k$  estimated using this technique for curves with a bend angle of  $40^\circ$  was 0.33, while the maximum calculation of  $k$  was 0.65; for  $\theta = 20^\circ$  the minimum value of  $k$  was 0.23, with a maximum of 0.45 (Table 5.3; Figure 5.5).

These values of  $k$  are in contrast to the theory discussed in Section 2.2, where it was suggested that  $k$  could not be less than 1. These lower than anticipated values for  $k$  could in part be attributed to the superelevation equation not accounting for the effects of friction with the channel bed and banks. Therefore, if energy losses to friction were taken into account, the value for  $k$  would inevitably be greater. Furthermore, whilst the values expressed for  $k$  are significantly below those suggested earlier, there is still some variation in the value of  $k$  with the largest figure (0.65) being almost two times greater than that of the smallest (0.33) for  $\theta = 40^\circ$ . Consequently, if  $k$  was uniform, as expected in such situations where flow conditions are identical, then this possible range in value

could have a significant influence on the resultant magnitude of predicted superelevation (Figure 5.6).

In conclusion, an average value for  $k$  of 0.45 fits the experimental data most accurately (Figure 5.4), although it is difficult to say definitively whether this figure should be used more widely, and more specifically for naturally occurring debris flows without further research to ascertain its role and value further.

Value for $k$	Rc = 0.7 m; $\theta = 20^\circ$	Rc = 0.7 m; $\theta = 40^\circ$	Rc = 0.55 m; $\theta = 40^\circ$	Rc = 0.4 m; $\theta = 40^\circ$
<b>Minimum</b>	0.23	0.33	0.40	0.34
<b>Maximum</b>	0.45	0.63	0.65	0.58
<b>Mean</b>	0.36	0.46	0.53	0.46

**Table 5.3:** Summary of 'k' values for each bend geometry.

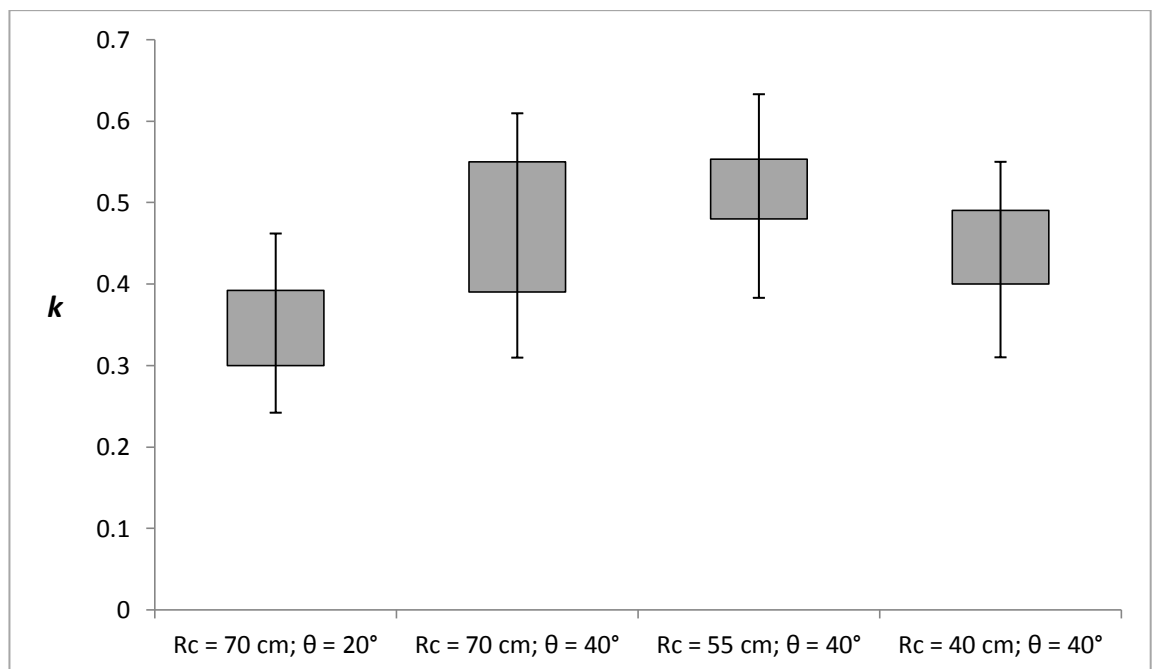


**Figure 5.5:** Box and whisker plot summarising 'k' values for each bend geometry.

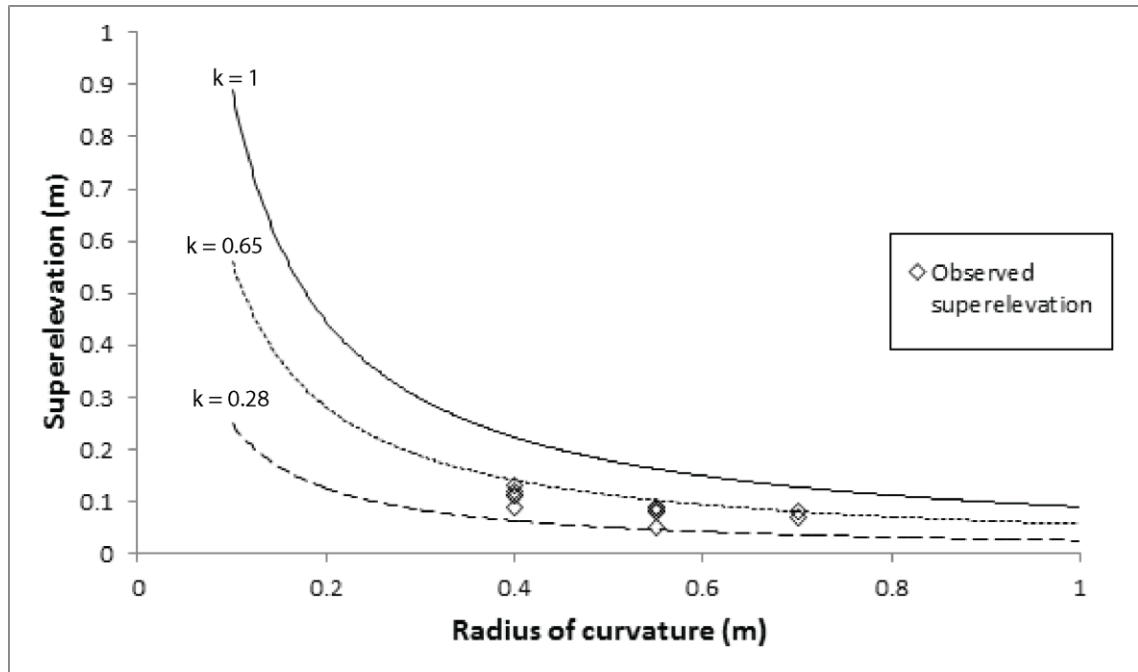


**Figure 5.6:** Demonstrating how the variability of  $k$  can influence predicted superelevation curves. Equation parameters:  $b = 0.14 \text{ m}$ ,  $v = 2.5 \text{ m s}^{-1}$ .

#### 5.4. Future investigations

The data collected in this investigation have led to the successful completion of the research objectives. However, further improvements could be made by expanding the dataset. An increase in the number of repetitions at each bend geometry and channel configuration would be useful in determining the experimental consistency and reliability of the results. For example, as demonstrated in Section 4.3.1, the trend exhibited between BEV and superelevation for bends with  $R_c = 0.7 \text{ m}$  is weak therefore increasing the number of runs may improve the relationship. Furthermore, although three debris flow experiments were conducted at each channel configuration to ensure repeatability, a larger data set would be preferable to perform an appropriate statistical analysis.

Measuring additional channel slopes between  $17\text{-}23^\circ$  would provide a greater understanding of the relationship between superelevation and channel slope. At both bend geometries where  $R_c = 0.7 \text{ m}$ , observed superelevation at a channel slope of  $17^\circ$  exceeded that recorded at  $23^\circ$ ; an unexpected and seemingly anomalous relationship. Thus, incorporating additional channel slopes between  $17\text{-}23^\circ$  into the methodology may help to better establish whether the relationship exhibited at present is anomalous or, as suggested in Section 5.2.3., an apparent threshold value.

Further, the investigation of superelevation over a greater range of bend configurations is important. In this study, the influence of bend angle upon superelevation was only investigated at one radius of curvature. Therefore, to examine this relationship more thoroughly it would be necessary to incorporate a greater range of radii of curvature into the investigation, across which bend angle is varied, and perhaps also an increase in the variety of bend angles tested in addition to 20° and 40°. Also, to further analyse the influence of radius of curvature upon superelevation, it would be required to expand the number of bends with varying radii of curvature.

At present, the debris flow mixture is relatively fluid in nature. Therefore, increasing the viscosity of the mixture by further adjustments to the sediment composition, such as increasing the fine, cohesive material content would promote laminar flow conditions, which are generally observed in naturally occurring debris flows. Further, it is not possible to ensure conservation of mass at a given location across all the debris flow experiments because flow depth is partially dictated by flow velocity, which varied throughout this investigation. However, this influence is not expected to have been a severe limitation of the study.

A limitation of this research is the technique which is used to measure superelevation. It is widely regarded that the passage of the frontal bore around a channel curve can cause the occurrence of splash marks which may exaggerate the magnitude of superelevation. However, because the method of recording superelevation measured the relative height difference of the debris marks on each channel wall, these splash marks may have introduced some inherent error into the data. Consequently, to reduce the error associated with the superelevation measurements it may be possible to use two video cameras to record the passage of debris flows down the channel, and then create a Digital Elevation Model (DEM) of the flow surface. This technique has been used to study the dynamics of channel beds in rivers and flumes previously (Chandler *et al.*, 2001a; Chandler *et al.*, 2001b; Chandler *et al.*, 2003; Shiono *et al.*, 2008), while recently it has been successfully applied to the flow surface of a flooding river in motion with an accuracy of  $\pm 5$  mm (Chandler *et al.*, 2008). This technique has shown some promise and therefore could potentially be used to record superelevation more precisely.

The superelevation equation is a commonly used method to back-calculate velocity estimates from debris flow deposits. However, having compared observed and predicted measurements this study has revealed some additional drawbacks of this technique. Further research is required into the superelevation equation to improve its accuracy,

and particularly the role of  $k$  in the equation. Moreover, the introduction of a parameter to account for the influence of bend angle upon superelevation is a requirement, as this can be a determining factor upon the magnitude of observed superelevation.

The reduced-scale environment in which this investigation is set provides an opportunity to closely study debris flow behaviour in curved and straight channels. Debris flow experimentation in the flume produced the same distinctive characteristic features as observed in naturally occurring debris flows, such as a dry granular front, a long and more fluid tail, and superelevation around channel bends. However, some characteristics observed in this investigation, such as a uniform, non-deformable channel with a lack of an available sediment supply, would not be found in the field and therefore the results obtained and discussed here are only analogous of naturally occurring debris flows (Davies, 1988; Davies, 1990).

Scaling of data is important when studying experimental debris flows (D'Agostino *et al.*, 2010; Iverson, 1997). The most significant experimental investigations have been performed on the USGS flume, which provides intermediate conditions between laboratory based studies and naturally occurring debris flows (Iverson, 1993; Iverson, 1997; Iverson *et al.*, 2010). Iverson (1997) and D'Agostino *et al.* (2010) used two dimensionless scaling parameters for analysing their results: Reynold's number and a number to ascertain pore pressure diffusion normal to the direction of flow. Similarly, Iverson *et al.* (2010) used a series of complex parameters to perform a scaling analysis for experimental and natural debris flows. Although no formal scaling analysis has been adopted in this investigation, it would be reasonable to assume that the velocity and magnitude of superelevation in naturally occurring debris flows would be between 1-2 orders of magnitude greater than those observed from this investigation owing to elevated flow volumes, wider channels with a greater depth and channel bends with much larger radii of curvature.

Similarly, it is necessary to analyse the material properties of debris flows, for sediment composition can be an important controlling factor on debris flow mobility. Although the debris flow mixture used in this investigation has a broad range of grain sizes, it is only a representative mixture of those found in naturally occurring debris flows. Furthermore, the influence of material properties and sediment composition of a debris flow were not directly investigated in this research. However, Fairfield (2011) extensively discussed the implications of material properties upon debris flow motion

by testing a large number of different mixture compositions in the same reduced-scale facility, and this informed the choice of debris flow mix used in this study.

Despite these drawbacks, because of the dearth of information about debris flow superelevation and its determining factors, there is still considerable scope for studying these phenomena on a small, reproducible scale in a laboratory setting.

## Chapter 6: Conclusions

This aim of this study was to investigate debris flow dynamics in curved channels and assess the factors controlling debris flow superelevation. The research objectives have been successfully achieved through experiments conducted in hardware model, and recorded using a combination of video-based and direct measurements. These findings have contributed to the understanding of the role of channel morphology and flow characteristics upon superelevation. This chapter summarises the main findings from this investigation (as discussed in Chapter 5); sets out the main conclusions from the study; and makes suggestions for further work.

### 6.1. Summary

The initial experimental configuration involved a continuous section of straight channel, enabling the relationship between channel gradient and debris flow velocity to be determined. Results demonstrate a strong linear relationship ( $p$ -value of 0.01 for average velocity and average terminal velocity) which is consistent with a Newtonian laminar flow model (Section 4.2.; Figure 4.2). However, further analysis of debris flow hydraulics suggests that flow conditions were more similar to Newtonian turbulent flow, with a power-law relationship between channel gradient and debris flow velocity (Section 5.1.2.).

A positive linear relationship between debris flow bend entry velocity (BEV) and superelevation was evident in all four of the investigated bend configurations, although it was most prevalent in the tighter channel curves (Sections 4.3.1-4.3.4; Figures 4.11 and 4.14). Curiously, superelevation at a channel slope of  $17^\circ$  exceeded that at  $23^\circ$  for the two bends with a radius of curvature of 0.7 m. With this occurring at two differing bend geometries, and at the same radius of curvature, this may suggest a non-linear relationship or threshold which initiates a change in debris flow behaviour, causing this pattern of results.

The radius of curvature and bend angle of a channel curve can also strongly control the magnitude of superelevation (Sections 4.3.3 and 4.3.4.). As radius of curvature decreased, superelevation increased in a non-linear association (Figures 4.17 and 4.18). Theoretical data suggests that a power law relationship should be exhibited between radius of curvature and superelevation, but it is not possible to explore this trend further or apply a statistical analysis with only three data points available for a constant bend

angle. Conversely, superelevation is greater for a bend angle of  $40^\circ$  than at  $20^\circ$ , suggesting that this is an as yet unaccounted control upon superelevation (Figure 4.19).

Comparison of the predicted and observed superelevation values has demonstrated a consistent overestimation of the predicted data by the superelevation equation, overestimating superelevation on occasion by over 200% (Section 5.3.1.; Table 5.1). The results are consistent with some previous investigations which regard the predicted superelevation as maxima. However, the magnitude of overestimation observed in this research suggests that the superelevation equation needs additional research to improve its accuracy.

Rearrangement of the superelevation equation enabled the ' $k$ ' coefficient to be analysed for the experimental data (Section 5.3.3.). The value of  $k$  was not uniform, as expected, but varied greatly between experiments with the largest values (0.65; 0.45) being almost two times greater than the smallest (0.33; 0.23); this is contrary to the initial theory that  $k$  cannot be less than 1. This apparent range in the value of  $k$  could have a significant impact upon the magnitude of predicted superelevation (Figure 5.6)

## 6.2. Primary conclusions

1. Debris flow velocity has a linear relationship with channel gradient.
2. The magnitude of superelevation observed in a channel bend is strongly controlled by a combination of debris flow velocity, the radius of curvature and bend angle of a channel curve.
3. The bend angle of a channel curve is a strong and, as yet, unquantified influence upon superelevation, and therefore it is important that a parameter defining this be introduced to the superelevation equation.
4. Back-calculated velocity estimates should be regarded as maxima.
5. Further research is required to improve the accuracy of the superelevation equation, and particularly evaluate the value and interpretation of the ' $k$ ' coefficient.

## 6.3. Suggestions for further research

Knowledge from literature and previous investigations documenting superelevation of debris flows is very limited. This study has improved the understanding of some of the key factors which determine superelevation, although further research is required to

improve this knowledge base. Detailed recommendations to supplement this research are described in Section 5.4. and focus on expanding the database. Briefly, this includes: increasing the number of experimental runs for each channel configuration; introducing additional radii of curvature into the study; and increasing the variety of bend angles investigated. These modifications would enhance understanding of the controlling factors affecting superelevation. Moreover, this research has highlighted some of the weaknesses of the superelevation equation for predicting superelevation. In particular further research into the suitability of  $k$  and introducing a parameter for bend angle are important.

---

## References

- Akhtari, A.A., Abrishami, J. and Sharifi, M.B. (2009) Experimental Investigations Water Surface Characteristics in Strongly-Curved Open Channels. *Journal of Applied Sciences*, 9 (20), 3699-3706
- Apmann, R.P. (1973) Estimating discharge from super-elevation in bends. *Journal of the Hydraulics Division*. 99 (HY1), 65-79
- Arattano, M. and Marchi, L. (2000) Video-derived velocity distribution along a debris flow surge. *Physics and Chemistry of the Earth (B)*, 29 (9) 781-784.
- Ashida, K., Takahashi, T. and Arai, M. (1981) Study on debris flow control; debris flow in bends of rectangular section. *Annals, DPRI*, 24B-2: 251-263 (*in Japanese*)
- Berger, C., McArdell, B.W. and Schlunegger, F. (2011a) Direct measurement of channel erosion by debris flows, Illgraben, Switzerland. *Journal of Geophysical Research*, 116 (F01002), 1-18
- Berger, C., McArdell, B.W. and Schlunegger, F. (2011b) Sediment transfer patterns at the Illgraben catchment, Switzerland: Implications for the time scales of debris flow activities. *Geomorphology*, 125 (3), 421-432
- Berti, M., Genevois, R., Simoni, A. and Tecca, P.R. (1999) Field observations of a debris flow event in the Dolomites. *Geomorphology*, 29 (3-4), 265-274
- Berzi, D. and Jenkins, J.T. (2009) Steady inclined flows of granular-fluid mixtures. *Journal of Fluid Mechanics*, 641, 359-387
- Blott, S.J. and Pye, K. (2006) Particle size distribution analysis of sand-sized particles by laser diffraction: an experimental investigation of instrument sensitivity and the effects of particle shape. *Sedimentology*, 53 (3), 671-685
- Bovis, M.J. and Jakob, M. (1999) The role of debris supply conditions in predicting debris flow activity. *Earth Surface Processes and Landforms*, 24 (11), 1039-1054
- Bowman, E. and Davies, T. (2008) The recognition and identification of debris flow hazards for proposed development sites in New Zealand. Auckland, New Zealand. *18th New Zealand Geotechnical Society (NZGS) Geotechnical Symposium 2008*, 4-6 Sep 2008.
- British Standards Institution (1989) Testing Aggregates Part 103: Methods for Determination of Particle Size Distribution. Section 103.1: Sieve Tests (AMD 6003). *BS 812-103.1*
- British Standards Institution (1999) Particle Size Analysis. Laser Diffraction methods. General principles. *BS ISO 13320-1:1999*

- Buffin-Bélanger, T., Reid, I., Rice, S., Chandler, J.H. and Lancaster, J. (2003) A casting procedure for reproducing coarse-grained sedimentary surfaces. *Earth Surface Processes and Landforms*, 28 (7), 787-796
- Buffington, J.M., Dietrich, W.E. and Kirchner, J.W. (1992) Friction angle measurements on a naturally formed gravel stream bed: Implications for critical boundary shear stress. *Water Resources Research*, 28 (2), 411-425
- Bulmer, M.H., Barnouin-Jha, O.S., Peitersen, M.N. and Bourke, M. (2002) An empirical approach to studying debris flows: Implications for planetary modelling studies. *Journal of Geophysical Research*, 107 (E5), 1-15
- Carrigy, M.A. (1970) Experiments on the angles of repose of granular materials. *Sedimentology*, 14 (3-4), 147-158
- Chandler, J.H., Lane, S.N. and Shiono, K. (2001a) "Acquisition Of Digital Elevation Models At High Spatial and Temporal Resolutions Using Automated Digital Photogrammetry", *lboro.ac.uk website* (<http://www-staff.lboro.ac.uk/~cvjhc/HRWallRep.html>, accessed on 08/08/2011)
- Chandler, J.H., Lane, S.N. and Shiono, K. (2001b) Measuring flume surfaces for Hydraulics research using a Kodak DCS460. *The Photogrammetric Record*, 17 (97), 39-61
- Chandler, J.H., Buffin-Bélanger, T., Rice, S., Reid, I. and Graham, D.J. (2003) The accuracy of a river bed moulding/casting system and the effectiveness of a low-cost digital camera for recording river bed fabric. *The Photogrammetric Record*, 18 (103), 209-223
- Chandler, J.H., Wackrow, R., Sun, X., Shiono, K. and Rameshwaran, P. (2008) Measuring a dynamic and flood river surface by close range digital photogrammetry. In: *Silk Road for Information from Imagery, Beijing, 3-11 July 2008*. International Society for Photogrammetry and Remote Sensing, 211-216
- Chaudhry, M.H. (2008) *Open-Channel Flow*. Springer: New York
- Chen, C-L. (1987) Comprehensive review of debris flow modeling concepts in Japan. In: Costa, J.E. and Wieczorek, G.F. eds. *Reviews in Engineering Geology, vol VII. Debris flows/ Avalanches: process, recognition, and mitigation*. The Geological Society of America: Boulder, CO, 13-29
- Chow, V.T. (1959) *Open-Channel Hydraulics*. McGraw-Hill: New York
- Contreras, S.M. and Davies, T.R.H. (2000) Coarse-grained debris-flows: hysteresis and time-dependent rheology. *Journal of Hydrological Engineering*, 126 (12), 938-941
- Costa, J.E. (1984) Physical geomorphology of debris flows. In: Costa, J.E., Fleisher, P.J. eds. *Developments and Applications of Geomorphology*. Springer, Berlin, 268-317

- Coussot, P. and Piau, J-M. (1994) On the behaviour of fine mud suspensions. *Rheologica Acta*, 33 (3), 175-184
- Coussot, P. and Meunier, M (1996) Recognition, classification and mechanical description of debris flows. *Earth Science Reviews*, 40 (3-4), 209-227
- Coussot, P., Laigle, L., Arattano, M., Deganutti, A. and Marchi, L. (1998) Direct determination of rheological characteristics of debris flow. *Journal of Hydrologic Engineering*, 124 (8), 865-868
- Crudden, D.M. and Lu, Z.Y. (1992) The rockslide and debris flow from Mount Cayley, B.C., in June 1984. *Canadian Geotechnical Journal*, 29 (4), 614-626
- D'Agostino, V., Cesca, M. and Marchi, L. (2010) Field and laboratory investigations of runout distances of debris flows in the Dolomites (Eastern Italian Alps). *Geomorphology*, 115 (3-4), 294-304
- Davies, T.R.H. (1986) Large debris flows: a macroviscous phenomenon. *Acta Mechanica*, 63 (1-4), 161-178
- Davies, T. R. H. (1988) Debris flow surges – a laboratory investigation. In *Mitteilungen der Versuchsanstalt für Wasserbau, Hydrologie und Glaziologie* 96. Technischen Hochschule Zürich.
- Davies, T.R.H. (1990) Debris flow surges – experimental simulation. *Journal of Hydrology (N.Z.)*, 29 (1), 18-46
- Davies, T.R., Phillips, C.J., Pearce, A.J. and Zhang, X.B. (1992) Debris flow behaviour – an integrated overview. *Erosion, Debris Flows and Environment in Mountain Regions*, 209, 217-225
- Deangeli, C. (2008) Laboratory granular flows generated by slope failures. *Rock Mechanics and Rock Engineering*, 41 (1), 199-217
- Deangeli, C. (2009) Pore water pressure contribution to debris flow mobility. *American Journal of Environmental Sciences*, 5 (4), 486-492
- DeGraff, J.V. (1994) The geomorphology of some debris flows in the southern Sierra Nevada, California. *Geomorphology*, 10 (1-4), 231-252
- Denlinger, R.P. and Iverson, R.M. (2001) Flow of variably fluidized granular masses across three-dimensional terrain. 2. Numerical predictions and experimental tests. *Journal of Geophysical Research*, 106 (B1), 553-566
- Denlinger, R.P. and Iverson, R.M. (2004) Granular avalanches across irregular three dimensional terrain: 1. Theory and Computation. *Journal of Geophysical Research*, 109 (F01014), 1-14
- Enos, P. (1977) Flow regimes in debris flow. *Sedimentology*, 24 (1), 133-142

- Eshel, G., Levy, G.J., Mingelgrin, U. and Singer, M.J. (2004) Critical evaluation of the use of laser diffraction for particle-size distribution analysis. *Soil Science Society of America*, 68 (3), 736-743
- Evans, S.G., Hungr, O. and Clague, J.J. (2001) Dynamics of the 1984 rock avalanche and associated distal debris flow on Mount Cayley, British Columbia, Canada; implications for landslide hazard assessment on dissected volcanoes. *Engineering Geology*, 61 (1), 29-51
- Fairfield, G. (2011) *Assessing the dynamic influences of slope angle and sediment composition on debris flow behaviour: An experimental approach*. MSc Thesis, Durham University: UK
- Genevois, R., Galgaro, A. and Tecca, P.R. (2001) Image analysis for debris-flow properties estimation. *Physics and Chemistry of the Earth (C)*, 26 (9), 623-631
- Guadagno, F.M., Forte, R., Revellino, P., Fiorillo, F. and Focareta, M. (2005) Some aspects of the initiation of debris avalanches in the Campania region: The role of morphological slope discontinuities and the development of failure. *Geomorphology*, 66 (1-4), 237-254
- Hampton, M.A. (1975) Competence of fine-grained debris flows. *Journal of Sedimentary Petrology*, 45 (4), 834-844
- Henderson, F.M. (1966) *Open Channel Flow*. The Macmillan Company: New York
- Hungr, O., Morgan, G.C., Kellerhals, R. (1984) Quantitative analysis of debris torrent hazards for design of remedial measures. *Canadian Geotechnical Journal*, 21, 663-677
- Hungr, O. (1995) A model for the rapid runout analysis of rapid flow slides, debris flows and avalanches. *Canadian Geotechnical Journal*, 32, 610-623
- Hungr, O. (2007) *Comms*. In Prochaska, A.B., Santi, P.M., Higgins, J.D. and Cannon, S.H. (2008a) A study of methods to estimate debris flow velocity. *Landslides*, 5 (4), 431-444
- Hürlimann, M., Rickenmann, D. and Graf, C. (2003) Field and monitoring data of debris flow events in the Swiss Alps. *Canadian Geotechnical Journal*, 40 (1), 161-175
- Ikeya, H. and Uehara, A. (1982) The behaviour of debris in S-shaped stream channel curves. *Materials for Civil Engineering Techniques (Dobuku Gijutsu Shiryo)*, 24 (12), 21-26 (in Japanese).
- Innes, J.L. (1983) Debris Flows. *Progress in Physical Geography*, 7 (4), 469-501

- Iverson, R.M. and LaHusen, R.G. (1993) Friction in debris flows: Inferences from large-scale flume experiments. In *Hydraulic Engineering '93. Proceedings of the 1993 Conference. Hydraulics Division of the American Society of Civil Engineers*. 2, 1604-9
- Iverson, R.M., LaHusen, R.G., Major, J.J. and Zimmerman, C.L. (1994) Debris flow against obstacles and bends: dynamics and deposits. (*Abstract Only*)
- Iverson, R.M. (1997) The Physics of Debris Flows. *Reviews of Geophysics*, 35 (3), 245-296
- Iverson, R.M., Reid, M.E. and LaHusen, R.G. (1997) Debris flow mobilisation from landslides. *Annual Review of Earth and Planetary Sciences*, 25, 85-138
- Iverson, R.M. and Denlinger, R.P. (2001) Flow of invariably fluidized granular masses across three-dimensional terrain. 1. Coulomb mixture theory. *Journal of Geophysical Research*, 106 (B1), 537-552
- Iverson, R.M. and Vallance, J.W. (2001) New views of granular mass flows. *Geology*, 29 (2), 115-118
- Iverson, R.M. (2003) The debris-flow rheology myth. In Chen, C.L. and Rickenmann, D. eds. *Debris flow Mechanics and Mitigation Conference*. Mills Press: Davos, 303-314.
- Iverson, R.M., Logan, M., LaHusen, R.G., and Berti, M (2010) The perfect debris flow? Aggregated results from 28 large scale experiments. *Journal of Geophysical Research*, 115 (F03005), 1-29
- Johnson, A.M. (1970) *Physical Processes in Geology*, Freeman Cooper: San Francisco
- Johnson, A.M. and Rodine, J.R. (1984) Debris flow. In: Brunsden, D. and Prior, D.B. eds. *Slope Instability*. Wiley: Chichester, UK, 257-361
- Julien, P.Y. and Paris, A. (2010) Mean Velocity of Mudflows and Debris Flows. *Journal of Hydraulic Engineering*, 136 (9), 676-679
- Lorenzini, G. and Mazza, M. (2004) *Debris-Flow Phenomology and Rheological Modelling*. WIT Press: Southampton
- Mangeney, A., Roche, O., Hungr, O., Mangold, N., Faccanoni, G. and Lucas, A. (2010) Erosion and mobility in granular collapse over sloping beds. *Journal of Geophysical Research*, 115 (F03040), 1-21
- Massoudi, M. and Phuoc, T.X. (2004) Flow of a generalised second grade non Newtonian fluid with variable viscosity. *Continuum Mechanics and Thermodynamics*, 16 (6), 529-538
- McGlinchey, D. (2008) *Bulk Solids Handling: Equipment Selection and Operation*. Blackwell: Oxford

- Miller, R.L. and Byrne, R.J. (1966) The angle of repose for a single grain on a fixed rough bed. *Sedimentology*, 6 (4), 303-314
- Mizuyama, T. and Uehara, S. (1983) Experimental study of the depositional process of debris flows. *Trans-Japanese Geomorphological Union*, 4 (1), 49-64.
- Mora, C.F., Kwan, A.K.H. and Chan, H.C. (1998) Particle size distribution analysis of coarse aggregate using digital image processing. *Cement and Concrete Research*, 28 (6), 921-932
- Muñoz-Salinas, E., Manea, V.C., Palacios, D. and Castillo-Rodriguez, M. (2007) Estimation of lahar flow velocity on Popocatepetl volcano (Mexico). *Geomorphology*, 92 (1-2), 91-99
- Nichols, R.L. (1939) Viscosity of lava. *The Journal of Geology*, 47 (3), 290-302
- Phillips, C.J. and Davies, T.R.H. (1991) Determining rheological parameters of debris flow material. *Geomorphology*, 4 (2), 101-110
- Pierson, T.C. (1981) Dominant particle support mechanisms in debris flows at Mt Thomas, New Zealand, and implications for flow mobility. *Sedimentology*, 28 (1), 49-60
- Pierson, T.C. (1985) Initiation and flow behaviour of the 1980 Pine Creek and Muddy River lahars, Mount St. Helens, Washington. *The Geological Society of America Bulletin*, 96 (8), 1056-1069
- Pierson, T.C. (1995) Flow characteristics of large eruption-triggered debris flows at snow-clad volcanoes: constraints for debris flow models. *Journal of Volcanology and Geothermal Research*, 66 (1-4), 283-294
- Pouliquen, O. And Vallance, J.W. (1999) Segregation induced instabilities of granular fronts. *American Institute of Physics*, 9 (3), 621-630
- Prochaska, A.B., Santi, P.M., Higgins, J.D. and Cannon, S.H. (2008a) A study of methods to estimate debris flow velocity. *Landslides*, 5 (4), 431-444
- Prochaska, A.B., Santi, P.M., Higgins, J.D. and Cannon, S.H. (2008b) Debris-flow runout predictions based on the average channel slope (ACS). *Engineering Geology*, 98 (1-2), 29-40
- Pudasaini, S.P., Wang, Y., Sheng, L-T, Hsiau, S-S., Hutter, K. And Katzenbach, R. (2008) Avalanching granular flows down curved and twisted channels: Theoretical and experimental results. *Physics of Fluids*, 20 (073302), 1-11
- Rickenmann, D. and Zimmermann, M. (1993) The 1987 Debris Flows in Switzerland: documentation and analysis. *Geomorphology*, 8 (2-3), 175-189

- Rickenmann, D. (1999) Empirical relationships for debris flows. *Natural Hazards*, 19 (1), 47-77
- Rickenmann, D., Weber, D. and Stepanov, B. (2003) Erosion by debris flows in field and laboratory experiments. *Debris Flow Hazards Mitigation: Mechanics, Prediction and Assessment*, 1&2, 883-894
- Rodine, J.D. and Johnson, A.M. (1976) The ability of debris, heavily freighted with coarse clastic materials, to flow on gentle slopes. *Sedimentology*, 23 (2), 213-234
- Sciblogs (2010) "Shaken not stirred: Flooding, Landslides Force Millions out of Their Homes". *Sciblog.co.nz website*. (<http://sciblogs.co.nz/shaken-not-stirred/tag/debris-flow/>, accessed on 03/01/2011)
- Shiono, K., Spooner, J., Chan, T., Rameshwaran, P. and Chandler, J.H. (2008) Flow characteristics in meandering channels with non-mobile and mobile beds for overbank flows. *Journal of Hydraulic Research*, 46 (1), 595-605
- Statham, I. (1977) Angle of repose, angle of shearing resistance and angles of talus slopes – a reply. *Earth Surface Processes*, 2 (4), 437-440
- Stock, J.D. and Dietrich, W.E. (2006) Erosion of steepland valleys by debris flows. *Geological Society of America Bulletin*, 118 (9-10), 1125-1148
- Suwa, H. and Yamakoshi, T. (2000) Estimation of debris-flow motion by field surveys. In: Wieczorek, G.F. and Naeser, N.D. eds. *Debris Flow Hazards Mitigation: Mechanics, Prediction, and Assessment*. AA Balkema: Rotterdam, 293-299
- Takahashi, T. (1981) Debris Flow. *Annual Review of Fluid Mechanics*, 13, 57-77
- Takahashi, T. (2000) Initiation and flow of various types of debris flow, in Wieczorek, G.F. and Naeser, N.D. eds. *Debris Flow Hazards Mitigation: Mechanics, Prediction and Assessment*. AA Balkema: Rotterdam, 15-28
- Takahashi, T. (2007) *Debris flow: Mechanics, Prediction and Countermeasures*. Taylor & Francis: London
- Tipler, P.A. and Mosca, G. (2004) *Physics for Scientists and Engineers - 5<sup>th</sup> edition*. Freeman: New York
- Uddin, M.S., Inaba, H., Yasumasa, I. and Kasahara, M. (1998) Estimation of the surface velocity of debris flow with computer-based spatial filtering. *Applied Optics*, 37 (26), 6234-6239
- USGS (2001) Natural Hazards on Alluvial Fans: The Venezuela Debris Flow and Flash Flood Disaster. *USGS Fact Sheet*, 0103-01

- Van Burkalow, A. (1945) Angle of repose and angle of sliding friction: an experimental study. *Geological Society of America Bulletin*, 56 (6), 669-707
- Van Dine, D.F. (1996) Debris flow control structures for forest engineering. *British Columbia Ministry of Forests Research Program*, Working Paper 08/1996
- Van Steijn, H. and Coutard, J.P. (1989) Laboratory experiments with small debris flows: physical properties related to sedimentary characteristics. *Earth Surface Processes and Landforms*, 14 (6), 587-596
- Webb, R.H., Pringle, P.T., Reneau, S.L. and Rink, G.R. (1988) Monument Creek debris flow, 1984: Implications for formations of rapids on the Colorado River in Grand Canyon National Park. *Geological Society of America Bulletin*, 16 (1), 50-54
- Webber, N.B. (1965) *Fluid Mechanics for Civil Engineers*. E. & F. N. Spon: London
- Wieczorek, G.F., Larsen, M.C., Eaton, L.S., Morgan, B.A. and Blair, J.L. (2001) Debris-flow and flooding hazards caused by the December 1999 storm in coastal Venezuela. *U.S. Geological Survey*, Open File Report 01-0144, 1-40. *USGS website*.  
(<http://pubs.usgs.gov/of/2001/ofr-01-0144/>, accessed on 29/03/2011)
- Whipple, K.X. (1997) Open channel flow of Bingham Fluids: Applications in Debris Flow research. *The Journal of Geology*, 105 (2), 243-262
- Wohl, E.E. and Pearthree, P.P. (1991) Debris flows as geomorphic agents in the Huachuca Mountains of southeastern Arizona. *Geomorphology*, 4 (3-4), 273-293